Enzyme Mimic to Develop Antioxidant Nanoreactors: From Synthesis to Application

Inauguraldissertation

Zur

Erlangung der Würde eines Doktors der Philosophie

Vorgelegt der

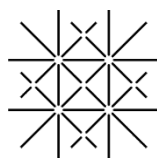Philosophische-Naturwissenschaftlichen Fakultät

der Universität Basel

Von

Vimalkumar Balasubramanian

Aus

Indien

UNI
BASEL

Basel 2011

Genehmigt von der Philosophisch-Naturwissenschaftlichen Fakultät auf Antrag von

Prof. Wolfgang Meier (Universität Basel)

PD. Dr. Cornelia Palivan (Universität Basel)
und

Asst. Prof. Andreas Taubert (Universität Potsdam)

Basel, den 21.06.2011

Prof. Dr. Martin Spiess
Dekan

Table of Content

Enzyme Mimic to Develop Antioxidant Nanoreactors: From Synthesis to Application

2. Structure- activity relationship (SAR) analysis to design an effective enzyme mimic

3. Synthesis and characterization of bi-functional enzyme mimic

4. Encapsulation of bi-functional enzyme mimics in polymeric vesicles

Impact of the work

Publications:

- **Vimalkumar Balasubramanian**, Maria Ezhevskaya, Hans Moons, Markus Neuburger, Carol Cristescu, Sabine Van Doorslaer and Cornelia Palivan, Structural characterization of a highly active superoxide-dismutase mimic, Phys. Chem. Chem. Phys., 2009, 11, 6778 – 6787.

- **Vimalkumar Balasubramanian**, O. Onaca, F. Axthelm, D. Hughes, M. Grzelakowski, W. Meier, C. G. Palivan, How to Reduce Superoxide Anion Concentration using Antioxidant Nanoreactors, Journal of Optoelectronics and Advanced Material, 2009, 1(6), 1083 - 1087.

- **Vimalkumar Balasubramanian**, Ozana Onaca, Maria Ezhevskaya, Sabine Van Doorslaer, Balasubramanian Sivasankaran, Cornelia G. Palivan, A surprising system: Polymeric nanoreactors containing a mimic with dual-enzyme activity, Soft Matter, 2011, DOI**:** 10.1039/C1SM05215B**.**

- **V. Balasubramanian**, O. Onaca, R. Enea, D. Hughes, C.G. Palivan, Proteins delivery: From conventional drug delivery carriers to polymeric nanoreactors, Expert. Opin. Drug Delivery, 2010, 7(1), 63-78.

- Cornelia G. Palivan, **Vimalkumar Balasubramanian**, Bernard A. Goodman, Global Structure-Activity Analysis in Drug Development Illustrated for Active Cu/Zn Superoxide Dismutase Mimics, Eur. J. Inorg. Chem., 2009, 31, 4634-4639.

- Ozana Onaca, David W. Hughes, **Vimalkumar Balasubramanian**, Mariusz Grzelakowski, Wolfgang Meier, Cornelia Palivan, SOD antioxidant nanoreactors: Influence of block copolymer composition on the nanoreactor efficiency, Macromol. Biosci., 2010, 10, 531-8.

- Pascal Tanner, Ozana Onaca, **Vimalkumar Balasubramanian**, Wolfgang Meier, Cornelia G. Palivan, Enzymatic Cascade Reactions inside Polymeric Nanocontainers – A Means to Combat Oxidative Stress, Chem. Eur. J., 2011, 17, 4552–4560.

- Egli, Stefan; Nussbaumer, Martin; **Balasubramanian, Vimalkumar**; Chami, Mohamed; Bruns, Nico; Palivan, Cornelia; Meier, Wolfgang, Biocompatible Functionalization of Polymersome Surfaces: A new Approach to Surface Immobilization and Cell Targeting using Polymersomes, J Am. Chem. Soc., 2011, 133 (12), 4476–4483.

- Pascal Tanner, Stefan Egli, **Vimalkumar Balasubramanian**, Ozana Onaca, Cornelia G. Palivan, and Wolfgang Meier, Can polymeric vesicles that confine enzymatic reactions act as simplified organelles? FEBS letters, 2011, DOI: 10.1016/j.febslet.2011.05.003.

Poster presentations:

• 4th EF EPR Summer School, COST P15 Training School and SUSSP 64, St Andrews, Scotland, Cu/Zn Superoxide dismutase mimics against oxidative stress, **V. Balasubramanian,** C.G. Palivan.

• Swiss Chemical Society – Fall Meeting, University of Zurich, Switzerland, Cu/Zn Superoxide dismutase- mimics: Is there a structure-activity relationship for the metal binding region? **V. Balasubramanian,** C.G. Palivan.

• Swiss Nano Conference 2009, Basel, Switzerland. How to detoxify O2$^-$ using antioxidant nanoreactors? Vimalkumar Balasubramanian, Ozana Onaca, Fabian Axthelm, David Hughes, Mariusz Grzelakowski, Wolfgang Meier and Cornelia G. Palivan.

• Fall Meeting of the Swiss Chemical Society 2009, Lausanne, Switzerland. Structural characterization of a high active superoxide-dismutase mimic. **V. Balasubramanian**, M. Ezhevskaya, H. Moons, M. Neuburger, S. Van Doorslaer, and C.G. Palivan.

• 7th European Federation of EPR groups meeting and Closing meeting of COST P15, Belgium. Structure determination by EPR spectroscopy as an aid to the design of effective Cu-based superoxide dismutase mimics. **V. Balasubramanian**, C.G. Palivan.

• Swiss soft day 1ST Workshop, Zurich, Switzerland. How to decrease O2- levels using nanoreactors based on enzyme mimics? **Vimalkumar Balasubramanian,** Ozana Onaca, David Hughes, Wolfgang Meier and Cornelia G. Palivan.

• Trends in Nanotechnology (TNT 2010) Conference, Braga, Portugal. Polymeric nanoreactors: a new way to improve antioxidant therapy **Vimalkumar Balasubramanian**, Ozana Onaca, Fabian Axthelm, Wolfgang Meier, Cornelia G. Palivan.

• Polycoll 2011, University of Geneva, Switzerland, Cellular interaction of polymeric nanoreactors. **Vimalkumar Balasubramanian,** Pascal Tanner, Ozana Onaca, Wolfgang Meier and Cornelia G. Palivan.

Summary of the thesis

The first chapter describes the general introduction to the self assembly of amphiphilic copolymers and their self assembled structures specially highlighted with nanoreactors. General concept of oxidative stress, natural antioxidant mechanisms and the recent strategies to improve antioxidant therapy are presented. Further, the motivation and concept of the thesis are also briefly presented.

In chapter two, the structure-activity realtionship(SAR) based on statistical analysis of all classes of already published copper based superoxide dismutase mimics (SODm) is investigated to distinguish the structural and geometrical specificity of highly active SODm. This will serve to streamline further the process of new drug discovery in relation with SODm. Combination of hyperfine coupling constants and distortion factors from EPR as structural parameters characterizing the first coordination sphere around the metal showed an almost linear relationship related to a high SOD like activity.

Chapter three presents the synthesis and characterization of a copper complex of 6-(2-hydroxy-benzaldehyde) hydrazono-as-triazine-3,5-dione (Cu^{II}ENZm). Cu^{II}ENZm studied in this work showed a change from a di-copper complex in the solid state to a mono-nuclear complex in solution. The superoxide dismutase and catalase like activity of the Cu^{II}ENZm were determined by a modified version of the conventional Nitro Blue Tetrazolium assay and Amplex red coupled fluorescence assay. Cu^{II}ENZm were able to completely detoxify the superoxide radicals and related peroxides.

In chapter four, we investigate the development of antioxidant nanoreators by encapsulating the bi-functional Cu^{II}ENZm inside polymeric vesicles made of PMOXA-PDMS-PMOXA block copolymers. We ensured that polymeric vesicles were not affected by the encapsulation procedure as indicated by light scattering and transmission electron microscopy. In addition, the structural conformation of Cu^{II}ENZm was preserved inside the polymer cavity, as demonstrated by electron paramagnetic resonance and UV-VIS spectroscopy.

Chapter five explains the detailed study of cellular interaction of Cu^{II}ENZm containing nanoreactors in THP-1 cells. The internalization of the nanoreactor in THP-1 cells was studied by confocal laser scanning microscopy and flow cytometry and intracellular localization through TEM.

No evident toxicity was found using MTS and LDH assays. As Cu^{II}ENZm remained active inside the vesicles therefore, these Cu^{II}ENZm-containing nanoreactors exhibited efficient antioxidant activity against paraquat mediated oxidative stress in THP-1 cells. Development of this simple, robust antioxidant nanoreactor represents a new direction in efficiently fighting oxidative stress.

Chapter six briefly summarize the results and achievements of the research work. Further investigations are suggested.

1.   Introduction

1.1. Copolymers

Block copolymers are macromolecules consisting of a minimum of two homopolymer subunits linked by covalent bonds or through an intermediate, non-repeating unit known as a junction block.[1] Block copolymers can be classified based on the arrangement and order of the homopolymer subunits, which are normally marked as A, B, C etc. The architectures of amphiphilic block copolymers exhibit the same variety as seen for homo polymers: linear, cycle, multi-arm star, comb, hyper-branched or dendrimeric shape. (Scheme 1) Amphiphilic (*amphi*: of both kinds; *philic*: having an affinity for) block copolymers consist of at least two subunits, one of them possessing hydrophilic properties while the other has a hydrophobic character.
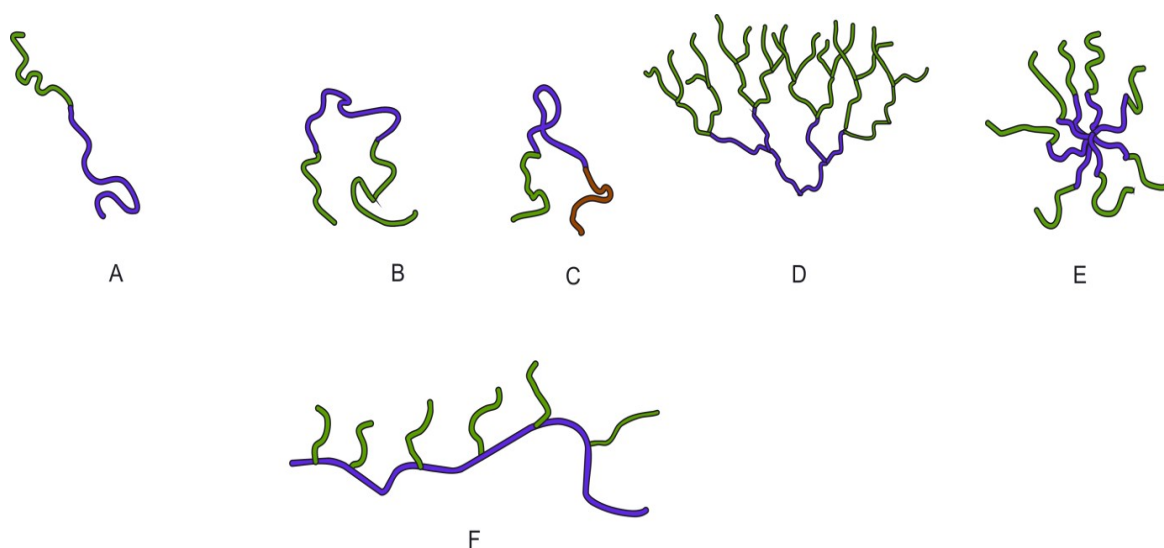
Scheme 1. Possible amphiphilic block copolymer architecture: A – AB – diblock, B – ABA triblock, C – ABC – triblock, D – dendrimer shape, E – star-shape, F – grafted.

1.2. General introduction to self-assembly

Self-assembly is a process by which a disordered system of components forms an organized structure or pattern due to local interactions between the components themselves, without any external guidance. Self-assembly can be either a static or a dynamic process. In static self-assembly, the ordered structures form at equilibrium and may require energy to form ordered

structures, which are stable after they formed. In dynamic self-assembly, interactions can occur only when the system is dissipating energy in order to form the organized structures.

Self assembly takes place in nature as a spontaneous process to generate well ordered biological structures or systems. For instance, self assembly of lipid bilayers leads to an increase in detailed internal organization of the cell membrane. Other biological structures, including membranes, proteins, nucleic acids and viruses, are also natural self-assembled super structures formed through intermolecular and/or intramolecular interactions. Proteins with a well-defined amphiphilic nature spontaneously form spatially-organized supramolecular structures to achieve biological functions. The mimicking of the self-assembly of biological structures has recently received attention for the creation of novel materials in the biomedical domain, especially in drug delivery approaches.

1.3. Self-assembly of amphiphilic block copolymers

Similar to conventional amphiphiles (lipids and surfactants), hydrophilic and hydrophobic blocks confer the amphiphilicity to block copolymers. The hydrophilic/hydrophobic nature and microphase separation of the amphiphilic copolymer chains can lead to molecular ordered super structures via self assembly,[2-4] mainly driven by non covalent hydrophobic interaction such as hydrogen bonds and van der Waals interactions. The solvent, which is selective for only one block, is unfavourable for the other block, and this triggers the self assembly process.[5] The covalent bond between the incompatible blocks prevents the macrophase separation.[6] Different morphologies of copolymers are generated by the self-assembly process, such as micelles, vesicles, tubes, rods, and lamellar structures. (Scheme 2)
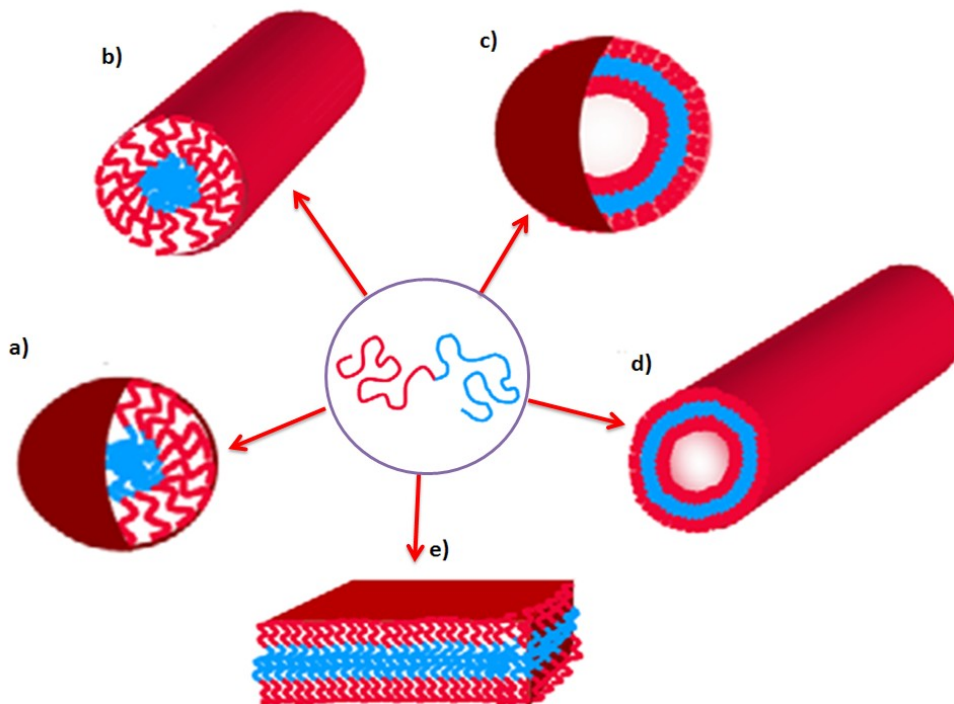
Scheme 2. Schematic representation of different morphologies generated by the self-assembly of amphiphilic copolymers: a) micelles b) rods c) vesicles d) tubes e) lamellar structures.

These morphologies can be obtaining by controlling the chemical nature of the blocks, copolymer concentration, temperature and the nature of the solvent.[7-9] The influence of polymer concentration was investigated on the formation of PS-*co*-PAA vesicles. Only a polymer concentration greater than 0.6 wt. % generates vesicles.[10] While PS-*co*-PAA copolymers in DMF form spherical aggregates, in tetrahydrofuran or dioxane vesicles are then formed. This indicates the effect of solvents on supramolecular morphology.[11] Self-assembly behavior of amphiphilic block copolymers has been found to depend on the weight fraction of the hydrophilic block as well. In the case of both poly (ethylene glycol)-poly (butadiene) (PEG–PBD) and poly (ethylene glycol)-pentaerythritol ethoxylate (PEG–PEE) copolymers, if the fraction of PEG is between 20 % and 42 %, the copolymers will self-assemble into vesicles. If the copolymer is considerably more hydrophobic, with a fraction of PEO < 20 %, the immobile hydrophobic blocks will sequester into solid-like particles. For fractions of PEO > 42 %, spherical micelles are typically formed.[12]

The main feature that makes amphiphilic block copolymers attractive for drug delivery applications is their chemical versatility, allowing control of size and morphology of the self-

assembled structures.[13,14] Micelles and vesicles are of major interest for drug delivery applications because of their appealing features, which fulfill the requirements for selective drug delivery.

1.4. Micelles

It has been reported that amphiphilic diblock copolymers dissolved in a solvent that is selective for one of the blocks will self-assemble and form micelles with a compact core of insoluble blocks surrounded by a soluble corona composed of a soluble block.[15] The micellar structures can be generated in two different forms based on the length of the blocks. If the hydrophilic block is longer than the hydrophobic part, star micelles with a small core and a longer corona are formed.[16,17] Oppositely, a copolymer with a hydrophobic block longer than the hydrophilic will form a crew-cut micelle.(scheme 3)[18,19]
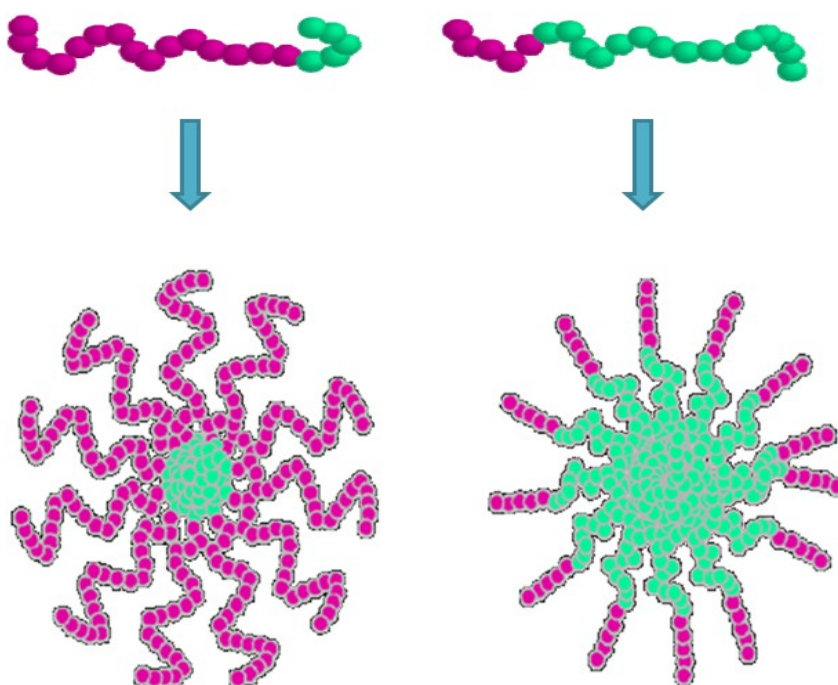
Scheme 3. Micelle types formed depending on the ratio of hydrophilic and hydrophobic blocks of AB copolymer a) star-like micelle b) crew-cut micelle.

The micellization process starts as the concentration of copolymer increases to reach a critical value called the critical micelle concentration (CMC) and it starts to associate to form a micelle in such a way that the hydrophobic part of the copolymer will avoid contact with the

aqueous environment. At the CMC, the solvent can be found inside the micellar core, which exhibits a larger size than the micelles formed at higher concentrations.[19] At those concentrations, the equilibrium will favour micelle formation, due to their low energy state configuration, and the remaining solvent will gradually be released from the hydrophobic core, resulting in a decrease in micellar size. Polymeric micelles are generally more stable than those formed of lipids, with a remarkably lower critical micellar concentration (CMC).[3]

Polymeric micelles have emerged as potential carriers for poorly water soluble drugs because they can solubilize those drugs in their inner core and they offer attractive characteristics such as small size (nm range) and a tendency to escape from the Reticulo Endothelial System (RES).[2] Hydrophobic drugs can be entrapped in the core of block copolymer micelles. An extensive variety of drugs such as doxorubicin,[20] paclitaxel,[21] cisplatin,[22] indomethacin[23] were incorporated into polymer micelles and studied for drug delivery applications. However, the physical stability of polymeric micelle is a critical issue, since rapid release of the incorporated drug may occur in vivo.[24]

1.5. Vesicles

Self-assembly of natural phospholipids in aqueous solutions generates the formation of liposomes. Similarly, copolymers with amphiphilic character have been used to generate vesicles. Vesicles are usually spherical, hollow spheres with a hydrophobic bilayer membrane and hydrophilic internal and external coronas. Polymer vesicles are more stable, robust and highly impermeable compared to lipid vesicles.[25] The hydrophobic part of the amphiphilic copolymer is protected within the bilayer with the hydrophilic part exposed to the inner and outer aqueous environments.[25] Scheme 4 schematically represents the polymeric vesicles formed by self-assembly of (a) di and (b) triblock copolymers.
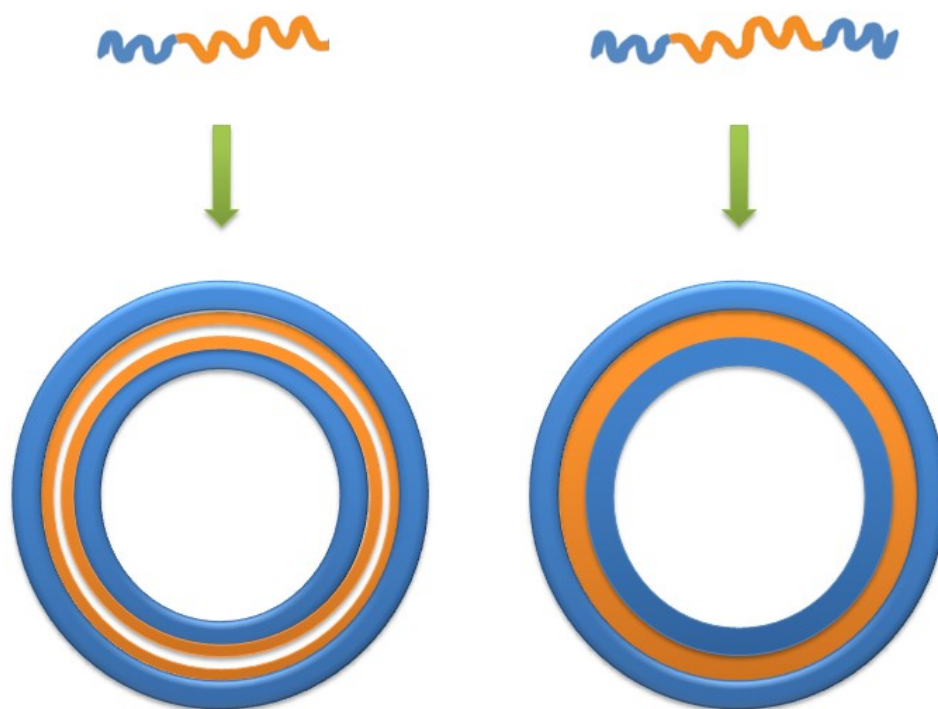
Scheme 4. Schematic representation of polymeric vesicles formed via self-assembly of (a) di block and (b) tri block copolymers.

The formation of vesicles occurs either through bilayer formation,[25] or by a sequence of intermediates[26] during the self-assembly process. In the classical way, first copolymers form a bilayer and, secondly, close-up to form a vesicle. Contact alone between the hydrophilic/hydrophobic interfaces is often sufficient to force a copolymer system to form bilayers. In another mechanism, first spherical micelles are formed, then worm-like micelles. These then form flattened disk-like micelles, which close-up and form vesicles. Bilayer formation followed by closing into vesicles, whether occurring spontaneously or during a series of intermediates, necessarily involves encapsulating the surrounding environment within the core of the vesicle. Recently, another mechanism has been postulated on the basis of dynamic simulations,[27] whereby small spherical micelles are initially formed because the segregation of the two blocks lags behind copolymer aggregation. These grow to large, energetically unfavourable spherical micelles. They therefore re-structure to yield vesicles.[28]

The size of vesicles ranges from nanometers to several micrometers, depending on the hydrophilic/hydrophobic block lengths of the copolymer, solvent ratios, concentration of the

polymer and method of preparation.[6,10,29,30] In addition, the size of a vesicle can also depend on membrane thickness, with bigger vesicles having thicker membranes and smaller ones having thinner membranes. However, no influence of membrane thickness on vesicle size has been found for the majority of polymeric vesicles.[31] The thickness, fluidity and permeability of the vesicular membranes can be controlled by tuning the copolymer compositions.[30] The stability of vesicles is an another important aspect to consider for technological and medical applications. To ensure that vesicle morphology is maintained and to prolong the circulation time in the body, the vesicle membrane is required to be as stable as possible.[32]

Polymeric vesicles have been widely reported in the literature and used as potential encapsulation devices for water-soluble molecules due to the large internal volume of the aqueous cavity. The chemical versatility of amphiphilic copolymers accounts for the generation of vesicles in a wide range of medium, from organic solvents to aqueous solution. The inner core of the vesicle can readily accommodate various guest molecules, ranging from small drug molecules to large protein molecules, by means of encapsulation. In addition, the hydrophobic bilayer membrane can also be used to trap hydrophobic entities such as dyes in order to facilitate the tracking and imaging of these vesicles in their roles as delivery and diagnostic tools.[33-35] Various targeting ligands can be attached to the surface of the vesicles, thereby increasing drug bioavailability, reducing undesirable side effects and minimizing nonspecific uptake. This then allows for specific targeting to certain cells within the cancer sites[36] or even intracellularly to specific organelles. In this way, a therapeutic effect can be delivered to the appropriate biological compartment in a so-called active targeting strategy based on surface functionalization with ligands, for the targeting of receptors expressed at cell surfaces with highly specific interaction.

1.6. Nanoreactors

Polymeric vesicles encapsulated with enzymes that are able to act *in situ* are termed as nanoreactors. Such a system confers the advantages of protecting the enzymes from proteolytic attack and allows the enzymes to act *in situ*. In a nanoreactor, an enzyme reaction is restricted in the confined cavity, which is contrary to a conventional release system where the enzymes need to be released to catalyze the reaction. Thus, the necessity of release from the polymer cage, as with the conventional drug release carrier, is eliminated. Therefore, nanoreactors do not need an

optimization process to control the release profile and avoid release into inappropriate sub-cellular compartments.

The copolymer membrane of a vesicle has a greater membrane thickness as compared to the lipid membrane, and thus reduces permeability while decreasing fluidity as compared to liposomes.[12] In the case of nanoreactors, access by substrates is necessary so as to support an enzymatic reaction *in situ* for the enzymes that are encapsulated. Various approaches are available to support substrate and enzyme combinations inside a nanoreactor: i) co-encapsulation of substrate together with enzymes ii) designing a nanoreactor that includes a substrate-permeable membrane, and iii) facilitating the substrate permeation by inserting channel proteins in the polymer membrane.[3] (Scheme 5)
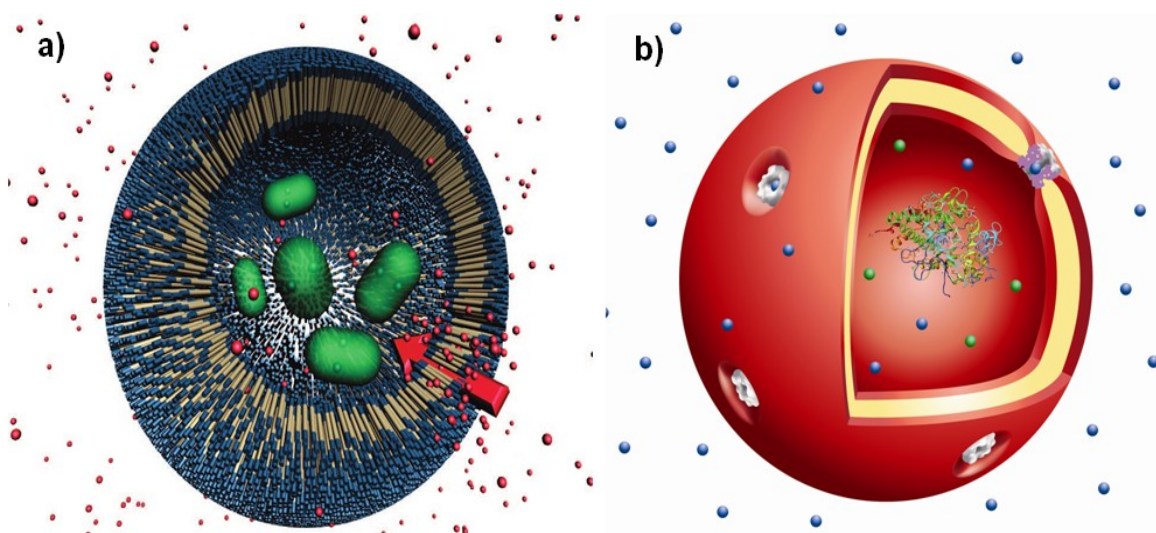
Scheme 5. Schematic representation of a nanoreactor formed by the self-assembly of amphiphilic block copolymers a) nanoreactor containing enzymes b) nanoreactors with channel protein containing enzymes.

The function of a nanoreactor depends on the activity of the encapsulated enzyme and this should be preserved during the encapsulation procedure. The preparation techniques may impose mechanical or chemical stress on the enzymes, with potential loss of activity. Studies on the catalytic properties of nanoreactors have proven that the enzymes not only maintain their activity inside,[37] but they lower K_m, due to favourable interactions with the polymeric membrane. It has been reported that the enzymatic activity is influenced by vesicle size. The smaller the vesicle

size, the greater the activity of the enzyme, indicating the advantageous interactions of the enzymes with the polymer membrane.[38]

These nanoreactors act as nanometer-sized reaction compartments, where one or several different enzyme types are encapsulated and shielded from proteolytic attack.[39] Various copolymers were investigated to develop nanoreactors, namely, poly(ethylene glycol)-block-oligo(desamino-tyrosyltyrosine octyl ester suberate)-blockpoly(ethylene glycol),[40] (poly(ethylene oxide)-block-poly(dimethylsiloxane)-block-poly(2-methyloxazoline))[41] and (poly(2-methyloxazoline)-poly(dimethylsiloxane)-poly(2- methyloxazoline)).[40-42] Nanoreactors served to perform specific reactions in the confined space for various enzymes such as acid phosphatase,[37] horseradish peroxidase, nucleoside hydrolase, thymidine phosphorylase. The enzymes are encapsulated in the aqueous cavity of nanoreactors, mainly intended for enzyme replacement therapy. More complex nanoreactors were formed by encapsulating two different enzymes to perform cascade reaction either inside the nanoreactors or within the membrane of the vesicles.[46]

1.7. Membrane permeability of nanoreactors

The permeability of the polymeric membrane to substrate molecules is an important parameter for the nanoreactors to perform catalytic reactions inside the aqueous cavity. Transport across the membrane can be achieved by incorporating channel proteins in the impermeable polymeric membranes or by using a substrate-permeable membrane.(Scheme 5) It has been shown that channel proteins can be successfully reconstituted in amphiphilic copolymer membranes that are closely identical to natural lipid bilayers. The copolymer membrane thickness (~20 nm) is considerably greater than lipid bilayers (3 − 5 nm) and the hydrophobic part of channel forming proteins may therefore be too small to fit into the thickness of the polymer membranes. However, the high flexibility and the conformational freedom of the polymer molecules, if they are appropriately designed in terms of hydrophobic domain, hydrophilic/hydrophobic ratio, allow for an adaption to the specific geometric requirements of membrane proteins without considerable loss of free energy.[47]

In the case of vesicles made of $PMOXA_n$-$PDMS_m$-$PMOXA_n$, which have an impermeable polymer membrane, different membrane proteins such as outer membrane protein (OmpF),[47] integral outer-membrane protein (Tsx),[44] transport protein (FhuA),[43] aquaporin water channel

protein (AqpZ),[48] and ion channel protein (LamB)[49] were reconstituted to support diffusion through the membrane. The nanoreactors with channel proteins that make the membrane permeable to the substrate have potential application in therapeutics. Nanoreactors represent a new strategy to cope with the necessity of increasing the concentration of the enzyme at biological sites without side effects or denaturation. The protein acts inside the nanoreactor and no release is required in order to obtain the biological effect.

1.8. Oxidative stress

Oxidative stress is caused by an imbalance between the production of free radicals, such as reactive oxygen species (ROS) and reactive nitrogen species (RNS), and the biological system's ability to detoxify them efficiently.[50] All forms of life maintain a reducing environment within their cells. This reducing environment is preserved by enzymes that maintain the reduced state through a constant input of metabolic energy. Disturbances in this normal redox state can cause toxic effects through the production of reactive oxygen species such as superoxide radicals, hydrogen peroxide, and hydroxyl radicals that damage all components of the cell, including proteins, lipids, and DNA.[51,52] The cells are exposed to a large variety of ROS from both exogenous and endogenous sources (Scheme 6). Exogenous agents including ionizing and non ionizing radiation, ozone, xenobiotics, drugs, food, pollutants and toxins can indirectly produce ROS in cells. Although the exposure of the organism to ROS from exogenous sources is extremely high, the exposure to endogenous sources is much more important, because it is a continuous process during the life span of every cell in the organism. Mainly, the mitochondria serve as a major source of ROS production in cells.

In addition, cytochrome P-450 detoxification reactions, phogocytic oxidative bursts, and peroxisomal leakage can generate significant amounts of ROS.[53] The continuous efflux of ROS from endogenous and exogenous sources results in continuous and accumulative oxidative damage to cellular components and alters many cellular functions. In humans, increasing evidence suggests that the cumulative damage caused by ROS contributes to numerous diseases, such as atherosclerosis, Parkinson's disease, heart failure, myocardial infarction, Alzheimer's disease, diabetes, rheumatoid arthritis, cancer and AIDS.[54-57]
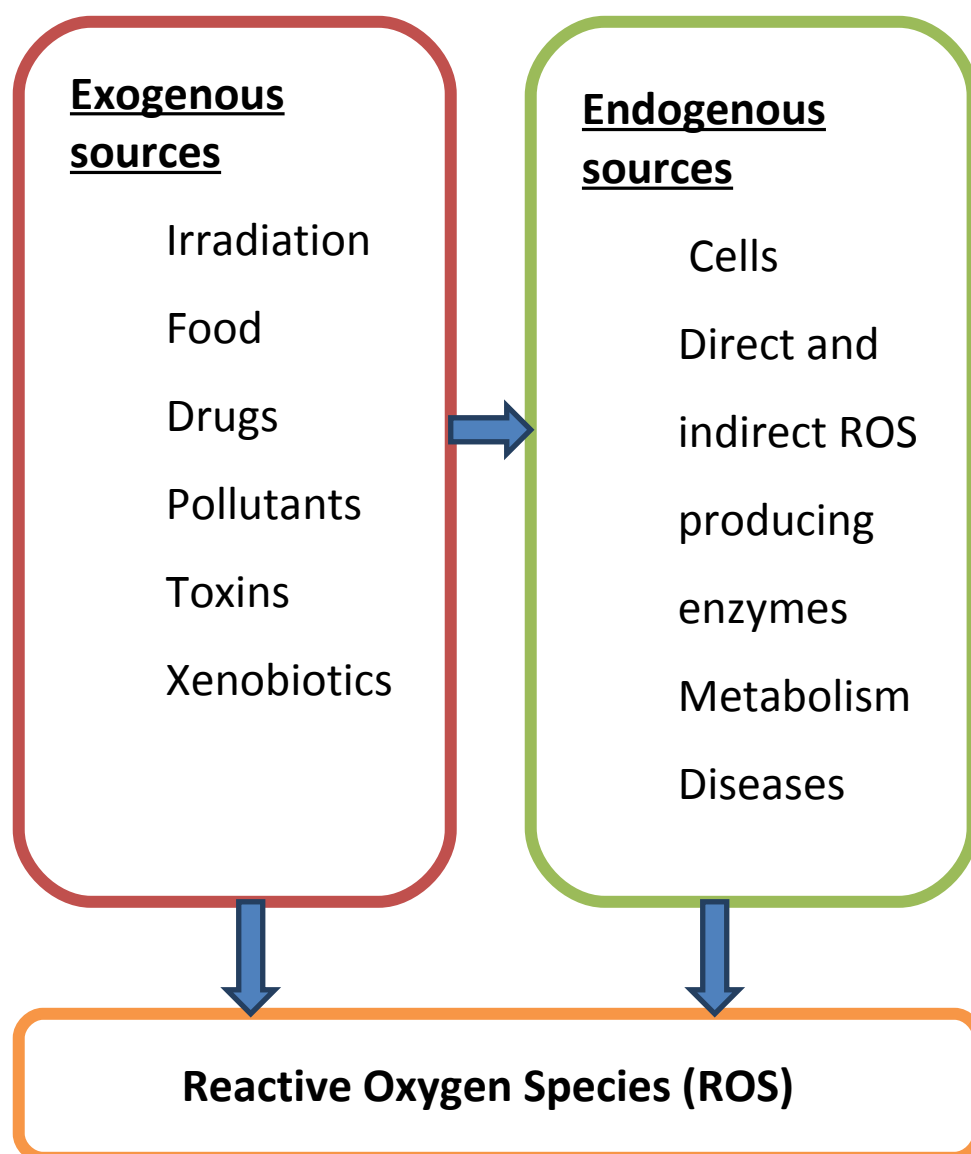
Scheme 6. Different sources of reactive oxygen species (ROS) from both exogenous and endogenous.

1.9. Natural antioxidant mechanism

Various antioxidants exist in cells to regulate the concentration of free radicals to help the body. Cells are protected from oxidative stress by an interacting network of both enzymatic and non-enzymatic entities. The main antioxidant defence mechanisms involve families of antioxidant enzymes such as superoxide dismutase (SOD), catalase (CAT) and peroxidases.[58-60] Various non-enzymatic small molecules, vitamins A, C, and E, and glutathione also contribute to cellular antioxidant defence. Other antioxidants include lipoic acid, mixed carotenoids, coenzyme

Q10, several bioflavonoid, and protein cofactors (folic acid, vitamins B1, B2, B6, B12). They act in synergy and against different types of free radicals.[61-64]

The superoxide dismutase (SOD) family contains metal ion cofactors that, depending on the isozyme, can be copper, zinc, manganese or iron. SOD enzymes are present in almost all aerobic cells and in extracellular fluids. In humans, the Cu/Zn SOD is present in the cytosol, while Mn-SOD is present in the mitochondrion. Cu/Zn-SOD is a dimeric-protein with two identical subunits; each contains one copper and one zinc ion respectively. The copper is the active metal center involved in the catalysis process of the enzyme. The basic catalytic mechanism of Cu/Zn SOD takes place in two steps, first superoxide reduces the copper center of SOD to form dioxygen and a second superoxide oxidizes the copper center to produce hydrogen peroxide (Equation 1).[58]

$$O_2^{\bullet-} + Cu(II)Zn\text{-}SOD \rightarrow O_2 + Cu(I)Zn\text{-}SOD$$

$$O_2^{\bullet-} + Cu(I)Zn\text{-}SOD + 2H^+ \rightarrow H_2O_2 + Cu(II)Zn\text{-}SOD \qquad \text{Equation 1}$$
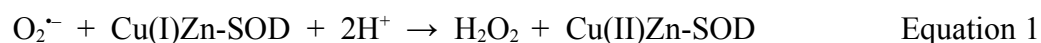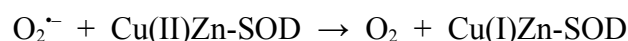
The end product of the reaction is H_2O_2, which is usually detoxified by catalase or various members of peroxidase family including glutathione peroxidase. Catalase converts the hydrogen peroxide into water and oxygen, via either an iron or a manganese cofactor. This enzyme is localized in peroxisomes in most eukaryotic cells. The enzyme consists of four protein subunits, each containing ferric ions in the haem group. The ferric ions are oxidized by the first H_2O_2 to produce Fe^{+4}. A second molecule of H_2O_2 reacts with Fe^{+4} to reform ferric ions and produce water and oxygen. (Equation 2).[59]

$$H_2O_2 + [Fe(III)]\text{-catalase} \rightarrow H_2O + Fe(IV)\text{-catalase}$$

$$H_2O_2 + Fe(IV)]\text{-catalase} \rightarrow H_2O + Fe(III)\text{-catalase} + O_2 \qquad \text{Equation 2}$$
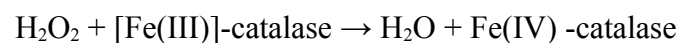
Peroxidases have a high affinity for H_2O_2 and can detoxify H_2O_2 even in low concentrations. For example, glutathione peroxidase found in the cytoplasm, mitochondria, and nucleus metabolizes hydrogen peroxide to water by using reduced glutathione as a hydrogen donor by the oxidation of glutathione (GSH) to its oxidized form, glutathione disulphide (GSSG) (Equation 3).[61]

Glutathione peroxidase

$$2\ GSH + H_2O_2 \longrightarrow GSSG + 2H_2O \qquad \text{Equation 3}$$

The synergic action of the various antioxidant enzymes keeps concentration of ROS in cells relatively low and able to be detoxified normally by the organismal ROS defence.

1.10. Antioxidant therapy

When the ROS concentration overwhelms the normal level of protection, the antioxidant system is not able to regulate the total amount of ROS. In such a condition, the antioxidant system of the organism should be reinforced by the administration of external antioxidants to prevent deleterious consequences of oxidative stress. It is important to deliver antioxidant agents at the biological site where a high concentration of ROS is present for efficient antioxidant therapy.

1.10.1. Administration of antioxidant enzymes

The clinical importance of enzymes in preventing ROS-related disease conditions was shown in various transgenic animal models that over expressed SOD from human origin. Clinically, SOD showed a beneficial and protective effect on animal models with different pathological conditions such as inflammatory conditions, Parkinson's disease, cancer, ischemia-reperfusion injuries in various organs like the heart, liver and kidney, and in pulmonary diseases. [65-69] The direct administration of native antioxidant enzymes does not show any effect on some pathological conditions, namely Parkinson's disease and stroke, due to the higher molecular weight that prevents the permeation through the blood-brain barrier. SOD and catalase/peroxidase have tremendous catalytic activity that protects cells from oxidative damage. However, as a result of a number of factors including the short half-life in plasma of around six minutes for both SOD and CAT, cell impermeability that prevents the uptake of these enzymes and effectiveness inside cells, non-human origin causing immunogenicity problem, high molecular weight and high cost of these enzymes, usage in clinical medicine is limited.[70,71] However, the role of SOD in preventing these clinical situations is demonstrated in transgenic animal models.[72]

There are various drawbacks to the direct administration of SOD in fighting oxidative stress. It is know that SOD can be denatured and damaged in the presence of hydrogen peroxide, formed during the dismutation of superoxide or spontaneously.[73] In order to solve the problem, the

Poznansky group cross-linked SOD with catalase, which can scavenge H_2O_2. In experimental animal models, the conjugation of catalase to SOD has shown efficient recovery from oxidative stress.[74] However, the heterogeneity and higher molecular weight are limiting factors for bifunctional enzyme efficiency. Another example is the peroxidase incorporation with SOD by chemical mutation, generating a bi-functional enzyme that reacts to combat both superoxide and H_2O_2. However, the peroxidase activity and the stability of the bifunctional enzyme is minimal as compared to the native enzymes.[75] In most cases, the protective effect of native enzymes requires high concentration and continuous dosage forms to obtain optimal therapeutic effects.[76-78] This requires other approaches than with the bi-functional enzyme obtained by conjugation of SOD with catalase or peroxidase.

Therefore, the administration of catalase or peroxidase together with SOD is necessary to convert the toxic, stable and cell membrane permeable H_2O_2 into non-toxic oxygen and water molecules. The balanced activity of these enzymes is important to have complete protection of the cells against oxidative damage.

1.10.2. Administration of enzyme mimics

To overcome intrinsic limitations of antioxidant enzyme administration, considerable attention is being paid to designing low molecular weight and low cost synthetic metal complexes such as SOD and/or catalase and peroxidase mimics. In designing such complexes, various synthetic approaches have been applied. A number of transition metal complexes, such as complexes of manganese, copper, iron and combination of different metal centers, have been investigated for enzyme-like activity.[79-82]

Although many metal complexes have been studied as enzyme mimics, the majority display poor thermodynamic stability and enzyme-like activity at different physiological pHs. The release of metal ions due to the degradation or instability of complexes causes toxic effects.[83] Therefore, high stability constants are required to avoid dissociation of the metal complex in a biological system. Thus, bio-distribution and clearance of the metal complex as well as its pharmacological specificity have to be taken into account when designing an enzyme mimic.

In addition, most of the reported enzyme mimics have significantly lower enzyme-like activity as compared to the native enzymes. Another key issue with enzyme mimics is the

solubility of metal complexes. Hidalgo and co-workers mentioned that 40% of metal complexes are not soluble in aqueous solution and that stops further development from reaching viable pharmaceutics.[84]

1.10.3. Strategies to improve antioxidant therapy

The direct administration of enzymes/mimics can lead to easy elimination from the blood[85] and rapid degradation in the gastrointestinal tract.[86] Different strategies have been followed to improve the bioavailability of antioxidants by changing the means of delivery of enzymes or enzyme mimics. Various attempts have been made to deliver the enzymes/mimics by protecting them through covalent conjugation with poly(ethylene glycol) (PEG) or phosphatidylcholine[87,88] and by encapsulation into liposomes.[89,90] However, these alterations did not improve the bioavailability of SOD, due to an excessive covalent modification with PEG that led to a decreased level of SOD activity.[91] Additionally, encapsulation of SOD into liposomes has serious drawbacks, due to intrinsic characteristics of liposomes, such as mechanical instability, interaction with high-density lipoproteins, and a short circulation lifetime.[92]

In order to solve this challenge it is necessary both to protect mimic molecules to preserve their antioxidant capacity and to reduce toxicity that results from degradation in biological compartments. In this respect, liposomes have been intensively investigated as carriers of enzyme or enzyme mimics (enzyme-m).[93-96] For example, Mn-porphyrin (chloro(-(5,10,15,20-tetrakis[1-hexadecylpyridinium-4-yl]-21H,23H-porphyrins) used to modify the surface of 1-palmitoyl-2-oleoyl-sn-glycero-3-phosphocholine liposomes preserved approximately 25% of native Cu/Zn SOD enzyme activity.[94] Liposomes were modified with Mn-HPyP as a ligand to obtain enzyme-like activity for both SOD and CAT. In this way, liposomes displayed dual enzyme-like function and were termed LIPOzymes (liposome + enzyme). However, the efficiency of detoxification $O2^{\bullet-}$ and H_2O_2 influenced by the membrane characteristics.[95,96]

Alternatively, SODm have been conjugated with polymers to increase their circulation half-life and bioavailability. The polymerizable SODm prepared from copolymerized Mn(III) Tetrakis[1-(3-acryloxy-propyl)-4-pyridyl]porphyrin (MnTPPyP-Acryl) cross linked with poly ethylene glycol diacrylate (PEGDA) reduced ROS damage in implantation with retention of high levels of SOD mimicking activity. Only at very high SODm concentration compared to the native SOD enzyme was an increase in activity reported.[97] Similarly polymer supported Mn-

SODm were synthesized by cross linking the polymers (4-vinylimidazole, methacrylic acid) with Mn^{2+} ion to create the coordination sphere like in native Mn-SOD enzyme[100] , but this approach dramatically reduced activity to as little as 0.1 % of the initial SOD-like activity. Moreover, synthesizing enzyme mimics that will have high catalytic activity and high stability together with low toxicity is still a challenging issue to be solved.

1.11. Motivation and Concept

The main focus of this thesis is to develop an efficient antioxidant system to fight oxidative stress. In this respect we designed and developed an antioxidant system based on several steps as follows,

    i.   Structure-Activity relationship (SAR) analysis to design a highly active enzyme mimic

   ii.   Synthesis and Charaterization of a highly active enzyme mimic

  iii.   Encapsulation of the enzyme mimic in polymeric vesicle to generate antioxidant nanoreators

  iv.   Studying the cellular interaction of nanoreators containing enzyme mimics

(i) A global structure-activity relationship (SAR) analysis applied to all classes of compound already proposed for a specific biological activity is a essential step towards optimization of a drug development strategy. Therefore we analyze most of the reported SODm statistically to determine whether spectroscopic parameters, which characterize the metal coordination, are consistently related to the activity of copper (II) complex to establish a structural model for a high SOD like activity.

(ii) Based on SAR analysis, we have synthesis a copper (II) complex (Cu^{II}ENZm) derived from triazine ligands with a high enzyme like activities that could be dependent on the conformation of the metal binding region. The structure will be investigated both in the solid state and in solution. The detailed characterization of the structural and electronic properties of these Cu^{II}ENZm clearly is a necessary step to identify the specific structural parameters that induce a high SOD/Catalase-like activity. This will serve to focus the synthetic efforts only on relevant aspects, rather than on factors which do not have a direct influence on activity.

(iii) Recently, the concept of antioxidant nanoreactors was introduced based on the encapsulation of SOD in polymer vesicles through the self-assembly of amphiphilic copolymers (poly (2-methyloxazoline)-poly (dimethylsiloxane)-poly-(2-methyloxazoline) (PMOXA-PDMS-

PMOXA) to improve the bioavailability.[99] The low solubility of the enzyme and its aggregating behavior not allowed to increase the concentration of SOD inside the vesicles therefore prevented the further improvement of the efficiency of the nanoreactors. Here we extend the concept of antioxidant nanoreactor by encapsulation of a Cu[II]ENZm, due to its high SOD/Catalase like activities. By using poly-(2-methyloxazoline)-poly(dimethylsiloxane)-poly(2-methyloxazoline), (PMOXA-PDMS-PMOXA)[99] we ensure the system membrane is oxygen permeable and thus fulfills a double role: to shield the antioxidant agent and to enable agent and substrate to react inside the polymeric "cage". In this way it is possible to improve the bioavailability of an antioxidant agent and to avoid the disadvantages of conventional drug release carriers, such as uncontrolled release of the antioxidant agent. The chosen block copolymers have good biocompatibility,[100] show low non-specific protein binding due to the hydrophilic PMOXA block, and form vesicles with stable membranes that are impermeable to saccharide ions and water.[48]

(iv) To use, these nanoreactors in antioxidant therapy, studying the interaction with cells is essential step. In this way, nanoreactor containing Cu[II]ENZm are tested for cellular uptake, cytotoxicity and *in vitro* antioxidant activity in monocyte (THP-1) cells to assess conditions for possible biomedical applications against oxidative stress. This type of nanoreactors is proposed to function as versatile antioxidants, able to escape the immune system, for medical applications.

2. Structure-Activity Relationship (SAR) analysis to design an efficient enzyme mimics

In this chapter, we present an essential step towards optimization of drug development strategy: a global structure-activity analysis of compounds already proposed for a specific biological activity. The statistical analysis can be applied to relate the structural parameters with biological activity for a family of drugs known as SODm that act as effective scavengers of the superoxide.

For several years, efforts have been made to design compounds with high Cu/Zn-SOD-like activity. Numerous copper complexes have been proposed as Cu-SOD-mimics (SODm) either as binuclear or mononuclear metal complexes based on different classes of ligands such as imidazole derivatives,[101] amine derivatives,[101g,h,n,102] pyridine derivatives,[101c,g,m,v,w,102a-c,e,g,103] sulfonamide,[101a,104] peptide derivatives,[101q,r,105] imine derivatives,[102f,106] salicylate derivatives,[101j,107] cyclodextrin derivatives,[108] curcumin derivatives,[109] triazine derivatives,[110] quinoline derivatives,[102h,105e,111] and other classes.[112] Although intensive efforts have been made to obtain better Cu-SODm, only a few studies that have tried to connect the SOD-like activity with structural parameters to model the interactions and conformations which promote a high SOD-like activity. It has been established recently that there is a linear relationship between the *log k_{cat}* for O_2^- and the metal-centered electrode potential,[103c,113] or that the modified distortion factor g_{ZZ}/P_{ZZ} obtained from EPR data can be correlated with the activity trend.[110a,b] But these findings are restricted to few classes of ligands, and a quantified relationship between geometrical environment of the metal and the biological activity is still missing.

2.1. Statistical SAR Analysis

By taking in account most of the Cu-SODm previously synthesized, we statistically analyze how the spectroscopic parameters which characterize the metal coordination can be related to their biological behavior, in order to propose a structural model for a very active SOD-mimic. Due to its property of allowing fluxional stereochemistry and variable coordination numbers between 4 and 6, the Cu(II) ion is well known to accommodate a large variety of geometrical arrangements in its first coordination sphere; these influence the interactions with the

ligand atoms and consequently its physical-chemical properties and behavior.[114] The sensitivity of the Spin Hamiltonian parameters to geometric changes in the coordination sphere of copper ion will give the possibility to connect their values with small changes in biological activity for a fine structure-activity screening, that cannot be obtained for other metals, such as Mn or Ni, specific for other families of superoxide dismutase, and used in SOD-m.[113,115]

The premise that we set out to test is based on the concept that the ligand dictates the catalytic activity by promoting or preventing a particular conformational structure. Consequently, we expect that the movement of one of the first coordination sphere nuclei out of the plane defined for the axial site will change the ability of the corresponding complex to function as a catalyst. We constructed a database with the classes of copper SOD-m previously reported by taking into account various parameters obtained by EPR and electronic spectroscopy, and activity values, as determined with the indirect method, first reported by McCord and Fridovich.[116] Even though the indirect assays possess inherent problems due to a possible participation of the compound being tested in a redox short circuit,[108a] they represent the conventional way to test a SOD-like activity. We did not included in our database the complexes those activity was tested by other assays, such as pulse radiolysis, or stopped-flow kinetics[117a,b] in order to have only one type of activity assay with its specific limits and errors, for all complexes. As activity parameter we took into account the concentration of copper complex required to attain 50% inhibition of the NBT reduction, the IC_{50} value, as it is indicative for its ability to catalyze superoxide radicals. Besides, every IC50 value can be compared to that of native SOD, or to other SOD-m. We included in this database complexes from various classes of ligands: imidazoles, amines (di and tri amines), imines, sulfonamides, peptides, salicylates, quinolines, pyridines and mixed ligands (combinations of any of the above mentioned ligands), others (such as: curcumin, valporate, cyclodextrins, and triazines) and also their derivatives.

Catalytic activity in Cu/Zn-SOD is expected to be favoured if the geometry of the first coordination sphere around the metal ion is imposed by the ligand in such a way that it facilitates superoxide binding to a vacant coordination site of the metal.[113] The copper has a sterically blocked axial site facing a hydrophobic region of Cu/Zn-SOD, whilst the active site, which is occupied by water in the native protein, faces a narrow hydrophilic channel. The degree of distortion at the copper site will therefore be influenced by the positions of the histidines in the protein and will have a direct effect on the size of the channel leading to the active site.[118] Such

structures, accurately determined by X-ray diffraction of single crystals, do not provide any information on changes in the symmetry, which might occur in solution, the native physical state of superoxide dismutase. In this respect the spectroscopic characterization of copper environment in solutions by EPR and UV-Vis complete with details for specific conformations closer related with the biological relevant structures. Therefore we took into account in our screening the hyperfine coupling constants and the distortion factors from EPR and the d-d-bands for the electronic spectra, as parameters characterizing the first coordination sphere around the metal.

Even if a wide range of copper complexes are reported as SOD-m, the large distribution of IC_{50} values ranging from 0.1μM to more than 200μM, made us to sort the compounds in two clusters: active complexes ($IC_{50} \leq 0.8$μM), and non-active ones (IC_{50} between 0.8μM and 200μM). Compared with the native SOD activity, reported to have an IC_{50} of 0.04μM, we choose the cluster of active SOD-m to not show a dramatic decrease in activity as is the case of the compounds classified as non-active. The cluster of non-active compounds is by far bigger than that of active compounds due to the basic requisites of functional SOD-m including an appropriate geometry of the metal coordination sphere, biocompatible metal redox couples and adequate stabilities for low-toxicity, which represent a difficult task to attain.

2.2. Analysis of individual spectroscopic parameters

First we analyzed the variation of IC_{50} values corresponds to the SOD like activity as function of single spectroscopic parameters, including the wavelength of d-d transitions in UV-Vis spectra- λ, the z component of the hyperfine interaction, Azz, and the ratio g_{zz}/A_{zz} (so called distortion factor F), obtained from the EPR spectra. A large distribution of activity values characterizes the whole group of reported complexes, without any specificity which could involve a characteristic trend, both in the case of λ (Figure 1 – a,b), and for each of the EPR parameters (Figure 2 – a,b,c,d). We could not correlate any of the individual structural parameters (d-d transitions, hyperfine interaction, or distortion factor) of Cu-SODm with their SOD-like activity. This indicates that individual spectroscopic parameter may not be the involved in contributing the higher SOD-like activity.
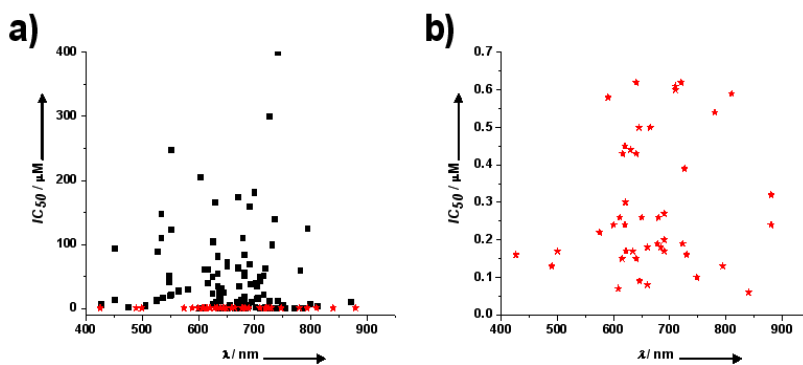
Figure 1. a) SOD-like activity as function of maximum of the d-d transitions in electronic spectra (□) for all classes of Cu-SODm. b) closer look containing only the active compounds.
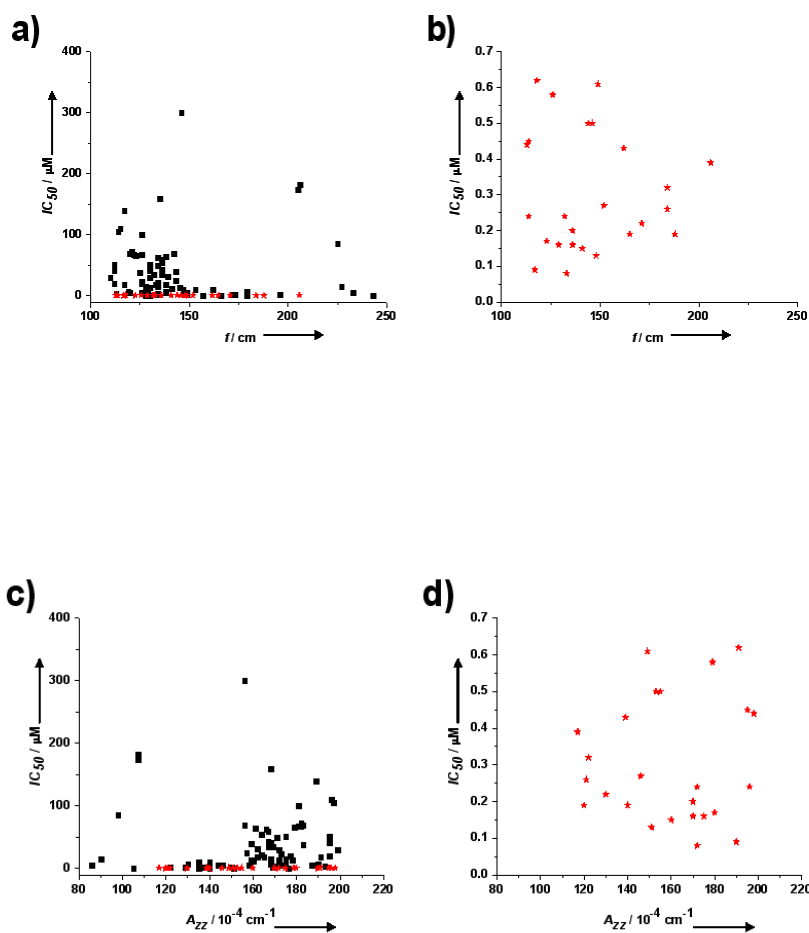

Figure 2. a) SOD-like activity as function of the distortion factor f for all classes of Cu-SODm. b) closer look containing only the active compounds. c) SOD-like activity as function of the

parallel hyperfine coupling constants (Azz) for all classes of Cu-SODm. d) Closer look containing only the active compounds. Black square: non-active compounds; red stars - active compounds.

2.3. Analysis of combination of spectroscopic parameters

We expand the analysis by taking into account the combinations of structural parameters: λ & Azz, λ & F (Figure 3 – a, b), and Azz & F, respectively (Figure 3c) in order to see if there are specific domains that could be connected with the active/non-active clusters of SOD-m. However no correlation was found that promote higher SOD like activity. The 3D graph combining the electronic transitions and each of the EPR parameters as function of SOD like activity do not show a specific trend which could allow to distinguish between the active and non-active compounds. But the 3D graph combining the EPR parameters with the IC_{50} values (Figure 4 – a,b) indicates for the active complexes an almost linear relationship, which cannot be put into evidence for the cluster containing the non-active ones. The similar trend was previously reported for the SOD-m copper complexes with triazine (asymmetric and symmetric) ligands.[110] However this linear relationship is general, and do not relate on specific ligand classes.
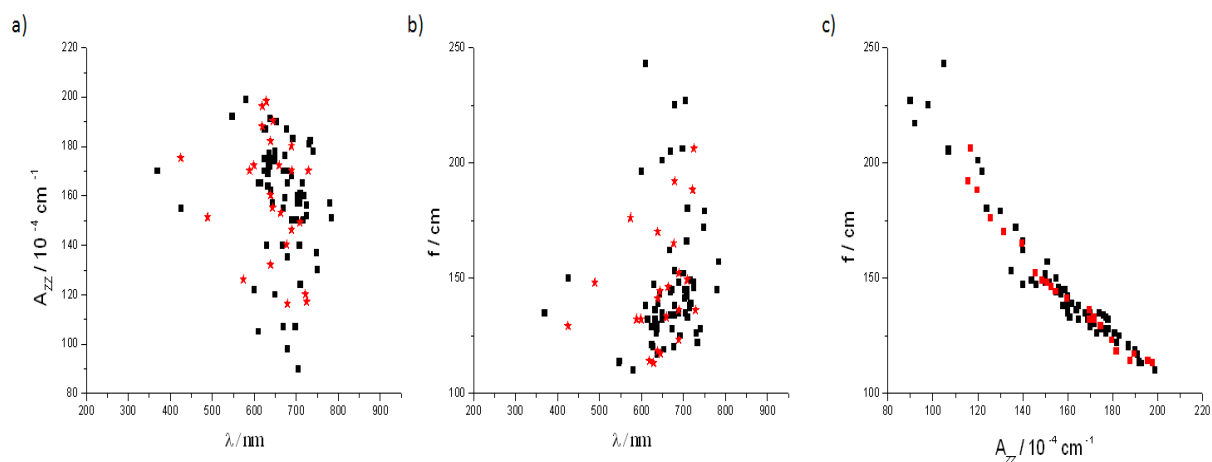

Figure 3. a) d-d transition (λ) as a function of parallel hyperfine coupling constant (Azz) for all classes of Cu-SODm b) d-d transition (λ) as a function of distortion factor f for all classes of Cu-SODm. c) parallel hyperfine coupling constants (Azz) as function of the the distortion factor f for all classes of Cu-SODm.
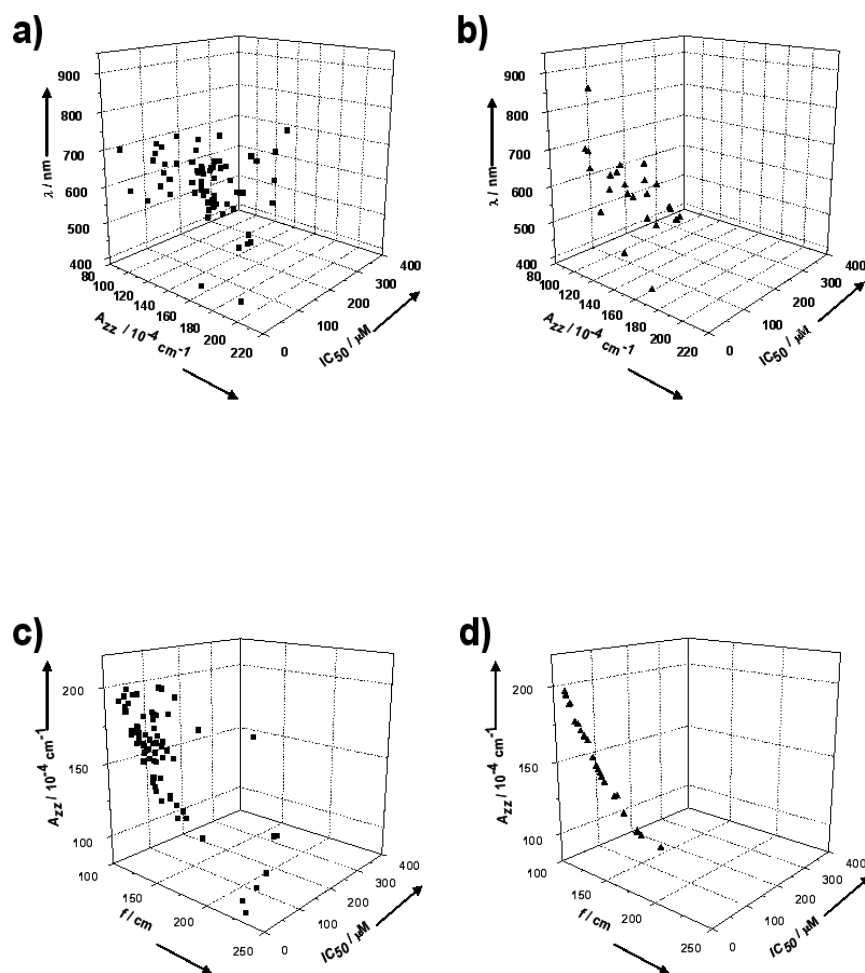
Figure 4. SOD-like activity as function of maximum of the d-d transitions in electronic spectra (λ) and of the parallel hyperfine coupling constants (A_{zz}) for non-active compounds a), and for active compounds b). SOD-like activity as function of the parallel hyperfine coupling constants (A_{zz}) and f for non-active compounds c), and for active compounds b).

2.4. Role of coordination numbers

By taking into account all SOD-mimics, which were published and characterized from the point of view of their electronic and EPR parameters, our focus is on the relation between the geometry of the first coordination sphere around the metal and its biological activity. As the coordination number of copper should make a difference in complexes' behavior, because a four-coordination sphere provides a different geometry for superoxide radical to access the metal compared with the fifth-coordination one, therefore, we also refined the analysis of the cluster of

active compounds to include a function of coordination number and we classified the active compounds as function of 4- or 5- coordination numbers (Figure 5). Both groups of compounds show an almost linear relationship and we fit each of them by a linear regression (Table 1).
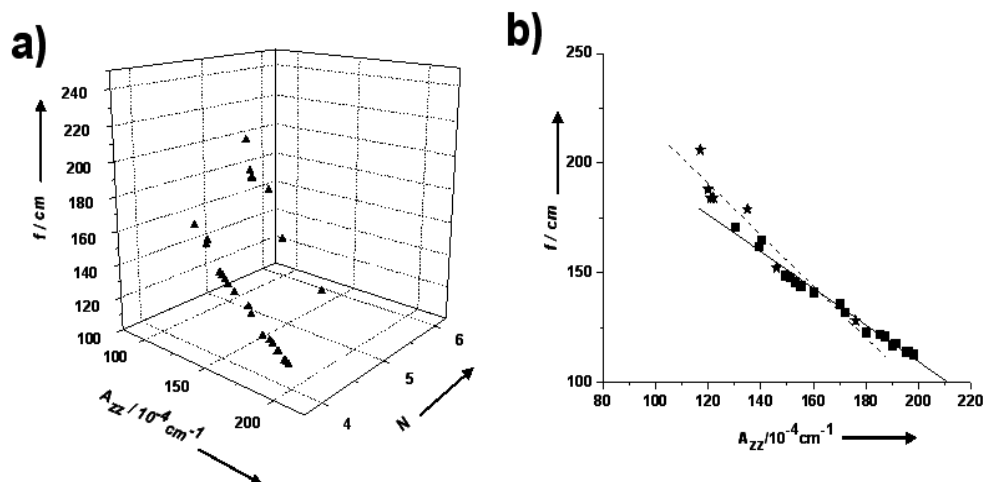

Figure 5. 3D representation of A_{zz}, f and coordination number of copper, N for active Cu – SODm a). Hyperfine coupling constants A_{zz} as function of the distortion factor f for active SOD-m b). Black stars: 5-coordinated copper complexes, black squares: 4-coordinated copper complexes.

Metal sphere	A	b	r*	σ_D*
4-coordination	277.2 ± 2.5	-0.84 ± 0.03	0.992	2.46
5-coordination	331.7 ± 20.3	-1.18 ± 0.15	0.961	7.83

* r – correlation factor, and σ_D – standard deviation.

Table 1. Parameters of the linear regression fit of F factor as function of the hyperfine coupling constant, A_{zz} (F = a + b x A_{zz}).

The overall EPR data suggest that the cluster of complexes with a 4-coordination sphere around metal contains by far the biggest number of compounds (around 50% (all active) 77% **(**according to the figure 5a**)** of the whole number of active compounds), and the square planar geometry with slight distortion induces, in general, higher catalytic activity than other geometries.

A smaller number of complexes with 5-coordination number ware active (around 44% (all active) 23% (according to the figure 5a) of the whole number of active compounds), and no 6-coordination number complex was active, indicating that there is a geometric specificity for an active SOD-m compound.

2.5. Role of ligand specificity

As we looked into the activity relationship with specific ligand classes, although we could not find exact correlation, it seems that imidazoles, sulfonamide and peptide based Cu-SODm are almost active. The imine, amine and pyridine derivatives having higher number of non active complexes. We could not conclude on ligand class - activity relationship, because all ligand classes having both active and non active complexes. The reason could be due to the important role played the structural parameters than the ligand specification.

Majority of the active Cu-SODm were mononuclear irrespective of the coordination number, contrary to many literature reports which claim that binuclear structure is important to have a better SOD mimicking activity. After a detailed look into various comparative data between active mono and binuclear Cu-SODm, we consider that it is not necessarily to have a binuclear compound, in order to get a high active SOD-m. The assumption that the binuclear compounds are more active that the mononuclear ones is related to the analogy of the metal binding region of the enzyme which contains a copper and a zinc atom, but this do not represent a structural requirement for a highly active compound. Besides, biological assays indicated that the role of Zn in native SOD is more related to the stability of the metal binding region, than to the catalytic activity. However, in the future synthetic efforts should be able to focus on potential compounds identified by theoretical methods as possessing physical properties that correlate with a high probability of possessing biological activity.

3. Synthesis and characterization of bi-functional enzyme mimics

Metal complexation of 6-(2-hydroxy-benzaldehyde) hydrazono-as-triazine-3,5-dione (**L)** was performed in a modified approach of an earlier procedure.[119] **L** (1mM) was dissolved under stirring in 20 ml NaOH (0.05mM) at 40°C and the pH was adjusted to 7.5 with NaOH (1M). A solution of $CuCl_2 \cdot 2H_2O$ (1mM) in 5ml of milli-Q water was added slowly drop wise for 20-30 minutes at 40°C. The mixture was cooled to 4°C and stirred continuously for 1 hour under atmospheric pressure, forming a green precipitate. The precipitate was filtered, washed successively with hot water, ethanol and acetone and was dried. The powder was re-crystallised in DMSO by slow evaporation method and formed small crystals after more than 2 months at room temperature.

3.1. Solid-state structure of the $Cu^{II}SODm$

3.1.1. IR spectroscopy

The characteristic peaks in the IR spectra of the powder of the free ligand **L** and its copper complex were compared to distinguish the probable coordination points of the ligand (Figure 6 and Table 2). Coordination of oxygen to the copper atom in the $Cu^{II}ENZm$ follows from the shift towards higher wavenumbers of the phenolic v(O-H) peaks in the IR spectrum of the copper complex (~3300-3355 cm^{-1}) when compared with the free ligand (~3250-3280 cm^{-1}), together with the appearance of a new peak at 1210 cm^{-1}, assigned to v(C-O). The shift towards lower wavenumbers of the IR peak atributed to v(CH=N) from 1648 cm^{-1} (free ligand) to 1631 cm^{-1} ($Cu^{II}ENZm$) and the shift towards higher wavenumbers of the peak of v(C=N) from 1565 cm^{-1} (free ligand) to 1584 cm^{-1} ($Cu^{II}ENZm$) support the metal binding of an imine nitrogen and a triazine nitrogen, respectively.[120] In addition, the new peaks at 490 cm^{-1} and 415 cm^{-1} are assigned to Cu-O and Cu-N, respectively.[121]
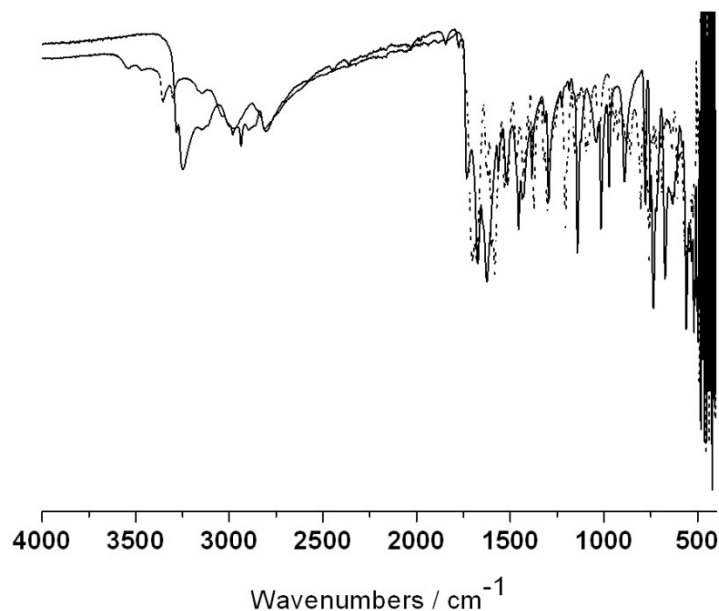
Figure 6. IR spectra of free ligand (solid lines) and Cu^{II}ENZm (dashes) in powder form.

Compound	IR (cm^{-1})				
	v(OH)	v(CH=N)	v(C=N)	v(NH)	v(C=O)
L	~3250-3280	~1648	~1565	~3150	~1680
Copper complex	~3300-3355	~1630	~1584	~3150	~1682

Table 2. IR-spectroscopic data for the free ligand **L** and the related Cu^{II}ENZm (powders)

3.1.2. X-ray crystallograpy

The molecular structure of the complex is presented in Figure 6. In the crystal, the compound forms a binuclear copper(II) complex being located on the inversion center 0.5, 0.5, 0.5, of the space group P-1. Each copper ion is five coordinated through two bridging chloride ions, two nitrogen atoms and one oxygen atom from the as-triazine ligand, which form a coordination sphere around the metal with a distorted square pyramidal geometry (Figure 7). The equatorial positions are defined by one triazine nitrogen atom, one imine nitrogen atom, one oxygen atom from the hydroxy group and one bridging chloride anion. The elongated axial

position is occupied by the second chloride anion, which is basal to the second copper of the dimer.
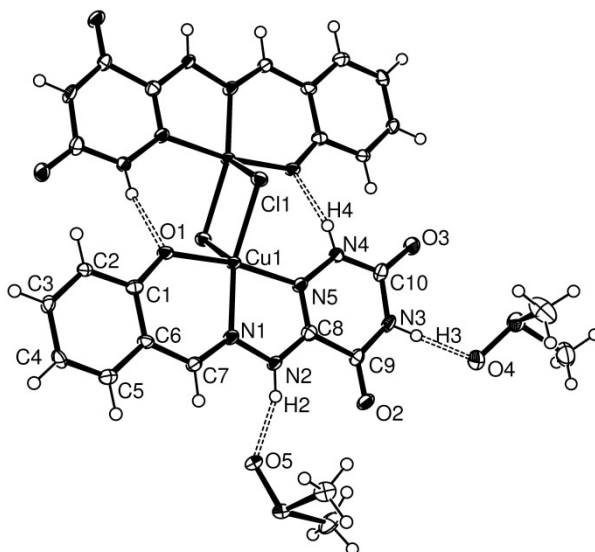

Figure 7. ORTEP diagram of the crystal structure of the Cu^{II}ENZm under study.

The crystallographic details are summarised in Table 3 and selected interatomic distances and angles of the copper complex are presented in Table 4.

Empirical formula	$C_{28}H_{40}Cl_2Cu_2N_{10}O_{10}S_4$
M	1000.2
Temperature/K	123
Wavelength/Å	0.71073
Crystal system	triclinic
Space group	P $\bar{1}$
a/ Å	8.2044(5)
b/ Å	10.5939(6)
c/ Å	12.6014(7)
α/°	111.339(2)
β/°	97.147(2)
γ/°	99.073(2)
Volume/ Å^3	987.54(10)
Z	1
d_{calc}/Mg m^{-3}	1.686
F (000)	514
Measured reflections	6575
Measured reflections	3974
Measured reflections	2607
R_{int}	0.033
wR(all data)	0.0623

Goodness-of-fit	1.1069
$\delta\rho_{max/min}$/ e Å^{-3}	0.77, - 0.47

Table 3. Crystal data and structure refinement details of Cu^{II}ENZm.

Bond lengths/ Å		Bond angles/ °	
Cu$_1$-N$_1$	1.964(3)	N$_1$-Cu$_1$-N$_5$	79.57(12)
Cu$_1$-N$_5$	2.000(3)	Cl$_1^i$-Cu$_1$-N$_5$	89.48(9)
Cu$_1$-O$_1$	1.900(2)	Cl$_1^i$-Cu$_1$-N$_1$	113.64(9)
Cu$_1$-Cl$_1$	2.308(1)	Cl$_1$-Cu$_1$- N$_5$	95.03(9)
Cu$_1$-Cl$_1^i$	2.645(1)	O$_1$-Cu$_1$-N$_1$	91.90(11)
Cu$_1$-Cu$_1^i$	3.468(1)	O$_1$-Cu$_1$-N$_5$	170.66(12)
		Cl$_1^i$-Cu$_1$-O$_1$	90.49(8)
		Cl$_1^i$-Cu$_1$-Cl$_1$	91.40(3)
		Cl$_1$-Cu$_1$-O$_1$	94.31(8)
		Cl$_1$-Cu$_1$-N$_1$	154.16(9)
		Cl$_1^i$ -Cl$_1$-Cu$_2$	88.60(3)

Table 4. Selected bond distances (Å) and the angles (°) for the Cu^{II}ENZm under study.

The bond distances between copper and the first order donor atoms of the ligand (Cu$_1$-N$_1$= 1.964(3) Å, Cu$_1$-N$_5$= 2.000(3) Å, Cu$_1$-O$_1$= 1.900(2) Å and Cu$_1$-Cl$_1$= 2.308(1) Å) are typical for the square base of pyramidal Cu^{2+} complexes.[99f] The molecular structure is in addition stabilized by intramolecular hydrogen bonds (N$_4$-H$_4$...O$_1^i$; i = 1-x, 1-y, 1-z and N$_4$-O$_1$ = 2.952(6) Å). A global view of the crystal structure of Cu^{II}ENZm is shown in Figure 8, and indicates the interactions present in solid state of this compound. There are two hydrogen bonds linking solvent molecules with each ligand molecule (N$_2$-H$_2$...O$_5$, N$_2$-O$_5$ = 2.660(6) Å,

N_3-H_3…O_4, N_3-O_4 = 2.714 Å). The distance between neighbouring complexes of 3.417 Å accounts for π-π interaction, which stabilizes a chain system along the crystallographic a axis. (figure 9)
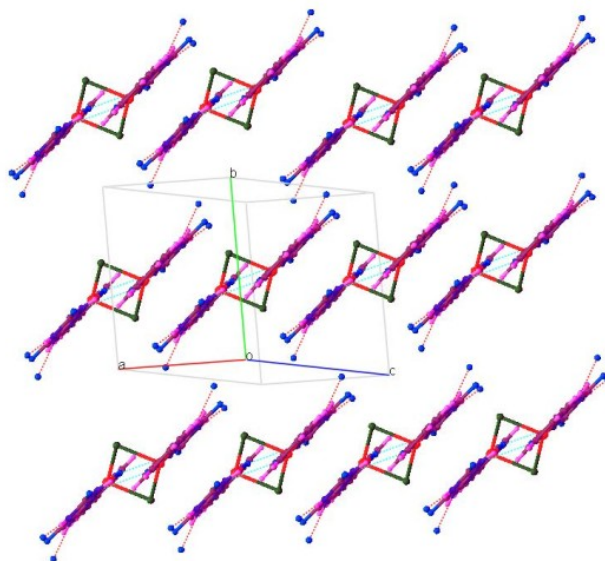

Figure. 8 Packing scheme of the crystal of the $Cu^{II}ENZm$ under study. View slightly off the crystallographic a-axis. Hydrogen atoms have been removed for clarity.
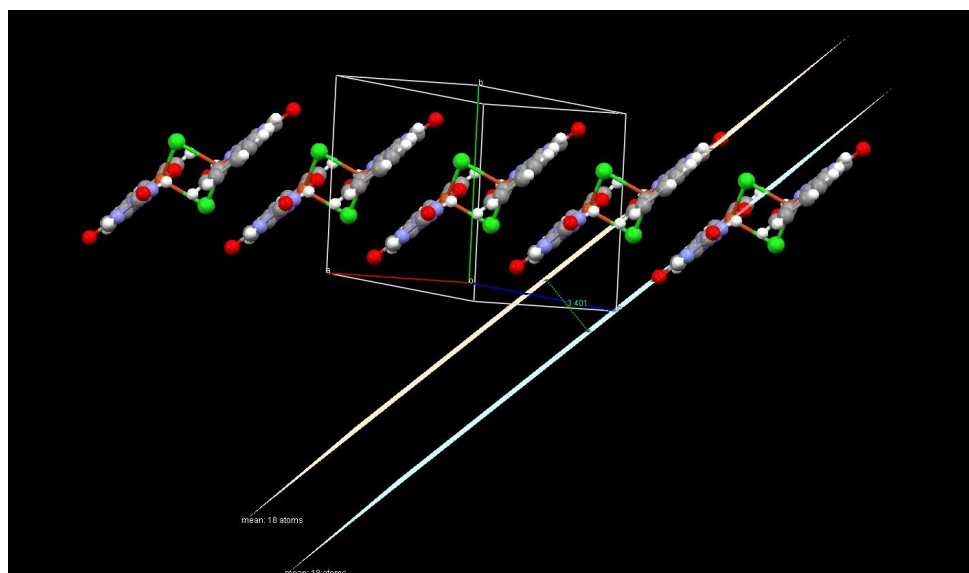

Figure. 9 The distance between neighbouring copper complexes along crystallographic a axis.

3.2. Structural changes upon dissolution of the Cu^{II}ENZm

3.2.1. UV-Visible spectroscopy

As the biological relevant conditions for Cu,Zn-SOD (and thus also Cu^{II}ENZm) are in solution, we determined whether and how the solid-state structure of the metal-binding region changes upon dissolution in dimethyl sulphoxide (DMSO). The electronic absorption spectra of free ligand and the copper complex at ambient temperature are presented in Figure 10 and Table 5. The electronic absorption band at 353 nm (ε = 11706 cm^{-1}M^{-1}) with a shoulder at 380 nm corresponds to π-π* intra ligand transitions. LMCT band of the copper complex is present at 428 nm with a shoulder at 482 nm.[122] The weak and broad absorption band at 678 nm (ε = 136 cm^{-1}M^{-1}) represents the d-d transition and suggest a predominantly 4-coordinated metal sphere with a distorted square planar geometry. However, additional weak axial ligations cannot be ruled out on the basis of these data.
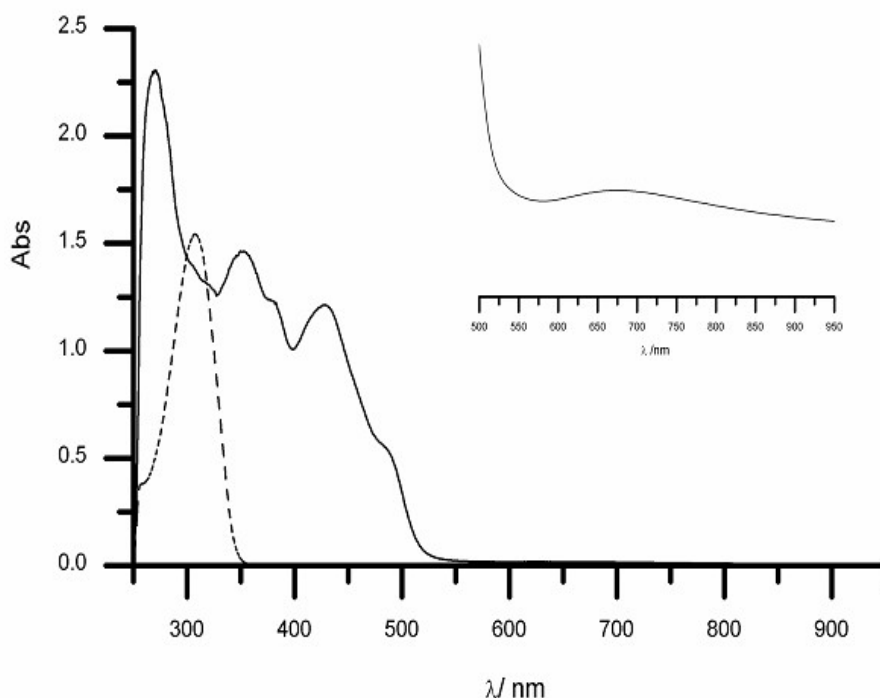

Figure 10. UV/Vis absorption spectrum of a DMSO solution of the Cu^{II}ENZm under study.

Compound	ILT	LMCT	λ_{max} (nm) d-d
L	303	-	-
Copper complex	353, 380(sh),	428, 482(sh)	678

Table 5. UV/Vis absorption spectra for the free ligand **L** and the related $Cu^{II}ENZm$ (in solution)

3.2.2. EPR spectroscopy

In order to gain more insight into the structure of the $Cu^{II}ENZm$ in solution, different EPR experiments were undertaken. If the dicopper structure as found by the XRD analysis is retained in solution, strong exchange coupling is expected to occur between the two Cu^{II} ions. Figure 11 shows the X-band CW-EPR spectrum of a frozen DMSO:toluene (1:1) solution of $Cu^{II}ENZm$ with its simulation.
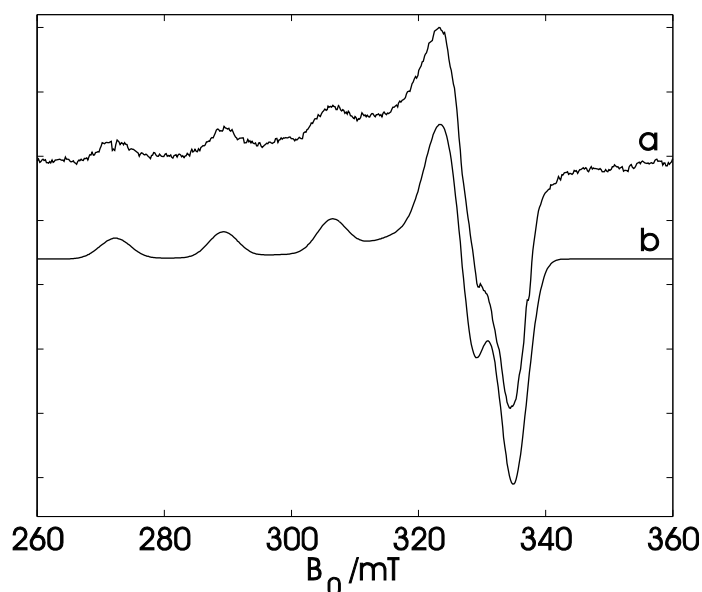

Figure 11. (a) Experimental X-band CW EPR spectrum of a frozen DMSO:toluene (1:1) solution of $Cu^{II}ENZm$ taken at a 100 K. (b) Simulation of (a) using the parameters in Table 6.

It was found that DMSO formed a bad glass leading to local clustering of the copper

complexes as is exemplified by figure 12. The broad signal underneath the type-2 Cu^{II} EPR spectrum is due to clustered copper complexes. The relative contribution of this broad signal increased upon increase of the concentration of the Cu^{II}ENZm. Addition of toluene largely solved this problem. Note that the complex was not soluble in pure toluene.
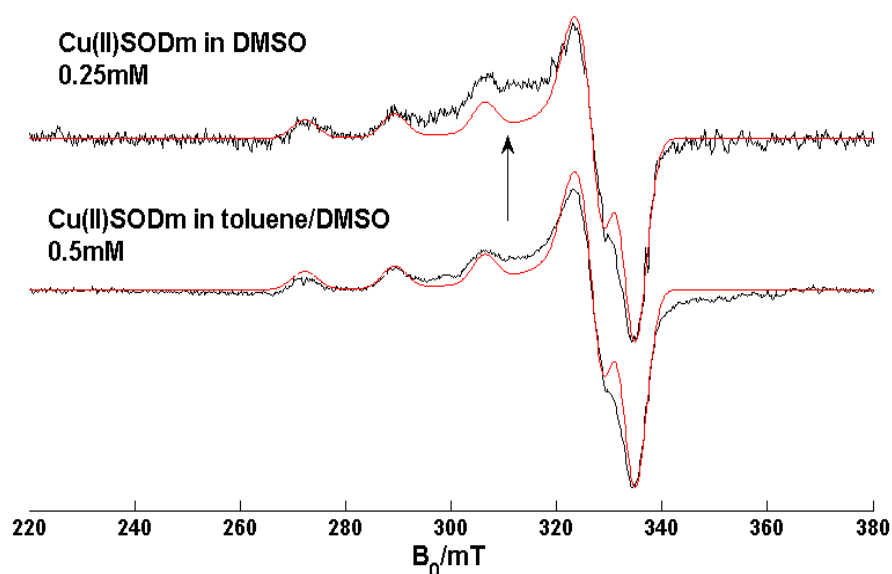
Figure 12. X-band CW-EPR spectra of the Cu^{II}ENZm in frozen DMSO and in frozen DMSO:toluene.

The principal *g* and copper hyperfine values (Table 6) are typical of a type-2 mono Cu^{II} complex, *i.e.* a square planar ligation of the Cu^{II} ion with possible additional weak axial ligations.[123] This confirms the UV/Vis data and implies rupture of the original structure. Similar breaking of the chloride bridges with subsequent rearrangement of the geometry of the Cu(II) center in solution compared to the single crystal structure has already been observed for other SODm and linked to their SOD-like activity.[124] The structure of the Cu^{II}ENZm under study thus differs from the tetrahedral surrounding of the copper ion found in bovine Cu,Zn-SOD (characterized by the smaller A_z value). The principal *g* and copper hyperfine values of the Cu^{II}ENZm resemble more those of lyophilized bovine Cu,Zn-SOD, whereby the imidazolate bridges between the copper and zinc ions are broken.[125]

Compound	g_x, g_y	g_z	A_x, A_y (MHz)	A_z (MHz)
Cu^{II}ENZm	2.057 (±0.004)	2.266 (±0.001)	5 (±20)	-525 (±2)
$[Cu(L1)_2(NH3)_2].2$ MeOH[a]	2.05	2.27	-	-516
$[CuA]^{2+b}$	-	2.310	-	-510
Cu–carc[c]	-	2.247	-	-560
Bovine Cu,ZnSOD	2.08	2.262	-	-401
Lyophilized bovine SOD	2.06	2.26	-	-450

[a]$[Cu(L_1)_2(NH3)_2].2$MeOH, (HL$_1$= N-2-(4-methylphenylsulfamoyl)-6-nitro-benzothiazole),, [b] $[CuA]^{2+}$, A = Ac-HisValHis-NH$_2$,[c] Cu-Carcinine.

Table 6. Principal g and copper hyperfine values of Cu^{II}ENZm in comparison with SOD, other SOD mimics.

Peisach and Blumberg[123] showed that the g_z and copper A_z values reveal information on the type of ligating atoms. Although this method is very course, the parameters of Cu^{II}ENZm agree with a 1N3O, 2N2O or a 3N1O surrounding. Based upon the XRD single crystal structure, a likely model of Cu^{II}ENZm in solution will be as given in Scheme 7. As the bond length of Cu-Cl$_1$ (2.308(1)Å) in the solid-state structure of Cu^{II}ENZm is significantly larger that the bond lengths of Cu-N and Cu-O (1.964(3) Å, and 1.900(2) Å, respectively), we suppose that the Cl$^-$ anion is easily detached from the Cu^{II} atom in solution, as previously reported for other complexes.[101d] X in Scheme 1 is therefore most probably a DMSO solvent molecule. Note that a weak axial ligation of solvent molecules to the Cu^{II} complex cannot *a priori* be ruled out.
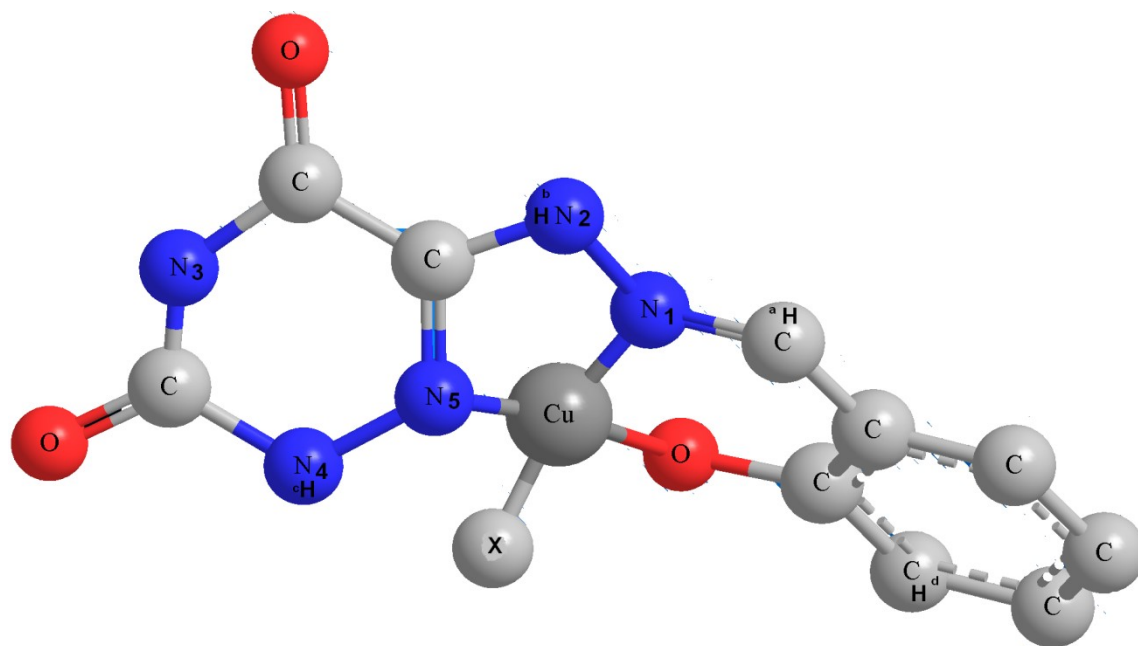
Scheme 7. Schematic representation of Cu^{II}ENZm in solution with X = most probably DMSO. The nuclei that are of importance in the discussion of the EPR data are indicated by numbering (nitrogens) and lettering (protons).

In order to obtain more detailed information on the Cu^{II}ENZm complex in solution, a number of pulsed EPR experiments were set up. Figure 13a shows the Davies-ENDOR spectrum of a frozen DMSO:toluene solution of Cu^{II}ENZm taken at an observer position corresponding with $g \approx g_{x,y} = g_\perp$. Weak mw pulses were used, so that mainly the weak proton couplings are visible in the spectrum. These weak proton interactions can be largely suppressed using strong microwave pulses, so that the stronger interactions can be studied (hyperfine contrast selective ENDOR[126] Figure 13b). Several contributions to the ENDOR spectrum, stemming from different nuclei, are visible in the latter spectrum. A pair of signals split by about 15 MHz and centered around the proton Larmor frequency can be clearly distinguished. Similar signals were observed at other observation positions. Furthermore, corresponding cross peaks are found in the different X-band HYSCORE spectra, confirming that these nuclear frequencies are linked to one type of proton nucleus (Figure 14a). Simulation of this proton ENDOR contribution (Figure 13c) reveals a largely isotropic hyperfine interaction (Table 7). The hyperfine coupling is in the same order of magnitude of what has been found for the imine-type protons of bis-(salicyldoximato) copper(II)[127] and N,N'-ethylene bis-(salicylideniminato)Cu^{II}[128] (Table 7). This indicates that we can ascribe this interaction to the imine proton labeled as H^a in Scheme 7.
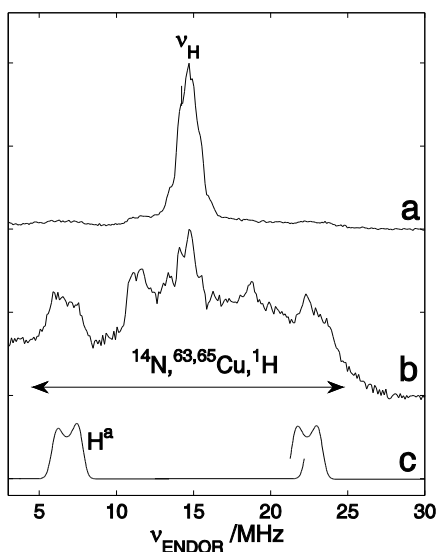
Figure 13. (a,b) Experimental Davies ENDOR spectra of a frozen DMSO:toluene (1:1) solution of Cu^{II}ENZm taken at 4 K ,at an observer position corresponding to $g\approx g_\perp$ (B_0=338 mT) with (a) t$\pi_{/2}$=200 ns, tπ=400 ns and (b) t$\pi_{/2}$=48 ns, tπ=96 ns. (c) Simulation of the H^a proton contribution to (b) using the hyperfine data in Table 7. V_H indicates the proton Larmor frequency.

Compound	A_x (MHz)	A_y (MHz)	A_z (MHz)
Cu^{II}ENZm (H^a)	17.4 (±0.3)	14.2 (±0.3)	14.2 (±0.5)
Cu(sal)$_2$^{a}	16.49	12.89	12.59
CuSalen^c	22.8 23.62	19.38 19.45	18.43 18.64

^{a}bis-(salicylaldoximato)Cu^{II} in bis-(salicylaldoximato)Ni^{II}, ^{b} N,N'-ethylene bis-(salicylideniminato) Cu^{II} in N,N'-ethylene bis-(salicylideniminato) Ni^{II}

Table 7. Experimental proton hyperfine values of H^a compared to those of other imine-like protons in Cu^{II} Schiff base complexes.
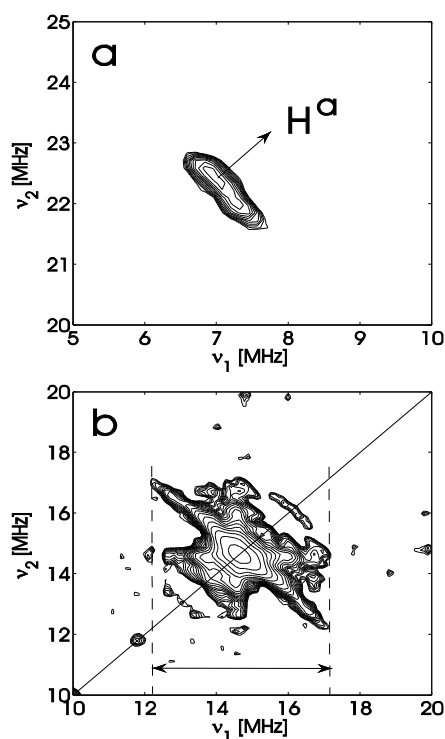
Figure 14. Matched proton HYSCORE spectrum (symmetrized) of a frozen DMSO:toluene (1:1) solution of $Cu^{II}ENZm$ taken at a 4 K at a high-field position (B_0=343.4 mT) . (a) Region agreeing with contribution of H^a. (b) Region around proton Larmor frequency.
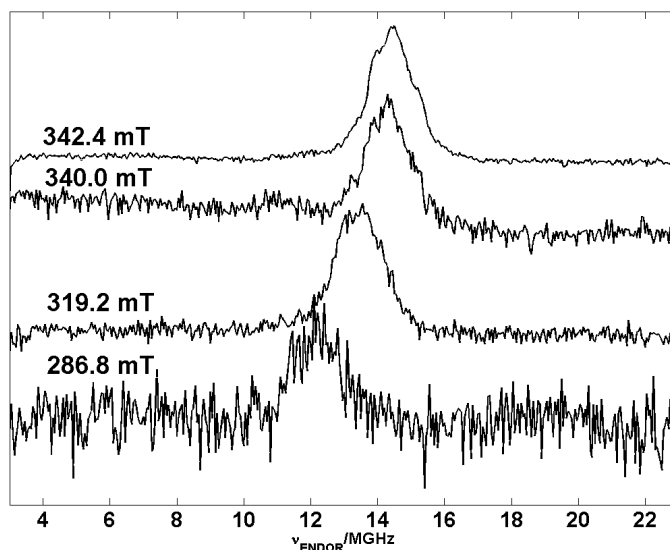
Figure 15. X-band Mims-ENDOR spectra of a frozen DMSO:toluene solution of the $Cu^{II}ENZm$ for different settings of the magnetic field (observer positions are given in the figure). All spectra are the sum of 30 τ values.

The remaining ENDOR signals in Figure 13b are strongly overlapping and stem from

contributions of different protons, the directly coordinated nitrogens N_1 and N_5 and from the ^{63,65}Cu hyperfine interaction (see Scheme 7 for numbering of the nitrogen nuclei). The X-band proton HYSCORE spectra allow an evaluation of the proton contributions. Besides the signal attributed to H^a, only a ridge with maximum width of ca. 4.9 MHz is found at the high-field observer positions near $g=g_\perp$ (Figure 14b). At $g \approx g_\parallel$ the maximum width is even lower (~2.5 MHz). This agrees with the X-band Mims ENDOR data (Figure 15) and with the Davies ENDOR spectra obtained with weak mw pulses (Figure 13a). This observation indicates that the largest part of the spectrum observed in Figure 13b thus stems from interactions with the copper nucleus and the directly coordinated nitrogens. The fact that the ENDOR signal is not exceeding 26 MHz, reveals that the hyperfine coupling of N_1 and N_5 is lower than ~50 MHz. A more detailed determination of the nitrogen hyperfine values is not possible based on the X-band Davies ENDOR measurements.
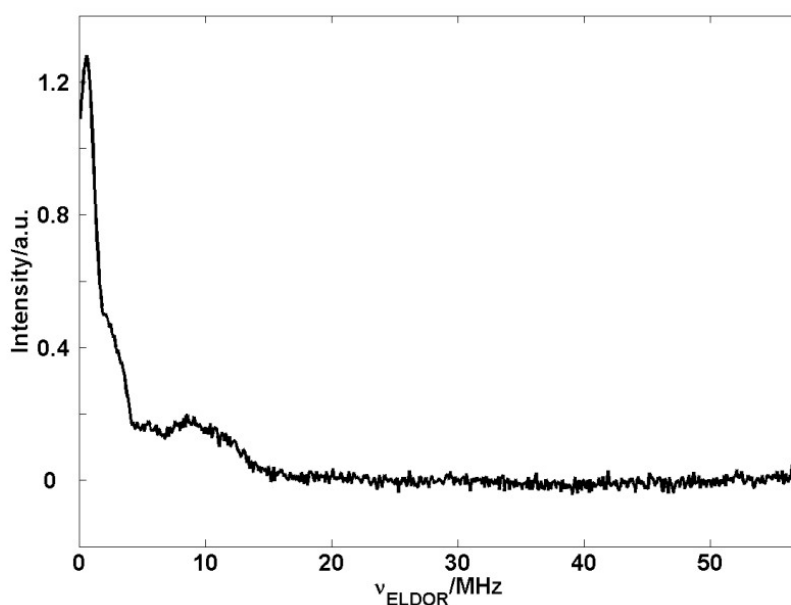
Figure 16. W-band ELDOR-detected NMR spectrum of a frozen DMSO:toluene solution of the Cu^{II}ENZm taken at an observer position corresponding with $g \approx g_\perp$.

Moreover, the Davies ENDOR spectra at the low-field settings were of very poor quality. In order to overcome this problem, W-band ELDOR-detected NMR experiments were undertaken, but proved to be insufficiently resolved to allow an unambiguous determination of the EPR parameters of the directly coupled nitrogens (Figure 16). The signal around 10 MHz is most probably due to the interaction with N_1 and/or N_3 (nuclear frequencies of the $m_S=1/2$

manifold). However, since the corresponding nuclear frequency of the m_S=-1/2 manifold is not observed, no definite attribution of the signal can be made.
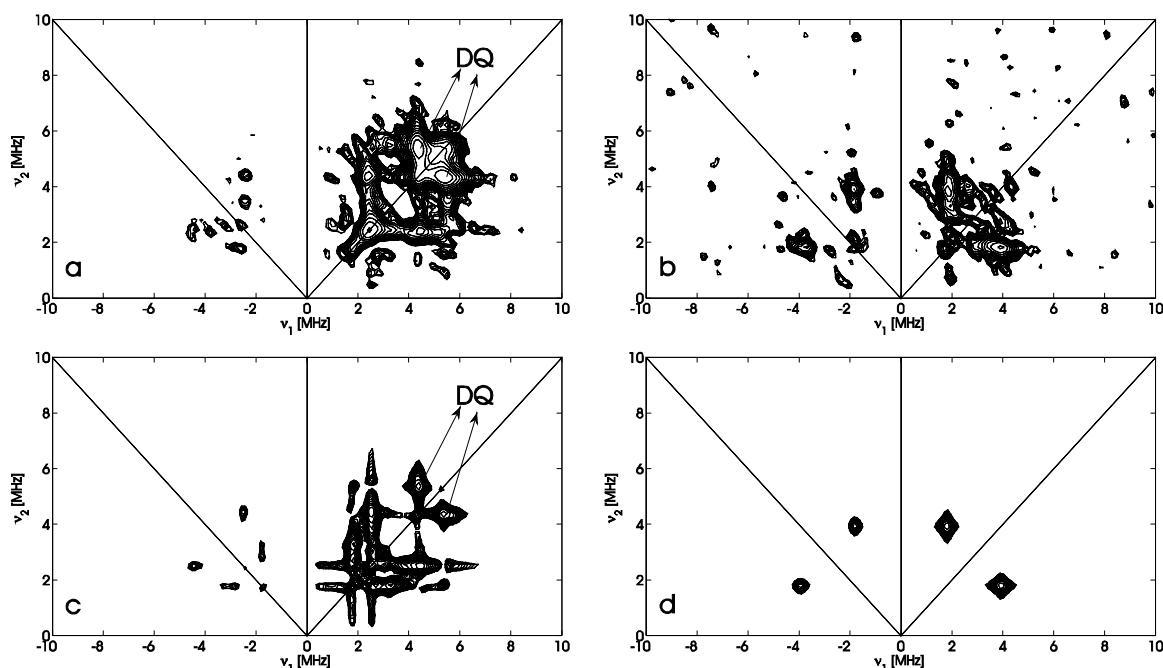
**Figure 17.** Experimental X-band ^{14}N HYSCORE spectra of a frozen DMSO:toluene (1:1) solution of Cu^{II}ENZm taken at a 4 K at observer position (a) B_0=343.4 mT ($g\approx g_\perp$) and (b) B_0=285.2 mT ($g\approx g_\parallel$, m_I=-3/2). (c,d) Simulation of (a,b) using the parameters in Table 8

Figures 17a and 17b show the ^{14}N HYSCORE spectra of Cu^{II}ENZm in the frozen DMSO:toluene solution taken at an observer position corresponding to $g\approx g_{x,y}=g_\perp$ and $g\approx g_z=g_\parallel$, m_I=-3/2, respectively. In the HYSCORE spectra taken at other observer positions are shown in Figure 18. In the HYSCORE spectrum of Figure 16a, a set of cross peaks linking the double-quantum (DQ) nuclear frequencies can be recognized. These DQ peaks are visible for all other magnetic field settings (Figure 17), except for the $g=g_\parallel$, m_I=-3/2 extremum position where only the cross peaks linking the single-quantum frequencies are visible (Figure 17b).

(a)

(b)

(c)

(d)
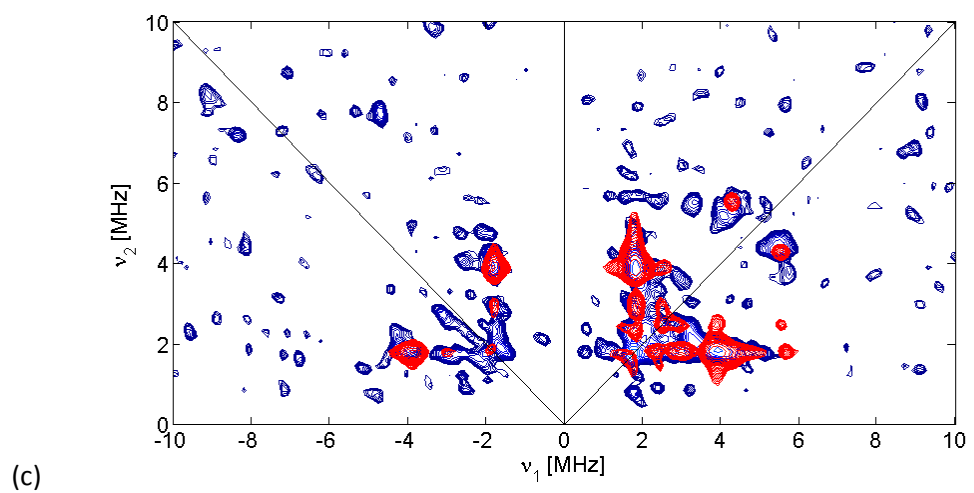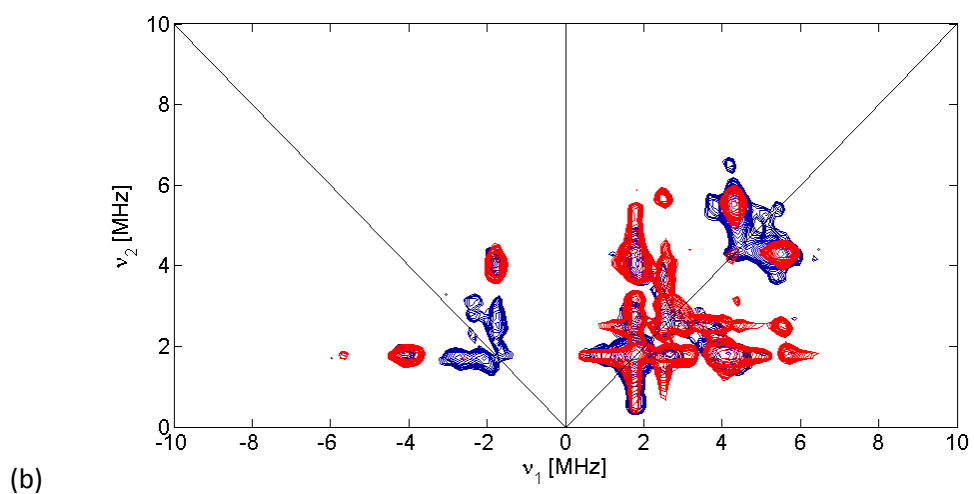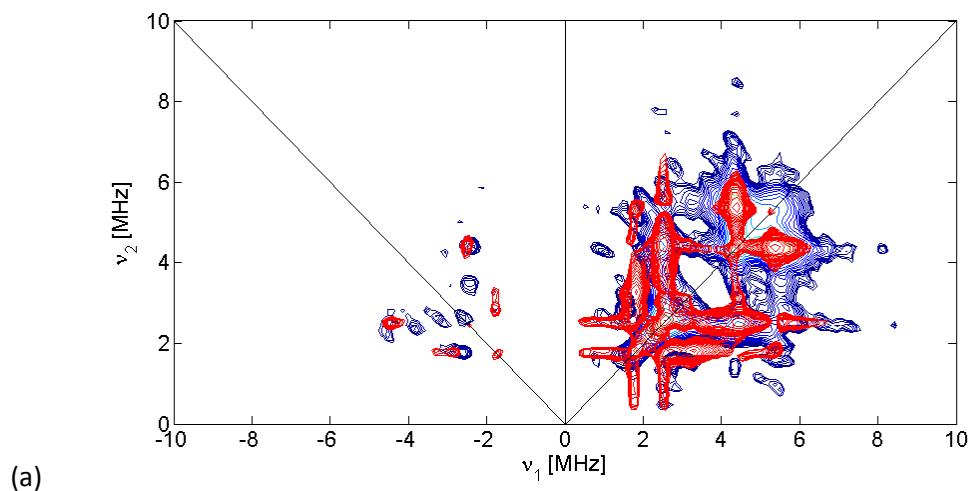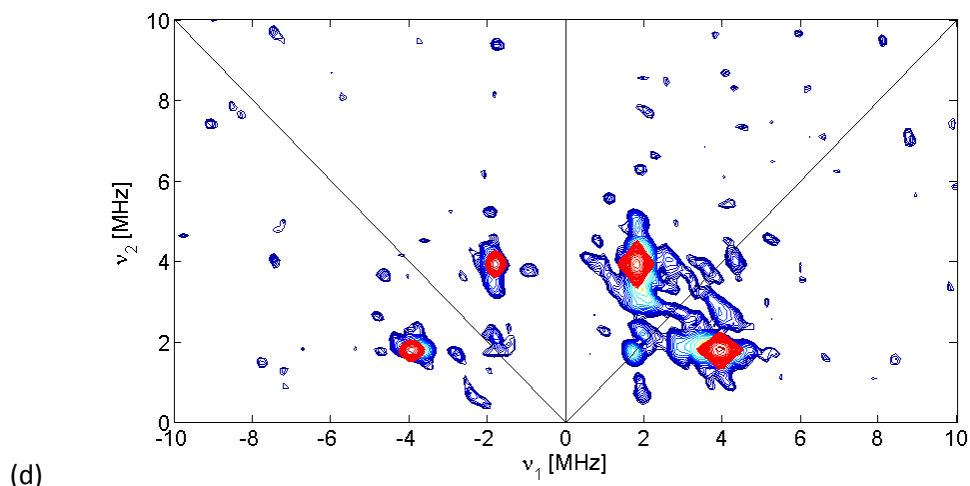
Figure 18. Experimental X-band HYSCORE spectra (blue) taken at observer positions (a) B_0=343.4 mT, (b) B_0=319.6 mT, (c) B_0=303.6 mT and (d) B_0=285.2 mT overlain with the simulation (red) assuming a two-spin (S=1/2, I=1) system and using the parameters given in Table 8 of the main text.

A first indication about the spin-Hamiltonian values of the nitrogen nucleus can be obtained from the formula,

$$v_{DQ}^{\pm} = \sqrt{(\frac{a}{2}+v_I)+K^2(3+\eta^2)} \qquad (1)$$

whereby a is the hyperfine value at the observer position, v_I is the Larmor frequency, $K=e^2qQ/(4I(2I-1)h)$ with Q the nuclear quadrupole moment and eq the electric field gradient. K and the asymmetry parameter η define fully the principal values of the nuclear quadrupole tensor $\boldsymbol{P}$ by

$$P_z = 2K; \eta = \frac{P_x - P_y}{P_z} \qquad (2)$$

Using Eq. (1), starting values can be obtained for the spectral simulation. Figure 17c,d show the simulations of the HYSCORE spectra in Figure 17a,b. The corresponding simulation parameters are given in Table 8. The small nitrogen hyperfine values indicate that we are dealing with 'remote' nitrogen(s), *i.e.* nitrogens that are not directly bound to the copper ion. N_2, N_3 and N_4 are possible candidates (see Scheme 7 for atom numbering).

In order to assign the ^{14}N spin Hamiltonian parameters to the correct nucleus, DFT computations were undertaken. Since it is not *a priori* clear whether the chloride anion is remaining bound to the Cu^{II} ion in solution and whether axial ligation can occur, different models were assumed: [Cu**L**Cl] (model A), [Cu**L**(DMSO)]$^+$ (model B), [Cu**L**(DMSO)$_2$]$^+$ (model C) and [Cu**L**(DMSO)$_3$]$^+$ (model D). At this stage, an optimized structure of a fifth model [Cu**L**(DMSO)Cl] could not be obtained. The optimized geometries of the four structures are given in the as well as the computed principal g values, copper hyperfine values and the hyperfine and nuclear quadrupole data for the nitrogens N_1-N_5 and protons H^a-H^d (Appendix). It should be noted that for model D, the optimized structure showed a strongly elongation of the bond to one of the two DMSO molecules (2.60 Å and 2.35 Å for the bond lengths to the axial DMSO molecules).

For all models, the magnitude of the nuclear quadrupole couplings of the remote nitrogens N_2 and N_4 are found to be similar and significantly larger than the ones of N_3 (Table 8). Comparison of these results with the experimentally observerd nuclear quadrupole data indicates that the cross peaks observed in the ^{14}N HYSCORE spectra (Figures 17a,b) stem from N_2 or N_4. This is corroborated by the magnitude of the observed hyperfine interaction, which is in the order of 1-2 MHz (in absolute value). The observed hyperfine parameters seem to match the theoretical values for N_2 best (Table 8). HYSCORE simulations showed that the observed HYSCORE spectra can stem from contributions of two nitrogen nuclei with hyperfine values with opposite signs as predicted theoretically for N_2 and N_4 (Figure 19). Furthermore, the small hyperfine of N_3 leads to shallow ESEEM modulation that are suppressed by the strong modulations of N_2 and N_4 and do not alter the HYSCORE pattern (Figure 20).
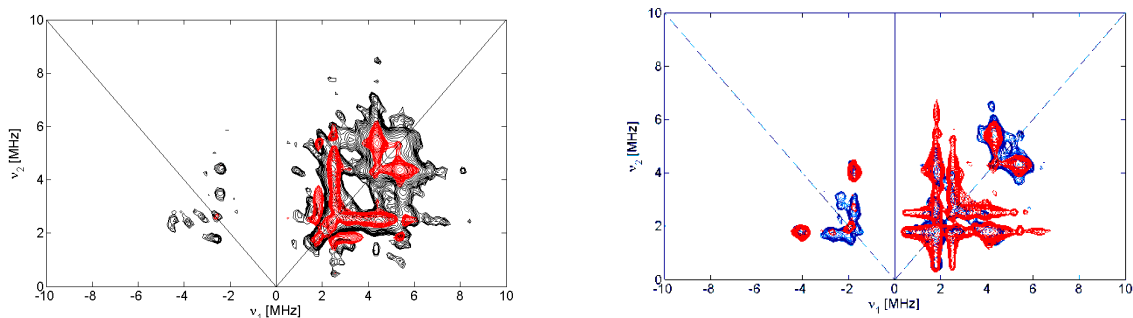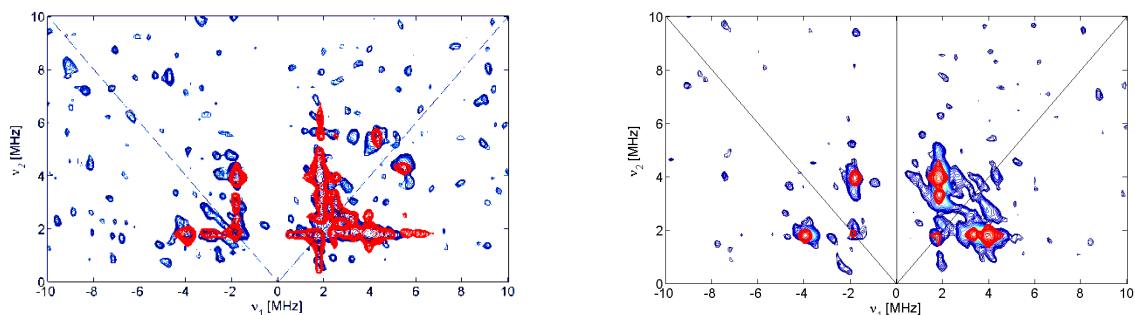
Figure 19. HYSCORE simulation (red) assuming a three-spin system ($S=1/2$, $I_1=1$, $I_2=1$) with A_1=[1 1.9 1.25 MHz], $(e^2Qq/h)_1$=-4.5 MHz and η_1=0.8 and A_2=[-1 -1.7 -1.9 MHz], $(e^2Qq/h)_2$=-4.5 MHz and η_2=0.8, with the hyperfine and nuclear quadrupole tensor of the second nucleus rotated 20° about the z axis. This simulates the contribution of a N_2-like and a N_4-like nitrogen (Appendix) and proves that the experimental data are consistent with the DFT data.
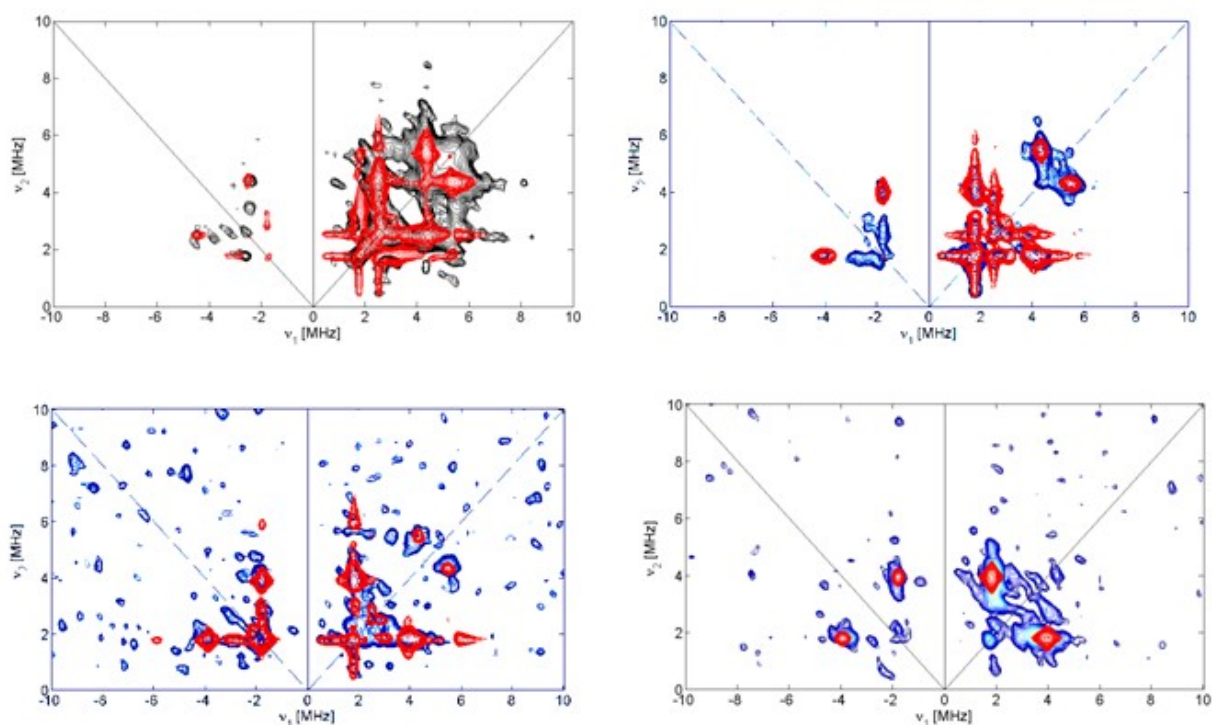
Figure 20. HYSCORE simulation (red) assuming a three-spin system ($S=1/2$, $I_1=1$, $I_2=1$) with A_1=[-1 -1.7 -1.9 MHz], $(e^2Qq/h)_1$=-4.5 MHz and η_1=0.8 and A_2=[-0.03 -0.09 0.16 MHz], $(e^2Qq/h)_2$=-3.4 MHz and η_2=0.265. α_2=90° for the $\mathbf{P}_2$ tensor, all other Euler angles of the hyperfine and nuclear quadrupole tensors are 0°. This simulates the contribution of a N_2 and a N_5-like nitrogen. The shallow modulation of the N_5 nucleus hardly alters the HYSCORE patterns (compare with Figure 18).

	A_x (MHz)	A_y (MHz)	A_z (MHz)	e^2qQ/h (MHz)	η	Method
Cu^{II}ENZm	±1.0 (±0.2)	±1.7 (±0.2)	±1.9 (±0.1)	±4.5 (±0.1)	0.8 (±0.1)	HYSCORE
Model A, N$_2$	-0.01	-1.0	-1.91	-5.07	0.49	DFT
Model A, N$_4$	1.06	0.09	0.34	-5.08	0.64	DFT
Model A, N$_5$	0.10	-0.08	-0.11	-3.42	0.27	DFT
Model B, N$_2$	-0.02	-1.04	-1.90	-5.03	0.53	DFT
Model B, N$_4$	2.05	1.02	1.25	-5.22	0.60	DFT
Model B, N$_5$	0.15	-0.03	-0.07	-3.43	0.28	DFT

Table 8. Comparison between the experimental ^{14}N spin Hamiltonian parameters derived from the HYSCORE spectra of Cu^{II}ENZm in toluene:DMSO and the ^{14}N data computed for two model structures.
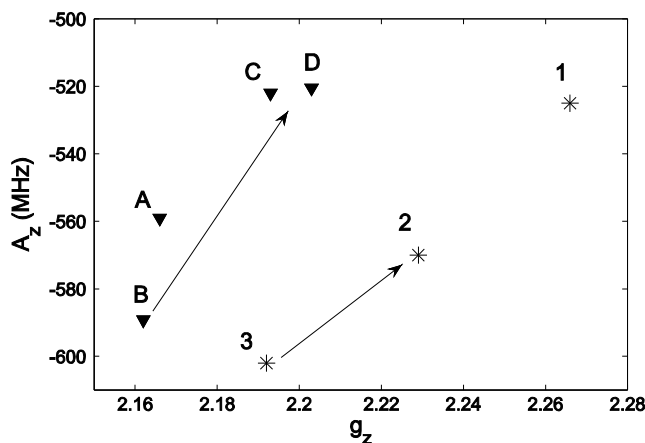
Figure 21. (g_z,A_z) plot for the theoretical models A, B, C and D (triangles) compared to the experimental points (asterisks) obtained for Cu^{II}ENZm (1), and CuJac (2), CuSalen (3). The values are given in Appendix (DFT) and Table 7 (EPR). The arrows indicate the parameter shifts upon axial ligation.

The agreement between the experimental data and the computed spin-Hamiltonian values for the different models is satisfactory, but far from perfect for any of the models. Nevertheless, a number of trends can already be deduced at this stage. The comparison of the computed g and copper hyperfine values of models B-D shows that upon axial ligation, the g_z value increases and the $|A_z|$ value decreases (Figure 8a). This trend is also found experimentally for Cu^{II} salen-type complexes. If we compare the parameters of CuSalen that bears no axial ligands with those of the CuJac complex that has axial methylbenzylamine binding, we see a similar trend (Table 7, Figure 21). For CuJac in toluene, g_z=2.190 and A_z=-

605 MHz (unpublished results), confirming this trend. The relatively large g_z and small $|A_z|$ of the $Cu^{II}ENZm$ seem to indicate weak (solvent) ligation. This is corroborated by the observed hyperfine coupling for H^a. In agreement with the experiment, the DFT computations predict a largely isotropic coupling for this proton (Appendix). Although the computed isotropic hyperfine is overestimated, a decrease in its value can be observed upon axial ligation, suggesting that the relatively small coupling of H^a is consistent with axial copper ligation. A similar decrease is seen in the computed hyperfine coupling of N_1 upon axial ligation (Appendix). Although it was impossible to determine the exact hyperfine couplings of N_1 and N_5 from the Davies-ENDOR spectra, an upper limit of 50 MHz was found. This value is below the computed couplings, matching the overestimation of the hyperfine values of H^a.

For the protons H^b and H^c maximal proton hyperfine couplings of ~10 MHz and ~7 MHz respectively, are predicted by DFT (Appendix). These values contradict the experimental findings, where all proton couplings other than H^a are below 4.9 MHz. Interestingly, H^b and H^c show strong H-bonding to DMSO (H^b) or a second **L** ligand (H^c) in the solid state (Figure 7). Although it is clear from the above analysis that the solid-state structure is not retained in solution, it is very likely that both protons will H-bond to the surrounding solvent molecules. This is not taken into account in the current DFT models, which may explain the overestimation of these proton couplings.

The last issue, which should be addressed, is the question whether chloride is still binding to the copper ion, or whether it has been replaced by solvent molecules. Figure 21 seems to indicate that the g and copper hyperfine values lie more in the line of a 2N2O surrounding with additional axial ligation as observed for Schiff base Cu^{II} complexes. Furthermore, the long Cu-Cl distance found for the solid-state structure of $Cu^{II}ENZm$ strongly suggests detachments of the chloride ion. The DFT computations on model A predict a large hyperfine coupling on the ^{35}Cl nucleus (A = [56.00 1.04   -0.63] MHz) if chloride is equatorially binding. Unfortunately, this interaction falls within the frequency area where also the contributions of the N_1, N_5 and $^{63,65}Cu$ are found in the ENDOR spectrum in Figure 13b, preventing direct verification. The DFT results for model A are, however, not in a better agreement with the experimental results than the solvated models B-D. It is interesting to note that, up till now, all attempts to compute an optimized geometry for [Cu**L**(DMSO)Cl] failed due to detachment of the chloride anion. Although one has to be careful with interpreting this

failure, it may indicate that Cl⁻ detaches when put in competition with a solvent molecule.

3.3. SOD like activity assay

The SOD-like activity of the complex was determined by a modified version of the conventional NBT test, based on Dojindo's highly water-soluble tetrazolium salt, WST.[129] As WST produces a water-soluble formazan dye upon reduction with a superoxide anion, this avoids the disadvantages of the conventional assay such as poor water solubility of formazan and the interaction with the reduced form of xanthine oxidase. The IC_{50} value of our Cu^{II}ENZm, obtained from the plot of inhibition percentage versus complex concentration, is 0.38μM, thus comparable with previously reported active copper SODm. (figure 22)[105a,123]
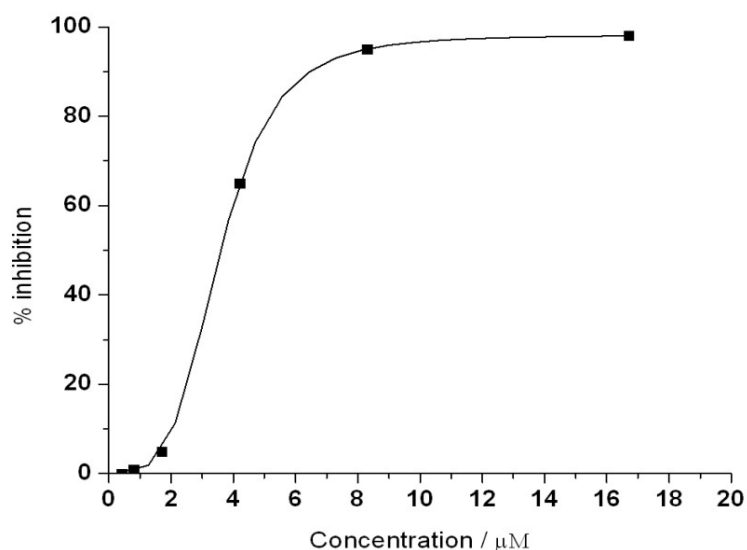
Figure 22. WST- SOD like activty assay. Different concentration of Cu^{II}ENZm inhibiting the formazan formation.

The metal binding region of native SOD is known to represent the catalytic active site, and in this respect its conformation in the case of a proposed SOD-mimic can explain its biological behaviour. Although the Cu^{II}ENZm under study takes on a square-planar mono-copper conformation upon dissolving, *i.e.* a structure strongly different from the tetrahedral surrounding of the Cu^{II} ion observed in Cu,Zn-SOD and Cu,Cu-SOD, it is probably exactly this mono-nuclear conformation that provides an easy accessibility to the O_2^- anion and thus contributes to its high catalytic activity.

It is interesting to note that Díaz *et al.*[107b] found a conciderably larger SOD like activity for thiosemicarbazone copper(II) complexes having $|A_z|$ values in the range of 500-580 MHz than those complexes having $|A_z|$ values around 420 MHz (although the latter value is closer to the Cu,Zn-SOD case). Jitsukawa *et al.*[102a] studied a number of copper complexes with tripodal polypyridylamine ligands and concluded that a five-coordinated square pyramidal or trigonal bipyramidal structure is more favourable for a good SOD like activity than a four-coordinated square planar structure. This seems to corroborate our suggestion of DMSO ligation in the current Cu^{II}ENZm, based on the combined EPR and DFT models.

3.4. Catalase like activity assay

As various SODm were reported to possess catalase-like activity, we also tested Cu^{II}ENZm as a catalase-mimic. The amplex red-coupled fluorescence assay provides a simple, sensitive measure of catalase-like activity. LPO reacts with H_2O_2 in the presence of amplex red and a highly fluorescent product, resorufine is formed. If catalase or an antioxidant compound is simultaneously present, it will compete for H_2O_2, and thus a lower amount of resorufine will be formed.[130] The decay in the fluorescence signal can be related to the catalase activity. The activity assay clearly indicated that Cu^{II}ENZm competes with LPO in catalyzing H_2O_2, similar to native catalase (Figure 23). Since Cu^{II}ENZm plays a dual role as an SOD- and a catalase- mimic, and will serve for complete ROS detoxification, both with respect to superoxide radicals and related peroxides.
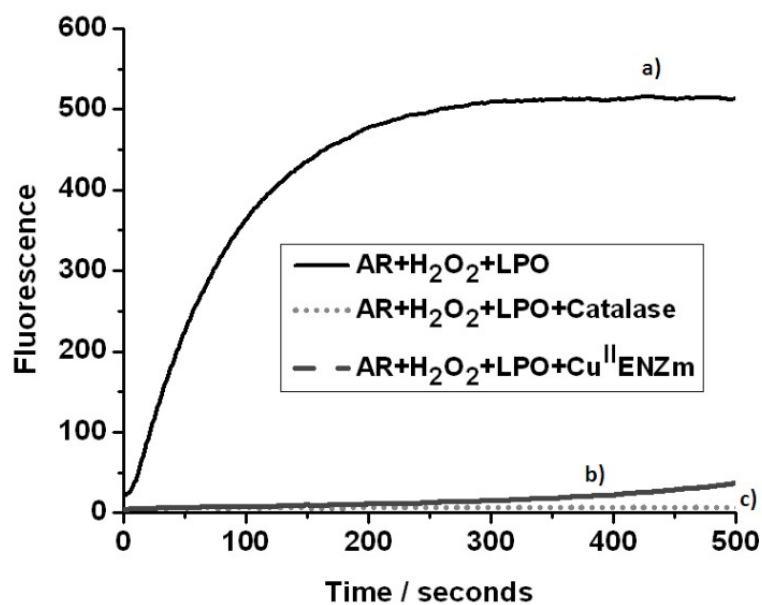
Figure 23. Amplex red-coupled fluorescence activity assay. Kinetics of resorufine formation in the presence of : a) Amplex red, lacto peroxidase and H_2O_2, b) Amplex red, lacto peroxidase, H_2O_2, and catalase (1 µM), c) Amplex red, lacto peroxidase, H_2O_2, and Cu^{II}ENZm. Buffer: PBS.

4. Encapsulation of bi-functional enzyme mimics in polymeric vesicles

To develop antioxidant nanoreactors, we encapsulate Cu^{II}ENZm inside polymeric vesicles that are formed by self assembly process. We chose the copper complex 6-(2-hydroxy-benzaldehyde) hydrazono-as-triazine-3,5-dione (Cu^{II}ENZm), for its bi-functional enzyme like activity. As an amphiphilic block copolymer for Cu^{II}ENZm encapsulation we used PMOXA$_{12}$-PDMS$_{55}$-PMOXA$_{12}$, which has already been reported as having an oxygen-permeable hydrophobic block.[29]

4.1. Characterization of Cu^{II}ENZm nanoreactors

It has been shown that amphiphilic triblock copolymer PMOXA-PDMS-PMOXA self-assemble spontaneously in dilute aqueous solutions into vesicular structures.[44,48,99] The size and shape of the polymeric vesicle before and after encapsulation of Cu^{II}ENZm were studied by light scattering (LS) and transmission electron microscopy (TEM).

4.1.1. Light scattering

The ratio ($\rho = Rg/R_H$) of the radius of gyration (Rg), obtained from static LS, to the hydrodynamic radius (R_H), from dynamic LS experiments was 0.96 for empty vesicles, 0.93 for vesicles containing Cu^{II}ENZm; these values are characteristic for hollow spherical objects (vesicular structures). The mean R_H value of 124 nm for empty vesicles decreased only slightly for Cu^{II}ENZm-containing vesicles (110 nm), indicating that the encapsulation procedure does not affect the size and shape of the self-assembled objects. This fact was also observed when SOD was encapsulated by a different encapsulation procedure inside polymeric vesicles with similar hydrophobic/hydrophilic blocks, revealing that neither the encapsulation procedure nor the molar mass of the encapsulated compound dramatically affected the formation of polymeric vesicles containing the compound inside their aqueous cavities.[99] Contrariwise, the hydrophobic and hydrophilic blocks were found to affect the size of the formed vesicles significantly, even when encapsulating the same compound.[29]

4.1.2. Transmission Electron microscopy

TEM micrographs of Cu^{II}ENZm-containing vesicles show spherical objects with homogeneous sizes in a range related to the R_H values obtained by LS (Figure 24). In addition, TEM micrographs show that Cu^{II}ENZm-containing nanoreactors do not differ significantly in shape and

size as compared to empty vesicles, reaffirming that Cu^{II}ENZm encapsulation does not influence the self-assembly of PMOXA$_{12}$-PDMS$_{55}$-PMOXA$_{12}$.
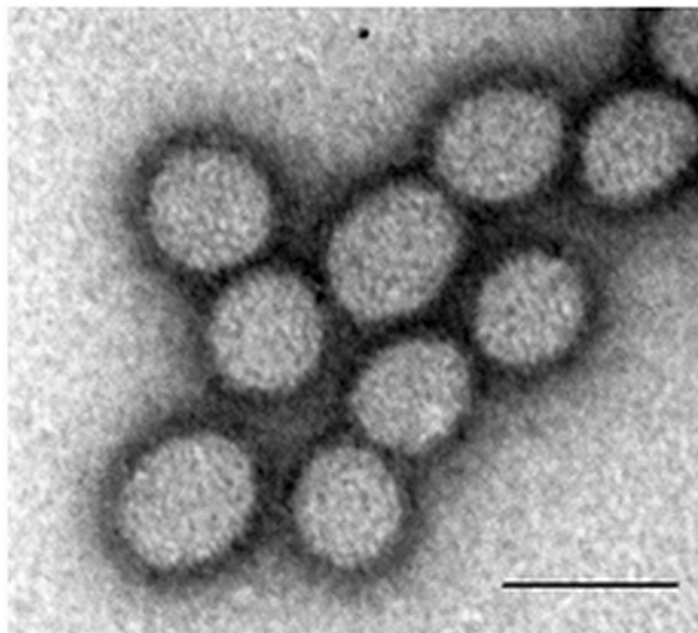
Figure 23. TEM micrograph of Cu^{II}ENZm encapsulated in PMOXA$_{12}$-PDMS$_{55}$-PMOXA$_{12}$ vesicles (room temperature, scale bar: 200 nm).

Taken together, TEM and LS results indicate that the encapsulation of antioxidant enzyme mimic during the auto-assembly process does not influence vesicle formation in terms of size and shape.

4.1.3. Electron Paramagnetic Resonance

A key point when Cu^{II}ENZm is encapsulated inside a carrier (liposome/polymer vesicles) is the preservation of its enzyme-like activity, which represents an important limiting factor that must be addressed. First of all, one must check whether the structure of the Cu^{II}ENZm is preserved after encapsulation. In principle, this can be done using CW-EPR spectroscopy. Indeed, we used this technique previously to characterize in detail the Cu^{II}ENZm structure. One of the big challenges in detecting the EPR spectra of the nanoreactors, however, is the low concentration of the vesicles. Figure 25a shows the EPR spectrum obtained for a frozen solution of the Cu^{II}ENZm nanoreactors. No signal arising from the Cu^{II} center can be discerned (the observed signal is a weak background signal due to the cavity). The fact that no signal is observed can be due, in principle, to one of three reasons: Either no Cu^{II}ENZm is included in the nanoreactors, or the overall concentration is below

the EPR detection limit, or a high number of $Cu^{II}ENZm$ complexes are encapsulated per vesicle. In the latter case, the local Cu^{II} concentration will be very high (despite the low overall Cu^{II} concentration) and strong dipolar interactions between different Cu^{II} centers may broaden the EPR spectrum beyond detection. The latter option can be easily tested by recording the EPR spectrum after breaking the vesicles with triton-X (2.5 %) (Figure 25b). If the third option is valid, $Cu^{II}ENZm$ will be dispersed in solution and the "normal" EPR spectrum of $Cu^{II}ENZm$ should be retrieved. We indeed observed the typical EPR features of the $Cu^{II}ENZm$, as can be seen by comparing the EPR spectrum of a frozen DMSO solution of $Cu^{II}ENZm$ (compare Figure 25b, 25c). Both EPR spectra can be simulated using the following spin Hamiltonian parameters: $g_{\parallel}= 2.266$, $g_{\perp}= 2.057$, $A_{\parallel}= 525$ MHz, $A_{\perp}= 25$ MHz (Figure 24d); only the line width differs somewhat for the two cases.
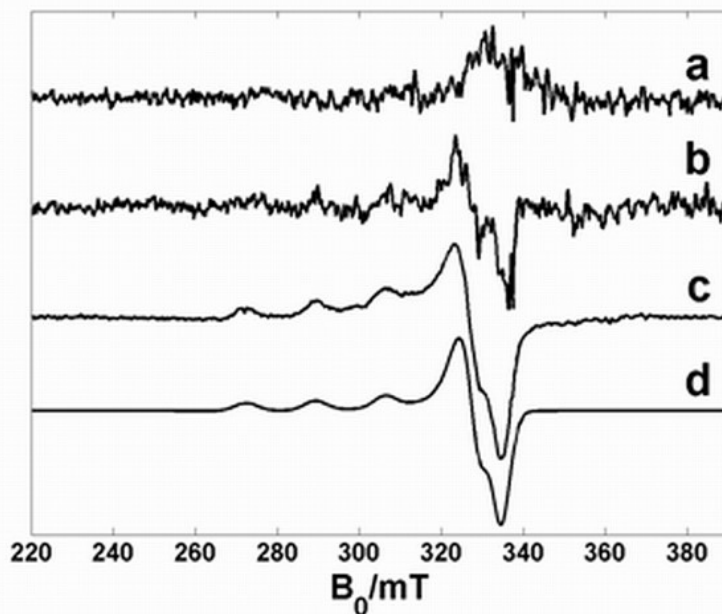
Figure 25. CW-EPR spectra taken at 100 K: a) Frozen solution $Cu^{II}ENZm$-containing PMOXA$_{12}$-PDMS$_{55}$-PMOXA$_{12}$ vesicles (in PBS buffer, pH 7.4). b) Frozen solution after $Cu^{II}ENZm$-release from PMOXA$_{12}$-PDMS$_{55}$-PMOXA$_{12}$ vesicles via addition of triton-X. c) Frozen DMSO solution of $Cu^{II}ENZm$, and d) the simulation of the EPR spectra b and c.

These findings indicate that no significant structural changes occurred during the encapsulation/release procedure. Due to the mild self-assembly using amphiphilic copolymers, the encapsulation procedure affects neither the structure of the coordination sphere of $Cu^{II}ENZm$, nor

the stability of the compound. It has already been shown that the geometry of native SOD is also preserved after encapsulation in PMOXA-PDMS-PMOXA vesicles, but in that case only a few SOD molecules were encapsulated per vesicle.[99]

4.1.4. UV-Visible spectroscopy

The UV-Vis spectra of encapsulated $Cu^{II}ENZm$ were also compared to the free compound after a background correction based on the absorption spectrum of polymeric vesicles. The maximum of the absorption band at $\lambda = 425$ nm, corresponding to the LMCT transitions, did not shift after encapsulation (Figure 26), which confirms the EPR data showing that the encapsulation procedure affects neither the metal coordination sphere nor does it degrade the complex. The ligand bands appearing in the UV-Vis region of the encapsulated compound spectrum are, moreover, similar to those of the free compound.
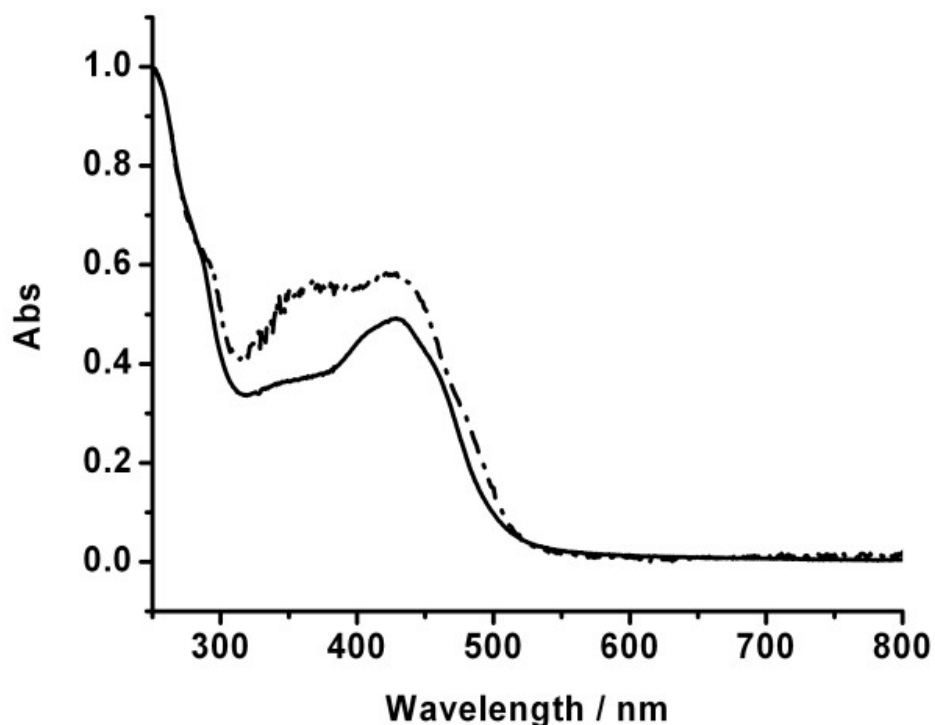
Figure 26. Normalized UV-Vis spectra: a) Free $Cu^{II}ENZm$ in PBS (straight line). b) $Cu^{II}ENZm$-containing $PMOXA_{12}$-$PDMS_{55}$-$PMOXA_{12}$ vesicles in PBS (dot-dash).

4.2. Encapsulation efficiency of Cu^{II}ENZm nanoreactors

The encapsulation efficiency of Cu^{II}ENZm inside polymeric vesicles was established by using the electronic spectra of Cu^{II}ENZm-containing vesicles compared with those of empty vesicles. The intense ligand to metal charge transition (LMCT) absorption band at approximately λ = 425 nm that is preserved after encapsulation permitted a direct estimation of the apparent value of Cu^{II}ENZm concentration, taking into account the total solution volume, which was determined to be ~138 μM (Figure 27). As our encapsulation procedure is based on the self-assembly process of vesicle formation, the concentration of Cu^{II}ENZm inside of vesicles is expected to be at least as high as the initial Cu^{II}ENZm amount used for encapsulation. In addition, if we take into account a polymer membrane thickness on the order of ~15 nm,[29,42] which decreases the overall volume by a factor of 0.64 to yield the cavity volume, this leads to an even higher value of Cu^{II}ENZm concentration inside vesicles.
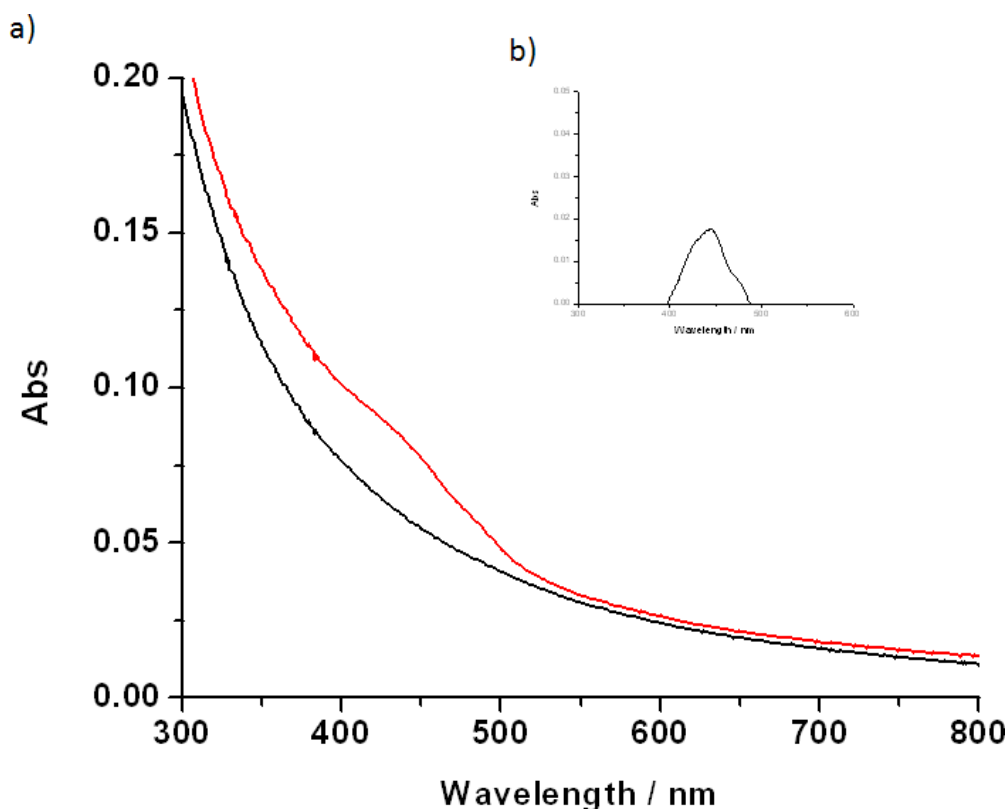
Figure 27. UV-VIS spectra of a) empty PMOXA$_{12}$-PDMS$_{55}$-PMOXA$_{12}$ polymeric vesicles (black), and Cu^{II}ENZm-containing PMOXA$_{12}$-PDMS$_{55}$-PMOXA$_{12}$ vesicles in PBS (red). b) Cu^{II}ENZm after background corrected with empty PMOXA$_{12}$-PDMS$_{55}$-PMOXA$_{12}$ polymeric vesicles (black).

In addition, different effects, such as steric and electrostatic interactions with the polymer membrane, may favour clustering of the Cu^{II} complexes inside vesicles. These effects of confinement lead to a significant decrease in the mean free path of molecules inside the inner cavity, and thus explain the presence of spin-spin interactions that broadened the EPR spectrum beyond the detection limit.

An encapsulation efficiency of approximately 46 % was calculated (for an initial Cu^{II}ENZm concentration of 300 μM). This indicates that the choice of a small molecular weight Cu^{II}ENZm leads to an improvement in encapsulation efficiency as compared to the reported SOD encapsulation efficiency of a maximum of 32 % with similar PMOXA-PDMS-PMOXA copolymer vesicles.[29] However, DMSO, the solvent of choice for Cu^{II}ENZm, affects the process of vesicle formation. Thus, initial concentrations of Cu^{II}ENZm higher than 300 μM should be avoided from a technical point of view.

4.3. Enzyme-like activity of Nanoreactors

4.3.1. SOD like activity

The SOD-like activity of Cu^{II}ENZm nanoreactors was determined with pulse radiolysis. High energy ionizing radiation generates primary radicals ($H^{\bullet}$, e^- (aq), $HO^{\bullet}$) that are rapidly and quantitatively converted into either superoxide $O_2^{\bullet-}$ or its protonated form, hydroperoxyl $HO_2^{\bullet}$, in the presence of formate.[117a] The kinetics of the decay of superoxide radicals in the presence of Cu^{II}ENZm-containing nanoreactors was compared to that of free Cu^{II}ENZm and empty vesicles (Figure 28). The obtained half-lives ($t_{1/2}$), and hence the rate of superoxide decay of Cu^{II}ENZm nanoreactors, clearly indicate that the Cu^{II}ENZm-nanoreactor is active at detoxifying superoxide radicals in a SODm concentration-dependent manner: higher Cu^{II}ENZm concentration inside the nanoreactor leads to considerably faster decay of superoxide (Figure 29). In addition, the rapid decay reaction indicates high $O_2^{\bullet-}$ permeability of the polymeric membrane, in good agreement with previously reported studies on PMOXA-PDMS-PMOXA copolymers with different hydrophobic/hydrophilic blocks.[25]
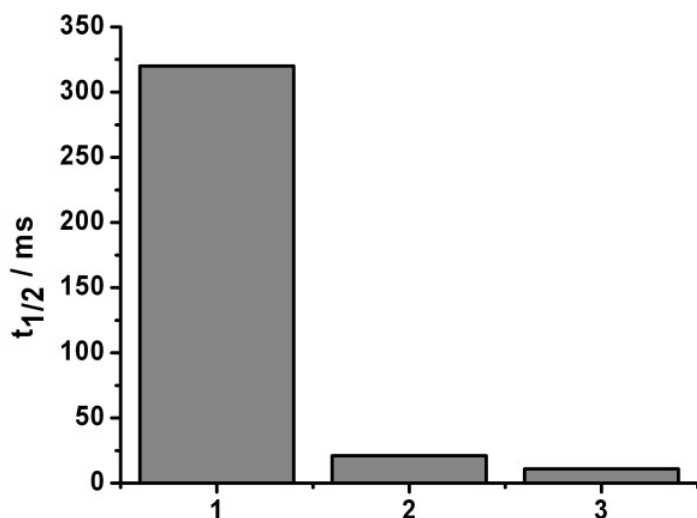
Figure 28. Pulse radiolysis assay. 1) Uncatalyzed decay observed at 280 nm for 80 µM superoxide produced by a 50 ns pulse of an aerated solution of 1.0 M formate and 10 mM phosphate, pH 8, in the presence of PMOXA$_{12}$-PDMS$_{55}$-PMOXA$_{12}$ vesicles. 2) Superoxide decay catalyzed by Cu^{II}ENZm (ca. 4.0 µM) encapsulated in PMOXA$_{12}$-PDMS$_{55}$-PMOXA$_{12}$ vesicles (10 mg polymer). 3) Superoxide decay catalyzed by free Cu^{II}ENZm (ca. 5.0 µM).
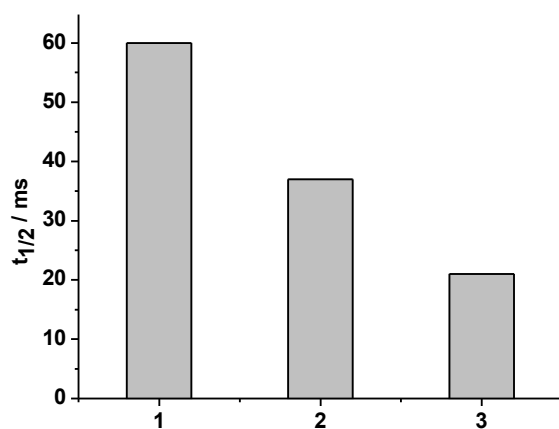
Figure 29. Pulse radiolysis assay. Superoxide decay catalyzed by Cu^{II}ENZm encapsulated in PMOXA$_{12}$-PDMS$_{55}$-PMOXA$_{12}$ vesicles as function of the Cu^{II}ENZm concentration: 1) ca. 1.6 µM, 2) ca. 2.7 µM, 3) ca. 4 µM.

4.3.2. Catalase like activity

The catalase like activity of $Cu^{II}ENZm$ nanoreactors was tested by the same assay as for free $Cu^{II}ENZm$ in solution that is amplex red-coupled fluorescence assay. The impermeability of amplex red and LPO through the nanoreactor membrane limits the reaction of H_2O_2 with LPO to form resorufine. We should to take into account that simultaneous encapsulation of LPO enzyme and substrate (amplex red) is required together with $Cu^{II}ENZm$ inside nanoreactors in order to analyze the resorufine formation. This represents a significant limiting factor of this assay in the detection of catalytic reaction of H_2O_2 by $Cu^{II}ENZm$.

However, since free $Cu^{II}ENZm$ plays a dual role as an SOD- and a catalase- mimic, and its structure is not affected by the encapsulation procedure, the mimic, once inside polymeric vesicles, will serve for complete ROS detoxification, both with respect to superoxide radicals and related peroxides.

5. Cellular interaction of nanoreactors containing bi-functional enzyme mimics

To evaluate the efficiency of the antioxidant nanoreactors as pharmaceutical candidate, it is very important to understand the cellular interactions, cellular uptake, intracellular processing and cytotoxicity in targeted cells. In this respect, we studied the internalization and toxicity assessment of nanoreactors containing in THP-1 cells that play an important role in immune system.

5.1. Cellular uptake of $Cu^{II}ENZm$ nanoreactors

5.1.1. Flow cytometry

The quantitative uptake of nanoreactors in THP-1 cells irrespective of cellular localization was analyzed using flow cytometry. Flow cytometry have been used for many applications to measure both light scattering and fluorescence signal from nanoparticles and cells. Most flow cytometry measure side scatter (SSC) intensity with a photomultiplier and forward scatter (FSC) intensity with a photodiode. SSC has been used to show differences in the physical state of the cell, including nanoparticle uptake. Forward light scatter is routinely used as a measure for cellular size comparisons.[131]

After 24 h incubation with the nanoreactors, a shift in the cell population to a high sideward scatter signal (SSC) was observed, showing changed granularity in an SSC density plot (Figure 30b) compared to untreated cells (Figure. 30a). Cells that became granular indicated that nanoreactors had been taken up. Both, in cells treated with nanoreactors and in untreated cells, the intensity of FSC was maintained that reflects the size of a cell (Figure 30a, 30b). This indicates that the cells maintained their sizes during nanoreactor uptake.

The cells incubated with nanoreactors showed an increased fluorescent signal in the FL-1 (PE) fluorescence channel (Figure 30d) that corresponds to the internalized nanoreactors in the cells. The fluorescent intensity allowed us to quantify the uptake after 24 h incubation as approximately 11 %. No fluorescent signal was obtained for the untreated cells (Figure 30c).
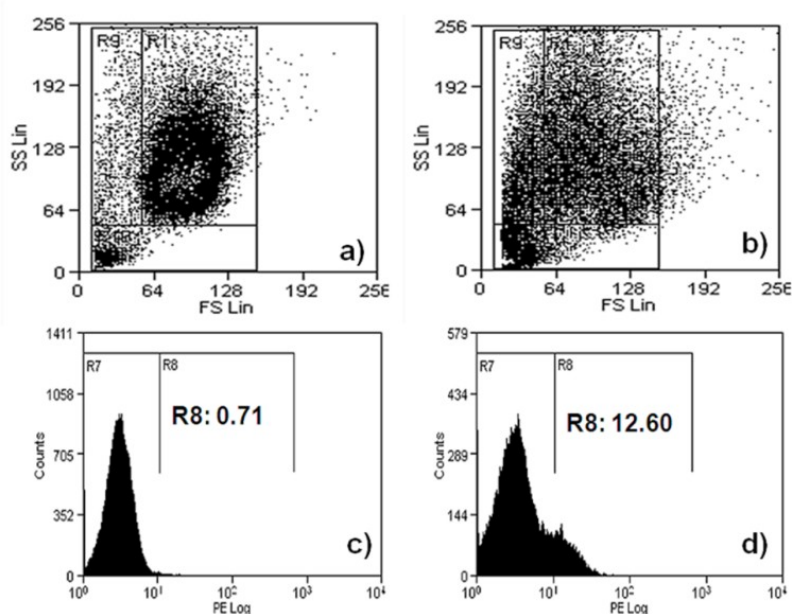
Figure 30. Flow cytometry analysis. Density plot of: a) THP-1 cells (control). b) THP-1 cells incubated with $Cu^{II}ENZm$- and sulforhodamine B-containing $PMOXA_{12}$-$PDMS_{55}$-$PMOXA_{12}$ vesicles for 24 h. Fluorescent intensity in FL-1 (PE) of: c) THP-1 cells. d) THP-1 cells incubated with $Cu^{II}ENZm$- and sulforhodamine B-containing $PMOXA_{12}$-$PDMS_{55}$-$PMOXA_{12}$ vesicles after 24 h.

5.1.2. Confocal Laser Scanning Microscopy (CSLM)

The intracellular localization of internalized nanoreactors was analyzed by Laser scanning confocal microscopy (CLSM). CLSM has been applied to wide range of investigations in the bio-sciences for imaging and recently to study the cellular uptake of nanoparticles. They are equipped with 3-5 laser systems controlled by high-speed acousto-optic tunable filters, which allow very precise regulation of different wavelength and excitation intensities. The spectral imaging detection systems further refine the technique by enabling the examination and resolution of different fluorophores with overlapping spectra as well as providing the ability to compensate for auto fluorescence. Advanced multi colour investigation of CLSM dramatically improves the collection and analysis of multiple colored image obtained from complex fluorescence experiments in live-cell imaging.[132]

THP-1 cells were incubated with nanoreactors containing co-encapsulated $Cu^{II}ENZm$ and sulforhodamine B and the CLSM micrographs were analyzed in order to observe their intracellular localization (Figure 31). The very low auto fluorescence of THP-1 cells excited at 543 nm was taken into account as background. As no uptake was found after 6 h of incubation, even at a high dose of nanoreactors (500 µg/ml), 24 h incubation allowed us to study the cell distribution: Most of the nanoreactors were located intracellularly and only few were present in the cell membrane (Figure 31a). By staining the cell membrane with a second dye, Deep Red, which emits at another wavelength value (Figure 31b), we were able to distinguish the extracellular and intracellular region of the cells, and thus localize the nanoreactors more precisely. For more detail on the internalization of nanoreactors, the cellular nucleus was stained with a third dye, DAPI. Nanoreactors were found to be present in the intracellular regions of the cells (Figure 31d), in agreement with the above analysis of $Cu^{II}ENZm$- and sulforhodamine B-containing nanoreactor micrographs. However, no $Cu^{II}ENZm$-containing nanoreactors were found to be present in the nucleus (Figure 31c).
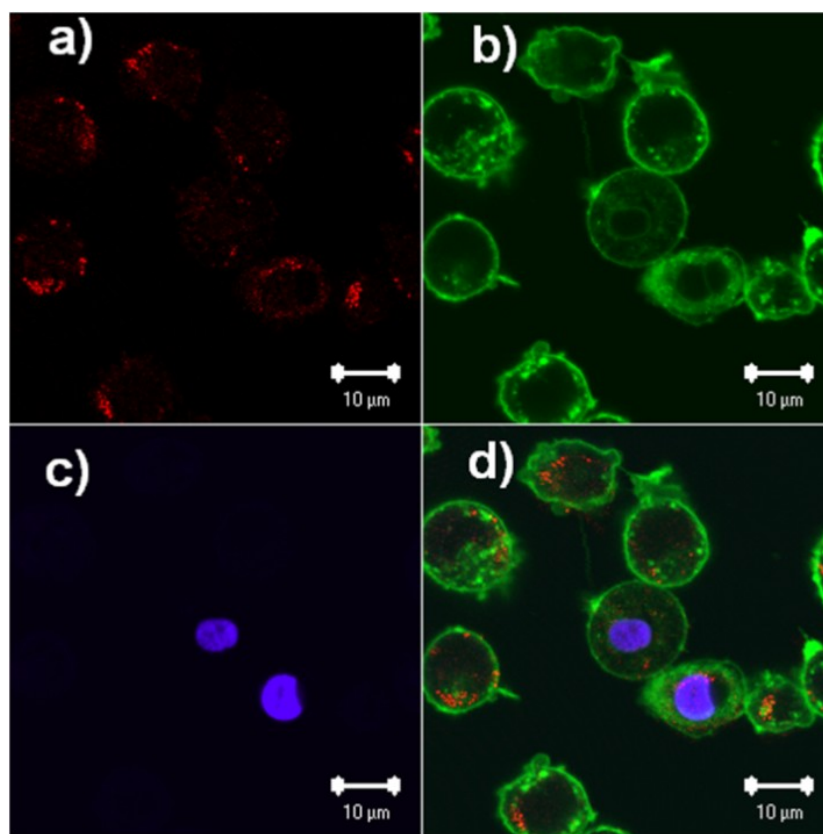
Figure 31. Confocal images of THP-1 cells after 24 h incubation with sulforhodamine B and $Cu^{II}ENZm$ co-encapsulated inside $PMOXA_{12}$-$PDMS_{55}$-$PMOXA_{12}$ vesicles. a) Internalized

Cu^{II}ENZm- and sulforhodamine B-containing vesicles, shown in the red channel. b) THP-1 cells membrane stained with Deep Red, shown in the green channel. c) THP-1 cell nucleus stained with DAPI, shown in the blue channel; d) Overlay of the micrographs from the red, green, and blue channels.

We observed only a limited number of cells containing internalized nanoreactors after 24 h incubation. This increased significantly after 48 h incubation (Figure 32). The number of cells containing nanoreactors as well as the number of internalized nanoreactors increased after 48 h incubation. This indicates the slower and time dependant uptake rate of nanoreactors containing Cu^{II}ENZm in THP-1 cells.
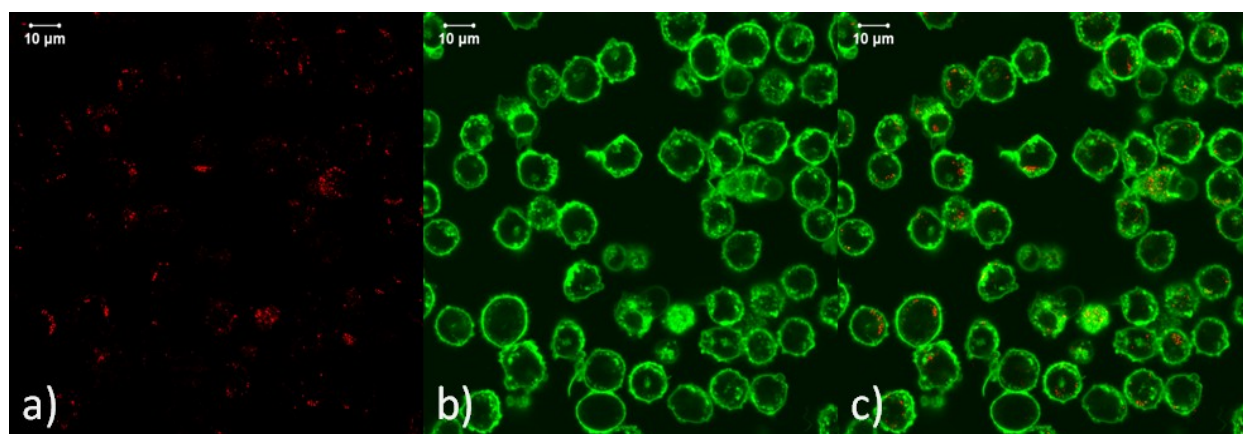
Figure 32. Confocal images of THP-1 cells after 48 h incubation with sulforhodamine B and Cu^{II}ENZm co-encapsulated inside PMOXA$_{12}$-PDMS$_{55}$-PMOXA$_{12}$ vesicles. a) Internalized Cu^{II}ENZm- and sulforhodamine B-containing vesicles, shown in the red channel. b) THP-1 cells membrane stained with Deep Red, shown in the green channel. c) Overlay of the micrographs from the red and green channels.

5.1.3. TEM

The intracellular localization of Cu^{II}ENZm-containing nanoreactors was visualized by TEM, which provides a higher resolution than CLSM. After 24 h cell incubation with nanoreactors, TEM images of THP-1 cells show that the nanoreactors were present in intracellular compartments that resemble endosomes (Figure 33a) and in cytoplasm (Figure 33b). The presence of nanoreactors in the endosome like intracellular compartments suggested an endocytic uptake. However it is

difficult to clearly differentiate polymeric vesicles from vacuoles and vesicular structures of the cell due to similarity in shape and size. Therefore, we analyzed the membrane structure in greater detail. Polymeric vesicles show alterations to their membranes in the form of deformational shrinkage, in contrast to vesicular structures of the cell. The image suggests that nanoreactors escaped the endosomes (Figure 33b, 33c) presumably due to the interaction of polymers with lipid membrane.

The number of intact nanoreactors present in the cytoplasm was significantly increased after 48 h incubation (Figure 34). This is in agreement with other studies that reported a time-dependent release of copolymer systems from endosomes.[133] No uptake of nanoreactors was recognized in the mitochondria or the nucleus, in agreement with other studies on polymer nanoparticles of similar sizes.[134] In the case of PLGA polymeric particles, uptake into the nucleus was reported, but no explanation for this response has been given.[135]
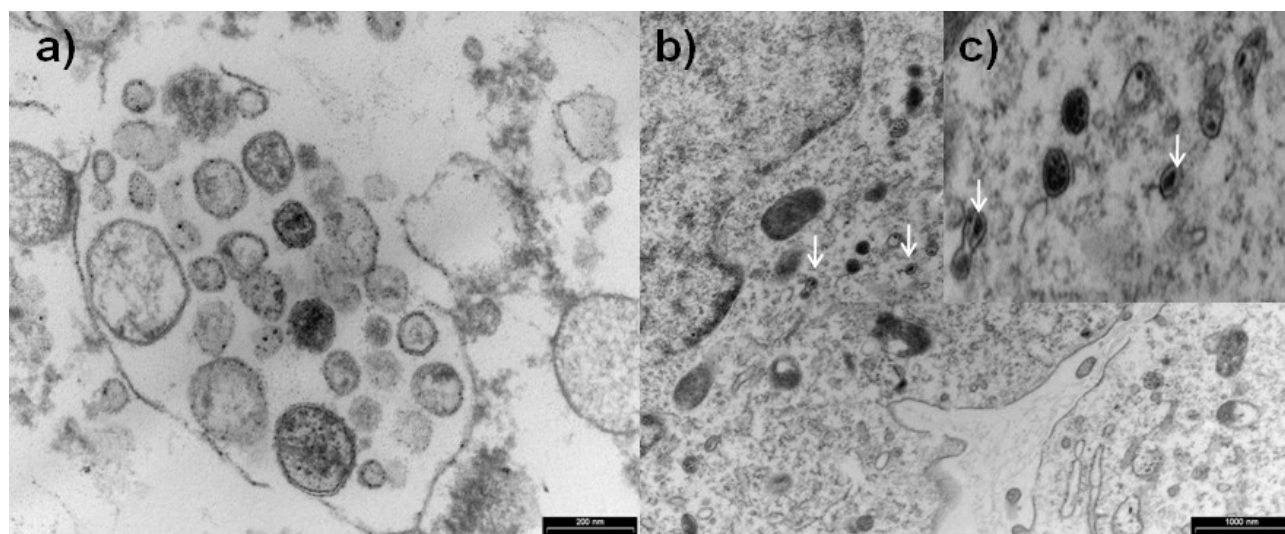
Figure 33. TEM images of THP1 cells incubated for 24 h with Cu^{II}ENZm-containing $PMOXA_{12}$-$PDMS_{55}$-$PMOXA_{12}$ vesicles: a) Intracellular area, as an endosome-like compartment; b) Cytoplasm area containing shrunken polymeric vesicles (indicated by arrows); c) Zoom of shrunken polymeric vesicles in the cytoplasm (indicated by arrows).
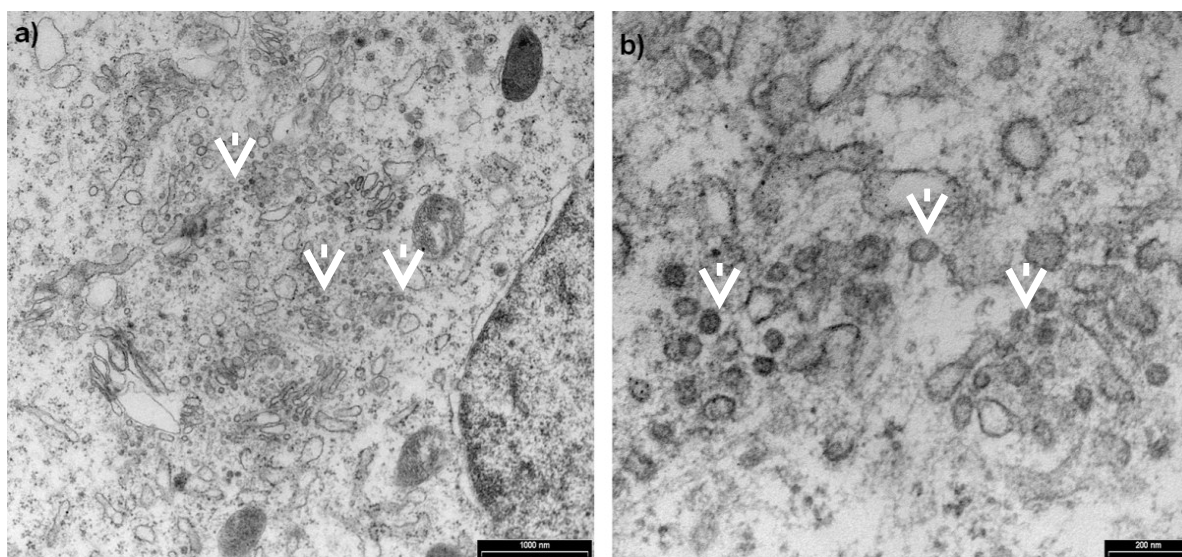
Figure 34. TEM images of THP1 cells incubated for 48 h with $Cu^{II}ENZm$-containing $PMOXA_{12}$-$PDMS_{55}$-$PMOXA_{12}$ vesicles: a) Cytoplasm area containing polymeric vesicles; b) Zoom of polymeric vesicles in the cytoplasm.

5.2. Cytotoxicity of $Cu^{II}ENZm$ nanoreactors

The cytotoxicity of $Cu^{II}ENZm$-containing nanoreactors was assessed with a colorimetric assay based on the formation of a colored formazan product when MTS is biologically reduced by metabolically active cells. As the amount of formazan relates to the metabolic state of the cells and cell viability,[136] the MTS assay allows an assessment of the toxicity of $Cu^{II}ENZm$-containing nanoreactors in comparison to empty polymer vesicles, or to free $Cu^{II}ENZm$. While free $Cu^{II}ENZm$ (20 µM) inhibited the proliferation of THP-1 cells after 24 h, and cell viability of approximately 79 % was shown (Figure 35a), a similar concentration of $Cu^{II}ENZm$ inside the nanoreactors exhibited significantly higher viability, up to 98 % (Figure 35b). This clearly indicates that encapsulation in polymeric vesicles prevents toxicity due to free $Cu^{II}ENZm$, in addition to providing a shielding effect that protects the compound from degradation. Moreover, empty polymer vesicles did not show a toxic effect in the cells after 24 h incubation, even at a high dose of polymer (300 µg/ml) (Figure 35c).
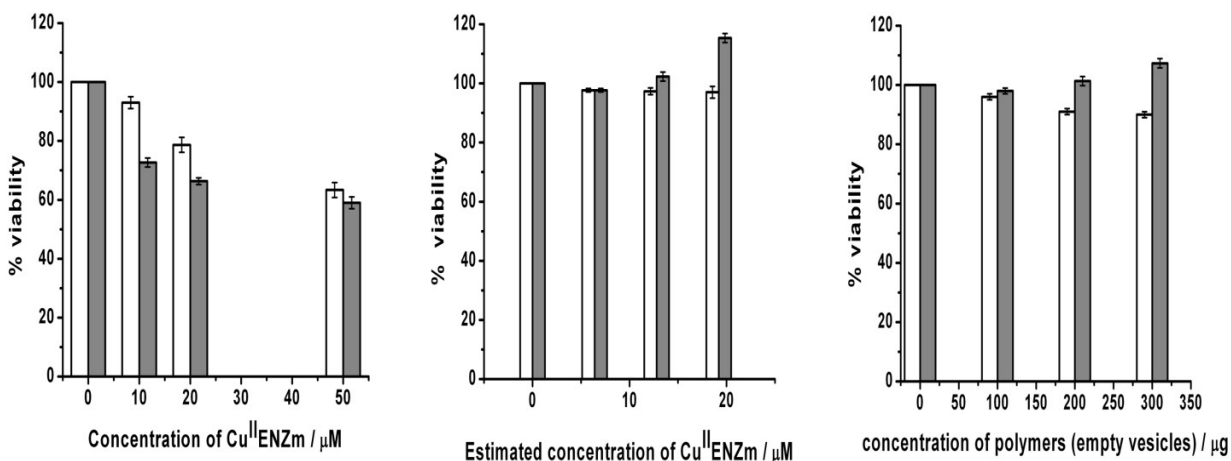
Figure 35. MTS assay. THP-1 cell viability after incubation with different concentrations of: a) free Cu^{II}ENZm. b) Estimated concentration of Cu^{II}ENZm inside PMOXA$_{12}$-PDMS$_{55}$-PMOXA$_{12}$ vesicles. c) Empty PMOXA$_{12}$-PDMS$_{55}$-PMOXA$_{12}$ vesicles. White bars: incubation time 24 h; grey bars: incubation time 48 h.

Increased viability was observed with polymer vesicles/nanoreactors after a prolonged incubation time of 48 h, depending on the concentration of polymeric vesicles. This is presumably due to the reaction of MTS with the O$_2$$^{\bullet-}$ that is produced by NADPH oxidase activity. This activity is sustained and relates to the prolonged and time-dependent uptake of nanoreactors/vesicles.[137,138] Increased viability of cells when incubated with different PMOXA-PDMS-PMOXA-based vesicles has already been reported, but not interdependent with vesicle concentration.[45]

LDH assay

Another approach to assess nanoreactor cytotoxicity was based on LDH assay that allows an estimation of membrane integrity by cytosolic enzyme release from cells.[139] The LDH assay was performed for THP-1 cells incubated with Cu^{II}ENZm nanoreactors, and compared to cells treated with empty vesicles or with free Cu^{II}ENZm (Figure 36). Cells treated with free Cu^{II}ENZm (20 µM) showed a release of less than 5 % LDH, as expected for a low molecular weight compound known to diffuse through the cell membrane without affecting membrane integrity.[140] A high dose of empty vesicles or nanoreactors (300 µg/ml polymer concentration) showed an increase in LDH of up to 24 %. However, the half-maximum inhibitory concentration (IC$_{50}$) was not reached after 24 h incubation, indicating that Cu^{II}ENZm-containing nanoreactors are not toxic at doses in the range of

100-300 μg/ml polymer concentration. In addition, these high doses are not expected to accumulate in biologically relevant conditions.
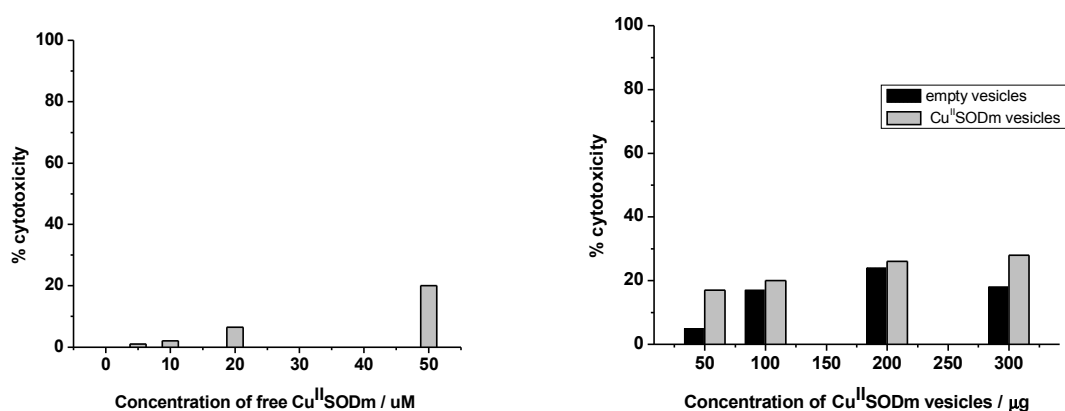
Figure 36. LDH assay. The cytotoxicity of different concentration of: a) Cu^{II}SODm, b) Cu^{II}SODm nanoreactors (grey bars) and empty vesicles (black bars), respectively.

5.3. *In vitro* activity of Cu^{II}ENZm nanoreactors

An essential point was to prove the *in-vitro* activity of Cu^{II}ENZm-nanoreactors. In this respect, we generated oxidative stress on THP-1 cells and analyzed the protective effect against paraquat-mediated cytotoxicity. Several studies suggested ROS involvement in the toxicity induced by paraquat, thereby enhancing cell death.[141-143] While THP-1 cells treated with 2 mM paraquat for 24 h exhibited approximately 48 % loss of viability, cells first treated with Cu^{II}ENZm nanoreactors for 24 h, and subsequently with paraquat for another 24 h showed a significant decrease in the loss of viability (maximum 23 %) (Figure 37). This indicates that Cu^{II}ENZm nanoreactors were active inside the cells and thus provided good protection against oxidative stress.

The increased population of cells containing nanoreactors after a 48 h incubation, as compared to a 24 h incubation (see CLSM micrographs), and the location, mainly in the cytoplasm (see TEM images), explain the protective effect of nanoreactors. Moreover, even if the mimic exhibits lower activity as compared to native enzymes, its higher concentration inside vesicles supports the protective effect we observed. We must also mention that nanoreactors and paraquat simultaneously co-incubated with THP-1 cells for 24 h provided a lower protective effect. This is assumed to be due to rapid paraquat uptake by cells, which induced oxidative stress and then

cytotoxicity that could not be prevented by the presence of Cu^{II}ENZm nanoreactors, as they were internalized more slowly compared to paraquat.

The fact that Cu^{II}ENZm is a dual mimic of SOD and catalase allows *in situ* detoxification of both superoxide radicals and related H_2O_2, and in this way a system is obtained that does not have the generation of ROS as a side effect. However, as our nanoreactor has a membrane which is not permeable to H_2O_2, its main role is to detoxify $O_2^{\bullet-}$ and the H_2O_2 product that develops inside the vesicles.
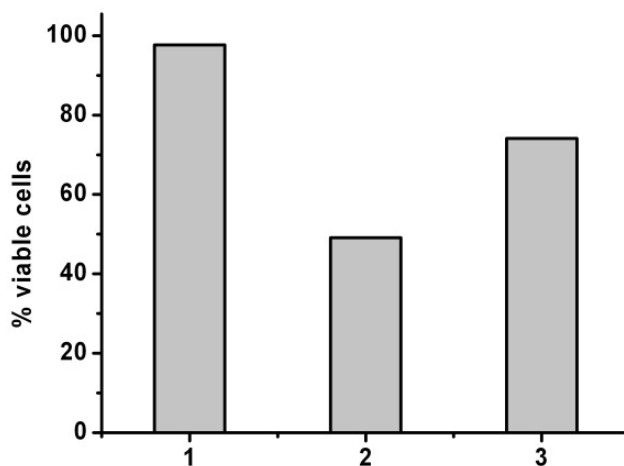
Figure 37. Flow cytometry analysis: *in-vitro* antioxidant activity of Cu^{II}ENZm nanoreactors. Viability of THP-1 cells after 24 h incubation with control, nanoreactors, and paraquat. 1) Viability of untreated control cells considered as 100 %. 2) Viability of cells after paraquat exposure. 3) Viability of cells pretreated with Cu^{II}ENZm nanoreactors for 24 h and sequentially treated by paraquat for additional 24 h.

6. General Conclusion and Outlook

We propose here a new concept of enzyme mimics containing nanoreactors in 4 different steps.

I.   Structure-Activity relationship analysis to obtain high active SODm model

We have demonstrated the first successful global structure–activity relationship based on statistical analysis of all classes of copper complexes proposed to have a SOD like activity. We took into account all copper-based SODm with electronic and EPR parameters that have been published, and established the specificity of the geometry around the metal as an essential criterion for a highly active SODm. The model we obtained for highly active SODm is that a slightly distorted square planar geometry seems to favour high catalytic activity for 4-coordination sphere in agreement with the geometry of native SOD[144] and for 5-coordinated SODm is square pyramidal, with a slightly distorted basal plane.

II.   Synthesis and characterization of a high active Cu^{II}ENZm

We have successfully synthesized a highly active enzyme mimics (Cu^{II}ENZm). The detailed structure of Cu^{II}ENZm in solid state as well as in solution was studied by X-ray crystallography and Electron paramagnetic resonance. Cu^{II}ENZm is shown to a change from a di-copper complex in the solid state to a mono-copper complex in solution and obtained a square-planar conformation. Upon a weak ligation of the solvent molecule, it preserves a pyramidal structure, as established by the combined pulsed EPR and DFT analysis. In this respect, the flexible solvent coordination site of Cu^{II}ENZm can be related to its high SOD activity. The presence of a solvent molecule in an equatorial position may be related to the labile bridge present in native SOD between Cu and Zn centers, which breaks to allow the geometric change during the catalytic reaction.[144] Therefore, the structural geometry of Cu^{II}ENZm can be related to the obtained structural model for highly active SODm based on SAR analysis.

III.   Encapsulation of Cu^{II}ENZm in polymeric nanoreactors

We developed a robust antioxidant nanoreactor based on the encapsulation of highly active Cu^{II}ENZm that permits higher encapsulation efficiency as compared to a nanoreactor

containing the enzymes themselves. This is attributable to intrinsic properties of the Cu^{II}ENZm, such as improved solubility and elimination of the severe constraints required to avoid enzyme denaturation. Cu^{II}ENZm was encapsulated inside the aqueous cavity of polymeric nanovesicles generated by the self-assembly of PMOXA-PDMS-PMOXA amphiphilic copolymers. The mild, structure-preserving procedure used to encapsulate Cu^{II}ENZm had no affect on the size/shape of the vesicles, as indicated by light scattering and TEM, or on the metal-coordination sphere that served as a center for catalytic activity, as demonstrated by EPR and UV-Vis spectroscopy.

IV. **Cellular interaction of Cu^{II}ENZm containing nanoreactors**

The cellular interaction of Cu^{II}ENZm containing nanoreactors was studied with THP-1 cells such as internalization, cytotoxicity, and *in vitro* activity. Approximately 11 % of cells contained internalized nanoreactors after 24 h incubation even without a functionalized vesicle surface to support a targeted approach. The antioxidant nanoreactors showed minimal cytotoxicity after 24 h incubation compared to free Cu^{II}ENZm. The population of THP-1 cells containing the antioxidant nanoreactors was significantly increased after 48 h incubation, and a protective antioxidant effect (23 %) against oxidative stress by paraquat was established. As Cu^{II}ENZm is both a mimic of SOD and of catalase, it serves to detoxify superoxide radicals and related H$_2$O$_2$ inside vesicles, preventing the generation of ROS as a side effect. The well pronounced antioxidant activity of nanoreactors in cells clearly points to a unique method to provide enzyme- mimics based antioxidant therapy, whereby encapsulating mimics in polymeric nanoreactors avoids mimic degradation within biological compartments and simultaneously allows Cu^{II}ENZm to act *in situ* when concentrated inside nanometer-range polymer cavities.

Compared with conventional drug nanocarriers made of liposomes or polymers, our system is more stable and combines the advantages of a polymer shield with an *in situ* active antioxidant compound. This type of nanoreactors is proposed to function as versatile antioxidants, able to escape the immune system, for medical applications. Development of this simple, robust antioxidant nanoreactor represents a new direction in fighting oxidative stress efficiently. However it is very important to investigate further the interaction of nanoreactors with biological systems such as cells, tissues, animal models in detail to understand the intracellular fate of nanoreactors,

such as internalization kinetics, intracellular trafficking, biodistribution and biocompatibility that are important to design more efficient nanoreactors for therapeutic applications.

7. Experimental Section

Materials

6-(2-hydroxy-benzaldehyde) hydrazono-as-triazine-3,5-dione (**L**) was received from Dr. C. Cristescu, National Institute for Chemical and Pharmaceutical Research, Bucharest. All reagents and solvents were purchased from Aldrich or Fluka with the highest purity grade and used as received. Cu/Zn-SOD from bovine erythrocytes, Lacto peroxidase (LPO) from bovine milk, Catalase from bovine liver (Sigma Aldrich), and the 6-(2-hydroxy-benzaldehyde) hydrazono-as-triazine-3,5-dione based Cu (II) complex (Cu^{II}ENZm) were used without further modification. RMPI-1640 cell culture medium (GIBCO), fetal calf serum (FCS), penicillin and streptomycin (Sigma Aldrich), as well as dimethylsulfoxide (Aldrich), chloroform (99.8 %; Fluka), paraformaldehyde (Fluka), glutaraldehyde (Fluka), osmium tetroxide (Fluka), phosphate buffered saline (PBS) , hydrogen peroxide 30% (w/w) and sodium formate (Sigma-Aldrich) were used as received. 10-acetyl-3,7-dihydroxyphenoxazine (amplex red), Sulforhodamine B, Cellmask^{TM} Deep Red, 4',6-diamidino-2-phenylindole (DAPI) and propidium iodide were purchased from Invitrogen. Polycarbonate membrane filters (Millipore), and sepharose 2B (Sigma Aldrich) were used.

Preparation of Cu^{II}ENZm

Metal complexation of **L** was performed in a modified approach of an earlier procedure. [119] **L** (1mM) was dissolved under stirring in 20 ml NaOH (0.05mM) at 40°C and the pH was adjusted to 7.5 with NaOH (1M). A solution of CuCl$_2$ ·2H$_2$O (1mM) in 5ml of milli-Q water was added slowly drop wise for 20-30 minutes at 40°C. The mixture was cooled to 4°C and stirred continuously for 1 hour under atmospheric pressure, forming a green precipitate. The precipitate was filtered, washed successively with hot water, ethanol and acetone and was dried. The powder was re-crystallised in DMSO by slow evaporation method and formed small crystals after more than 2 months at room temperature.

UV/Vis absorption spectroscopy

UV-VIS spectra were recorded with a Perkin Elmer Lambda 35 UV/VIS spectrometer in 0.5 ml silica glass cells between 200 nm and 950 nm, at 25°C. Cu^{II}ENZm and free **L** solutions (1mM) were prepared in DMSO.

IR spectroscopy

IR spectra of the powders of Cu^{II}ENZm were measured with a Shimadzu FTIR 8400S spectrometer from 400 cm^{-1} to 4000 cm^{-1} with a resolution of 1 cm^{-1}.

Continuous-wave (CW) EPR

X-band CW-EPR measurements were performed on a Bruker ESP 300E instrument, equipped with a liquid Helium cryostat (Oxford Inc.), at a microwave (mw) frequency of about 9.43 GHz. A mw power of 20 mW, a modulation frequency of 100 kHz and a modulation amplitude of 0.5 mT were applied. All spectra were taken at 100 K. The EasySpin program was utilized to simulate the CW-EPR spectra.[145] The Cu^{II}ENZm complex was dissolved in DMSO:toluene (1:1 to 1:4) mixtures. Addition of toluene was needed to obtain a good glass upon freezing.

Pulsed EPR

The X-band (9.76 GHz) pulsed EPR experiments were performed on a Bruker ESP380E spectrometer, equipped with a helium-gas flow cryostat (Oxford Inc.). The measurements were done at 4K, with a repetition rate of 1 kHz.

The standard HYSCORE (hyperfine sublevel correlation) experiments were performed using the $\pi/2 - \tau$ - $\pi/2$ - $t_1 - \pi$ - t_2 - $\pi/2 - \tau$ - echo sequence of pulses with $t_{\pi/2}$ = 16 ns and t_π = 16 ns. The time intervals t_1 and t_2 were varied in steps of 16 ns. The matched HYSCORE experiments were performed using the $\pi/2 - \tau - HTA - t_1 - \pi - t_2 - HTA - \tau -$ echo sequence with $t_{\pi/2}$ = 16 ns, t_π = 16 ns and τ =152 ns. The length of the high-turning-angle (HTA) pulse was taken to be 40 ns with ν_1=15.625 MHz to selectively enhance the proton signals. In order to get rid of unwanted echoes, an eight-step phase cycle was applied for all HYSCORE experiments. The time-domain HYSCORE spectra were baseline corrected with a third-order polynomial, apodized with a Hamming window and zero filled. The absolute-value spectra, obtained by two-dimensional Fourier transformation, were added for the different τ values to reduce the blind-spot effect. The HYSCORE spectra were simulated using a program developed at ETH.[146]

The Davies ENDOR (electron nuclear double resonance) experiments were performed using the mw pulse sequence $\pi - T - \pi/2 - \tau - \pi - \tau -$ echo, whereby a π radio-frequency (rf) pulse is

applied during time T. The parameters used were the following: $t_\pi = 96$ (400) ns, $t_{\pi/2} = 48$ (200) ns, $T = 31\mu s$, $t_{rf} = 29$ µs.

The Mims ENDOR experiments were performed with the mw pulse sequence $\pi/2 - \tau - \pi/2 - T - \pi/2 - \tau$ - echo. The parameters used were: $t_{\pi/2} = 16$ ns, $T = 30\mu s$, $t_{rf} = 28$ µs. The spectra were recorded and added for 15 τ values from 104 ns to 216 ns, in order to avoid $\Box \tau$-dependent blind-spots.

The W-band (94 GHz) pulse EPR experiments were performed on a Bruker ELEXSYS E680 spectrometer equipped with a helium-gas flow cryostat. All measurements were done at 5 K using a repetition rate of 200 Hz.

W-band ESE (electron spin echo)-detected EPR experiments were performed using the $\pi/2 - \tau - \pi - \tau$ – echo sequence with $t_{\pi/2} = 148$ ns, $t_\pi = 296$ ns and $\tau = 800$ ns.

W-band ELDOR-detected NMR experiments were performed using the mw sequence: $(HTA)_{mw2}$ - T - $(\pi/2)_{mw1} - \tau - (\pi)_{mw1} - \tau -$ echo sequence, with $t_{HTA} = 20$ µs, $t_{\pi/2} = 148$ ns, $t_\pi = 296$ ns, $T = 1$ µs and $\tau = 800$ ns. The second microwave frequency, mw2, was varied in steps of 120 kHz in the range mw1 $\pm$ 60 MHz.

Preparation of Cu^{II}ENZm-containing polymer vesicles

The synthesis and characterization of PMOXA$_{12}$-PDMS$_{55}$-PMOXA$_{12}$ copolymer has been reported elsewhere.[37] Vesicles of PMOXA$_{12}$-PDMS$_{55}$-PMOXA$_{12}$ in PBS at pH 7.2 were generated by the film rehydration method. A solution of polymer (5 mg/ml) dissolved in 1 ml of chloroform was slowly evaporated in a rotary vacuum evaporator at 40 °C at 50 rpm and 260 mbar vacuum (Buchi Rota vapor R-124 with vacuum controller B-721, Buchi Switzerland) until a film formed on the inside of the flask. The film was dried under vacuum (0.3 mbar) for at least four hours, then a PBS solution (1 ml) and a solution of Cu^{II}ENZm (300 µM/ml) were added and stirred for 48 h at room temperature. The mixture was extruded once with a polycarbonate membrane filter (pore size 400 nm), and 21 times with a polycarbonate membrane filter (pore size 200 nm) to decrease the size-polydispersity of the vesicles. Subsequently, the extruded solution was purified by SEC on sepharose 2B (10 × 300 mm) to remove the non-encapsulated Cu^{II}ENZm. Empty vesicles were generated under similar conditions, without addition of Cu^{II}ENZm solution.

Light scattering (LS)

Dynamic (DLS) and static (SLS) light-scattering experiments to determine the sizes and size distribution of empty and Cu^{II}ENZm-containing vesicles were performed on a ALV (Langen, Germany) goniometer, equipped with an ALV He-Ne laser (λ = 632.8 nm). Empty and Cu^{II}ENZm-containing vesicles were prepared by serial dilution to polymer concentrations ranging from 3.33 to 0.1 mg/ml. Light scattering was measured in 10-mm cylindrical quartz cells at angles of 30–150 ° at 293 K. The data for DLS were analyzed using a Williams-Watts function. The size polydispersity of the vesicles was determined according to the literature.[147]

Transmission electron microscopy (TEM)

The solutions of polymeric vesicles with and without Cu^{II}ENZm were negatively stained with 2% uranyl acetate, then mounted on a carbon-coated copper grid, and dried. The samples were analyzed with a Philips Morgagni 268D transmission electron microscope at 293 K.

Electron paramagnetic resonance (EPR)

An aqueous solution of Cu^{II}ENZm nanoreactors was prepared and measured with EPR (PBS buffer, pH 7.4). Next, a solution of 5% triton X was added (at a 1:1 (v/v) ratio) and the mixture, kept for 48 h at room temperature, was then measured by EPR. X-band CW-EPR spectra were obtained with a Bruker ESP 300E spectrometer, equipped with a liquid Helium cryostat (Oxford Inc.). The EPR spectra were recorded at 100 K. A microwave power of 5 mW, a modulation frequency of 100 kHz and modulation amplitude of 0.5 mT were applied. Each spectrum was the accumulation of 50 scans. The Easy Spin tool for Matlab was utilized to simulate the CW-EPR spectra.

Encapsulation efficiency of Cu^{II}ENZm nanoreactors

Solutions of Cu^{II}ENZm-containing vesicles were measured by detecting light absorption at λ = 425 nm (UV/Vis absorption spectrometer: Perkin Elmer, Lambda 35 spectrophotometer). The concentration of Cu^{II}ENZm inside vesicles was obtained with a standard calibration curve in the range of 10-400 μM, after background correction of the polymer absorption. The encapsulation efficiency was calculated as the ratio between encapsulated Cu^{II}ENZm concentration and the initial concentration of Cu^{II}ENZm.

SOD mimicking activity assay

To measure the activity of Cu^{II}ENZm nanoreactors, pulse radiolysis was used with a 2 MeV Febetron 705 accelerator (Titan Systems Corp., San Leandro, CA, USA) at 20 °C in a 1 cm quartz cell. The oxygenated sodium formate (1 M) solution at pH 8.0 was irradiated to generate $O_2^{\cdot-}$ in the environment of Cu^{II}ENZm nanoreactors. SOD-like activity was calculated from rates of decay of $O_2^{\cdot-}$, measured at $\lambda = 280$ nm, in the presence/absence of Cu^{II}ENZm.

Catalase mimicking activity assay

The catalase-like activity in solution was assessed by using an amplex red-coupled fluorescence assay. The solutions containing 50 µL of LPO (0.5 µM) and 30 µL of amplex red (10 µM) under three different circumstances, with catalase, without catalase, and with Cu^{II}ENZm, were mixed in a quartz cuvette and the fluorescence intensity of resorufin (λ_{ex} =530 nm, λ_{em} = 580 nm) was followed after the addition of 45 µL of H_2O_2 (16 µM). The fluorescence intensity was recorded in a PerkinElmer LS55 fluorescence spectrometer (Waltham, Massachusetts, USA) in the kinetic mode at ambient temperature.

Cell culture

THP-1 cells were kept in RPMI-1640 growth medium supplemented with 10% fetal calf serum, 1% penicillin (10,000 units/ml) and streptomycin (10,000 µg/ml), 2 mM L-glutamine and 1 mM pyruvate. Cells were grown in a humidified incubator (HERA Cell 150, Thermo scientific, Germany) at 37 °C in a 5% CO_2 atmosphere.

Cellular uptake of Cu^{II}ENZm nanoreactors

Cellular uptake of Cu^{II}ENZm nanoreactors was established by flow cytometry, confocal laser scanning microscopy (CLSM) and transmission electron microscopy (TEM). Cu^{II}ENZm and sulforhodamine B were simultaneously encapsulated during the formation of vesicles, as mentioned above. THP-1 cells were cultured in a 6-well plate at different densities of cells per well (2×10^5 for CLSM and flow cytometry analysis, and 1×10^6 for TEM) in RPMI medium and incubated with a nanoreactor solution containing co-encapsulated sulforhodamine B and Cu^{II}ENZm, for 24 h at 37 °C in a humidified CO_2 incubator.

Flow cytometry analysis

Cells treated with a solution of co-encapsulated Cu^{II}ENZm- and sulforhodamine B-containing nanoreactors prepared as above were washed with PBS to deplete the free nanoreactors and analyzed for the quantitative uptake of Cu^{II}ENZm nanoreactors with a flow cytometry set-up (CYAN, BD biosciences). A total of 20,000 events were analyzed for each condition.

Confocal laser scanning microscopy

Cells pre-treated with a solution of nanoreactors co-encapsulated with Cu^{II}ENZm- and sulforhodamine B were incubated at 37 °C with freshly prepared Deep Red (cellmask^{TM}) plasma membrane stain (5 μg/ml) for 5 min, followed by DAPI nucleic acid stain (300 nM) for 5 min. They were then washed with PBS buffer and visualized with a confocal laser scanning microscope (Carl Zeiss LSM510) equipped with 63× water emulsion lens (Olympus), and three lasers (λ_i = 405, 543, and 633 nm). The measurements were performed in multi-track mode, and the intensity of each fluorescent dye was adjusted individually: sulforhodamine B excited at 543 nm in channel 3, Deep Red excited at 633 nm in channel 2, and DAPI nuclear stain excited at 405 nm in channel 1. The images containing the superposition of all three dyes were processed using Carl Zeiss LSM software (version 3.99).

Transmission electron microscopy (TEM)

THP-1 cells pre-incubated with a nanoreactor solution containing co-encapsulated sulforhodamine B and Cu^{II}ENZm were fixed with a solution of 3% paraformaldehyde in PBS, and 0.5% glutaraldehyde in PBS containing 1.5% saccharose (pH 7.3), and then post-fixed in 0.5% aqueous osmium tetroxide. The samples were then dehydrated in a graded series of ethanol and block-stained in 6% of uranyl acetate and embedded in LR white resin. Ultra thin sections were contrasted with 0.3% lead citrate and imaged using a Philips Morgagni 268D.

Cytotoxicity assay of Cu^{II}ENZm nanoreactors

The cytotoxicity of the Cu^{II}ENZm-containing nanoreactors was evaluated based on mitochondrial function and membrane integrity of THP-1 cells by using the MTS-(3-(4,5-

dimethylthiazol-2-yl)-5-(3-carboxymethoxyphenyl)-2-(4-sulfophenyl)-2H-tetrazolium) and a lactose dehydrogenase (LDH) assay.

MTS assay

Cells were cultured in a 96-well plate at a density of approximately 2×10^4 cells per well, and incubated with 100 µl of RMPI growth medium/well for 24 h. A series of empty vesicles, free Cu^{II}ENZm and Cu^{II}ENZm nanoreactors at different concentrations was added to different wells and incubated with cells for a period of time (24 and 48 h). Subsequently, 20 µl of CellTiter 96 Aqueous One Solution Cell Proliferation Assay (MTS) reagent (Promega) was added to each well and then incubated for 2 h. The absorbance of each well mixture was measured with a Spectromax M5e microplate reader (Molecular Devices) at λ = 490 nm. Cell viability (%) was calculated as $[A_{sample} / A_{control}] \times 100$. Errors are based on the standard deviation of three independent measurements.

LDH assay

The cytotoxicity of Cu^{II}ENZm nanoreactors was assessed by LDH leakage from THP-1 cells, with a CytoTOX 96 non-radioactive cytotoxicity assay (Promega). Cells were cultured in a 96-well plate at a density of approximately 2×10^4 cells per well, and incubated with 100 µl of RMPI growth medium/well for 24 h. Cells suspensions were then centrifuged at 250 RCF for 5 min, and 50 µl of supernatant were transferred from each well to a new plate. Substrate solution (50 µl) was added and incubated for 30 min. After incubation, a stop solution (50 µl) was added to the wells, and the mixture was immediately measured with a Spectromax M5e microplate reader (Molecular Devices), at λ = 490 nm. Control experiments were performed both for the maximum LDH release after cell lysis with 10 % (v/v) Triton®X-100, and for the LDH released spontaneously from intact cells. Cell culture medium with and without Cu^{II}ENZm nanoreactors was taken into account as background. Cytotoxicity of the samples was calculated according to the manufacturer's protocol.

In-vitro activity of Cu^{II}ENZm nanoreactors

To determine the antioxidant activity of Cu^{II}ENZm nanoreactors, oxidative stress was induced by paraquat and analyzed by flow cytometry (CYAN, BD Biosciences). THP-1 cells at a

density of 1×10^5 plated in a 6-well transparent microplate were first incubated with Cu^{II}ENZm nanoreactors (500 µg/ml) for 24 h, and subsequently with paraquat (2 mM) for further 24 h at 37 °C in a 5% CO_2 atmosphere. Cells were washed with PBS buffer and stained with propidium iodide (PI, 50 µg/ml) to determine cell viability. A total of 10,000 events were analyzed for each condition.

8. Appendix

A1. Optimized structures of models used in DFT computations

MODEL A, [CuLCl] - Optimized structure

Coordinates from ORCA-job

O	-7.190519	-1.471015	-0.137343
O	-5.302588	2.729449	-0.020150
O	0.018234	-1.426313	-0.107058
C	3.245777	1.208592	-0.020664
C	3.417168	-0.193990	-0.049435
C	2.328658	-1.048548	-0.078346
C	0.995596	-0.553066	-0.079982
C	0.823049	0.875484	-0.050613
C	1.965324	1.723580	-0.021379
C	-0.456146	1.505263	-0.047137
N	-1.589274	0.852058	-0.073340
N	-2.767943	1.554769	-0.062958
C	-3.895898	0.814194	-0.078360
N	-3.779328	-0.489297	-0.112237
Cu	-1.856326	-1.116730	-0.125525

Cl	-2.434933	-3.325606	-0.210093
N	-4.914501	-1.252004	-0.135411
C	-6.196085	-0.766785	-0.118828
N	-6.265906	0.637941	-0.078329
C	-5.204242	1.515436	-0.055667
H	-0.490736	2.593897	-0.020410
H	-2.793093	2.566427	-0.010891
H	-4.738692	-2.249959	-0.162157
H	-7.203433	1.034658	-0.064357
H	4.108474	1.869469	0.001773
H	4.422190	-0.612934	-0.048928
H	2.462277	-2.123597	-0.100152
H	1.805893	2.800626	0.000976

MODEL B, [CuL(DMSO)]$^+$ - Optimized structure
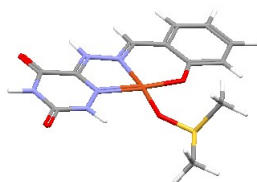
Coordinates from ORCA-job

O	-7.423745	-0.712978	-0.085716
O	-5.189028	3.307449	-0.354847
O	-0.282016	-1.310999	0.028527
C	3.200006	0.975020	-0.134864
C	3.228147	-0.432540	-0.023509

C	2.056833	-1.170207	0.027996
C	0.784191	-0.543628	-0.028506
C	0.754741	0.891165	-0.142954
C	1.978512	1.615613	-0.192590
C	-0.451438	1.653496	-0.211359
N	-1.647329	1.125143	-0.181160
N	-2.758393	1.926941	-0.252166
C	-3.947284	1.286554	-0.208652
N	-3.943513	-0.019548	-0.114125
Cu	-2.093602	-0.780494	-0.045717
O	-2.811240	-2.592435	0.111539
N	-5.137127	-0.685968	-0.079183
C	-6.375284	-0.094936	-0.124354
N	-6.324290	1.307203	-0.221970
C	-5.192629	2.092487	-0.270991
H	-0.368842	2.740040	-0.294496
H	-2.695332	2.937467	-0.296978
H	-5.055351	-1.695192	-0.001262
H	-7.225074	1.780580	-0.258322
H	4.125276	1.543896	-0.174542
H	4.184830	-0.950229	0.022648
H	2.079694	-2.254133	0.113331
H	1.931177	2.700023	-0.278724
S	-1.897349	-3.862090	-0.121672
C	-1.224092	-4.252141	1.516143
C	-3.122626	-5.185521	-0.278487
H	-2.042148	-4.312848	2.240872
H	-0.529930	-3.445100	1.765664

H	-0.688101	-5.204549	1.439811
H	-3.798635	-5.157180	0.581640
H	-2.579004	-6.135206	-0.326353
H	-3.663002	-5.014153	-1.213672

MODEL C, [Cu**L**(DMSO)$_2$]$^+$ - Optimized structure
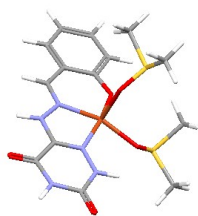
Coordinates from ORCA-job

O	-2.302400	-0.876937	-3.072378
S	-1.246324	-0.941387	-4.237406
C	-2.286826	-1.011216	-5.718045
C	-0.628318	-2.646061	-4.222681
H	-2.782614	-0.040532	-5.809770
H	-3.018718	-1.817729	-5.608377
H	-1.633963	-1.182591	-6.580595
H	-0.080406	-2.763845	-3.283980
H	0.045595	-2.769910	-5.077503
H	-1.471445	-3.342205	-4.277935
O	-6.807266	1.115812	-2.362653
O	-4.785770	3.128580	1.254541
O	0.094041	-0.697291	-1.473345
C	3.415564	0.253405	0.864121

C	3.499768	-0.612663	-0.246821
C	2.380452	-0.911263	-1.006575
C	1.102970	-0.365648	-0.702765
C	1.019266	0.519068	0.432348
C	2.189965	0.804632	1.186176
C	-0.188562	1.170313	0.849063
N	-1.342006	0.996936	0.268285
N	-2.446738	1.679630	0.720259
C	-3.563037	1.552599	-0.041952
N	-3.532886	0.729612	-1.054875
Cu	-1.750578	-0.213753	-1.260323
O	-2.400334	-2.008000	-0.123252
N	-4.652187	0.570651	-1.819962
C	-5.832923	1.248531	-1.643406
N	-5.818999	2.115305	-0.536844
C	-4.760338	2.352582	0.315496
H	-0.130382	1.854263	1.695594
H	-2.363338	2.435445	1.391022
H	-4.525195	-0.031666	-2.622541
H	-6.680256	2.631448	-0.368227
H	4.298671	0.483503	1.454716
H	4.458165	-1.055195	-0.514083
H	2.447559	-1.575386	-1.860134
H	2.100261	1.478584	2.037108
S	-1.632835	-3.348191	-0.274267
C	-0.529028	-3.465156	1.167986
C	-2.825660	-4.631663	0.208531
H	-1.109907	-3.321965	2.085522

Enzyme Mimic to Develop Antioxidant Nanoreactors: From Synthesis to Application

H	0.222829	-2.677099	1.062607
H	-0.044499	-4.447614	1.156350
H	-3.244640	-4.387020	1.190428
H	-2.307692	-5.596625	0.229771
H	-3.611037	-4.645285	-0.553230

MODEL D, [CuL(DMSO)₃]⁺ - Optimized structure
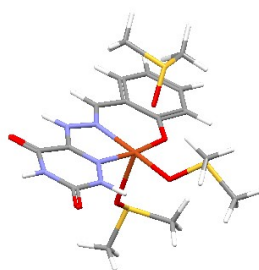
Coordinates from ORCA-job

O	-2.122556	-0.271557	-2.772047
S	-0.940660	-0.032970	-3.740268
C	-1.662360	0.771318	-5.204527
C	-0.553779	-1.641916	-4.501155
H	-2.002857	1.764115	-4.894639
H	-2.503987	0.173677	-5.571236
H	-0.884231	0.865578	-5.969954
H	-0.166533	-2.271356	-3.695122
H	0.211430	-1.490213	-5.270509
H	-1.464861	-2.071974	-4.931427
O	-6.945461	-1.315458	0.055699
O	-4.589620	2.355297	1.541651

O	0.175248	-1.665155	-1.157212
C	3.677921	0.488112	-0.459591
C	3.681685	-0.771756	-1.097390
C	2.504262	-1.467809	-1.310160
C	1.240436	-0.950368	-0.905434
C	1.241498	0.334104	-0.246482
C	2.471255	1.019208	-0.045930
C	0.056419	0.985656	0.234609
N	-1.137662	0.473765	0.143863
N	-2.215168	1.158098	0.647643
C	-3.425120	0.560955	0.497284
N	-3.473466	-0.605573	-0.082856
Cu	-1.652195	-1.266611	-0.695752
O	-2.456486	-3.006168	-1.297805
N	-4.672655	-1.240735	-0.206556
C	-5.882345	-0.735625	0.197755
N	-5.781381	0.527476	0.806148
C	-4.628410	1.259745	1.008031
H	0.171681	1.960293	0.709530
H	-2.134114	2.101283	1.008671
H	-4.618182	-2.129355	-0.686765
H	-6.657062	0.936287	1.126195
H	4.606723	1.029008	-0.296088
H	4.624721	-1.205459	-1.427473
H	2.507308	-2.434739	-1.799535
H	2.442651	1.988724	0.450266
S	-1.802154	-4.357928	-0.839771
C	-1.946381	-5.404035	-2.315041

C	-3.067900	-5.146402	0.192662
H	-1.641429	-6.420759	-2.044442
H	-1.263988	-4.998985	-3.068102
H	-2.979249	-5.384946	-2.677601
H	-3.157003	-4.518921	1.083110
H	-2.717127	-6.148822	0.461648
H	-4.012060	-5.196953	-0.359953
O	-1.663882	-2.523533	1.580854
S	-0.805600	-2.846309	2.818423
C	0.945452	-2.730947	2.324892
C	-0.852507	-1.371216	3.888734
H	1.563074	-2.900714	3.213849
H	1.149719	-1.749068	1.885560
H	1.125018	-3.518747	1.587348
H	-0.557060	-0.489117	3.310220
H	-0.175216	-1.529486	4.735181
H	-1.880789	-1.266012	4.247999

Computed spin Hamiltonian values

In the following Tables, the main computed spin Hamiltonian values are given for the different models. The numbering of the nuclei is given in Scheme 6.

Table A1. Computed g tensors for the different models for Cu^{II}SODm in a DMSO:toluene solution.

	g_x	g_y	g_z
Model A	2.041	2.060	2.163
Model B	2.048	2.051	2.162
Model C	2.055	2.077	2.193
Model D	2.060	2.075	2.203

Table A2. Computed copper A tensors for the different models for Cu^{II}SODm in a DMSO:toluene solution.

	A_x/MHz	A_y/MHz	A_z/MHz
Model A	20.8	-31.8	-558.8
Model B	3.25	-10.68	-589.2
Model C	29.3	109.5	-522.0
Model D	50.8	99.7	-520.5

Table A3. Computed proton A tensors for H^a in the different models for Cu^{II}SODm in a DMSO:toluene solution. (A_z is perpendicular to the **L** plane, A_x points in the direction of the copper ion).

	A_x/MHz	A_y/MHz	A_z/MHz
Model A	22.29	18.85	17.94
Model B	21.34	18.02	17.25
Model C	21.17	17.68	16.79
Model D	20.22	16.71	15.86

Table A4. Computed proton A tensors for H^b in the different models for Cu^{II}SODm in a DMSO:toluene solution. (A_x is approximately along the H-N bond, A_z is approximately perpendicular to the plane of **L**).

	A_x/MHz	A_y/MHz	A_z/MHz
Model A	11.07	6.73	5.62
Model B	11.44	6.93	5.85
Model C	9.68	5.14	4.17
Model D	9.98	5.50	4.52

Table A5. Computed proton A tensors for H^c in the different models for $Cu^{II}SODm$ in a DMSO:toluene solution. (A_x is pointing towards the copper ion, A_z is perpendicular to the plane of **L**).

	A_x/MHz	A_y/MHz	A_z/MHz
Model A	7.11	-0.65	1.13
Model B	6.24	0.27	-1.11
Model C	7.21	0.00	-0.06
Model D	7.27	0.74	-0.88

Table A6. Computed proton A tensors for H^d in the different models for $Cu^{II}SODm$ in a DMSO:toluene solution. (A_z is perpendicular to the plane of **L**, A_y is pointing in the direction of the copper ion)

	A_x/MHz	A_y/MHz	A_z/MHz
Model A	-1.83	1.74	-2.61
Model B	-1.80	2.10	-2.57
Model C	-1.78	1.83	-2.50
Model D	-1.71	1.82	-2.37

Table A7. Computed nitrogen hyperfine and nuclear quadrupole tensors for N_1 in the different models for $Cu^{II}SODm$ in a DMSO:toluene solution. (A_z is perpendicular to the plane of **L**, A_y is pointing in the direction of the copper ion. The largest nuclear quadrupole coupling is approximately along A_x, the smallest nuclear quadrupole value (in absolute value) is lying approximately perpendicular to the **L** plane)

	A_x/MHz	A_y/MHz	A_z/MHz	e^2qQ/h /MHz	η
Model A	45.03	58.40	46.96	3.775	0.412
Model B	45.86	59.75	47.89	3.779	0.396
Model C	41.76	54.44	43.70	3.779	0.530
Model D	41.68	53.97	43.55	3.826	0.600

Table A8. Computed nitrogen hyperfine and nuclear quadrupole tensors for N_2 in the different models for $Cu^{II}SODm$ in a DMSO:toluene solution. (A_z and P_z are quasi perpendicular to the plane of **L**,

	A_x/MHz	A_y/MHz	A_z/MHz	e^2qQ/h /MHz	η
Model A	-0.02	-1.02	-1.92	-5.00	0.52
Model B	-0.02	-1.04	-1.90	-5.03	0.53
Model C	-0.24	-1.21	-2.01	-5.04	0.51
Model D	-0.17	-1.04	-1.89	-5.09	0.49

Table A9. Computed nitrogen hyperfine and nuclear quadrupole tensors for N_5 in the different models for Cu^{II}SODm in a DMSO:toluene solution. (A_z is perpendicular to the plane of **L**, A_y is pointing in the direction of the copper ion. The largest nuclear quadrupole coupling is approximately along A_x, the smallest nuclear quadrupole value (in absolute value) is lying approximately perpendicular to the **L** plane).

	A_x/MHz	A_y/MHz	A_z/MHz	e^2qQ/h/MHz	η
Model A	39.27	49.14	40.95	3.680	0.298
Model B	36.46	45.96	38.07	3.708	0.288
Model C	34.23	43.22	35.80	3.731	0.457
Model D	33.98	42.71	35.55	3.786	0.508

Table A10. Computed nitrogen hyperfine and nuclear quadrupole tensors for N_4 in the different models for Cu^{II}SODm in a DMSO:toluene solution. (A_z and P_z are perpendicular to the plane of **L**, P_x is approximately parallel to A_y).

	A_x/MHz	A_y/MHz	A_z/MHz	e^2qQ/h/MHz	η
Model A	1.07	0.10	0.34	-5.03	0.66
Model B	2.05	1.02	1.25	-5.22	0.60
Model C	1.78	0.83	1.05	-5.04	0.62
Model D	1.72	0.81	1.01	-4.96	0.61

Table A11. Computed nitrogen hyperfine and nuclear quadrupole tensors for N_3 in the different models for Cu^{II}SODm in a DMSO:toluene solution. (A_z is perpendicular to the plane of **L**, P_z lies along A_y, P_y is approximately perpendicular to **L**)

	A_x/MHz	A_y/MHz	A_z/MHz	e^2qQ/h/MHz	η
Model A	0.10	-0.08	-0.11	-3.42	0.27
Model B	0.15	-0.03	-0.07	-3.43	0.28
Model C	0.13	-0.08	-0.04	-3.43	0.27
Model D	0.11	-0.06	-0.10	-3.43	0.26

9. References

[1] Kwon, G. S.; Kataoka, K. *Adv. Drug Deliv. Rev.* 1995, *16*, 295.

[2] Kwon, G. S.; Okano, T. *Adv. Drug Deliv. Rev.* 1996, *21*, 107.

[3] V. Balasubramanian, O. Onaca, R. Enea, D. Hughes, C.G. Palivan, Expert. Opin. Drug Delivery, 2010, 7(1), 63.

[4] Monica C. Branco, Joel P. Schneider, Acta Biomaterialia, 2009, 5, 831.

[5] Caruso, F., *Colloids and colloid Assembly*, 2004, Wiley-VCH GmbH & Co. KGaA.

[6] Kita-Tokarczyk, K., et al., Polymer, 2005, 46(11), 3563.

[7] Kwon, G. S. *Crit. Rev. Ther. Drug,* 1998, *15*, 481.

[8] Battaglia, G. and A.J. Ryan, Nat. Mater., 2005, 4(11), 876.

[9] Zhang, L.E., A., J. Polym. Sci., Part B: Polym. Phys., 1999, 37, 1469.

[10] Shen H., Eisenberg A. *Macromolecules* 2000, *33*, 2561.

[11] Yu Y., Eisenberg A. *J. Am. Chem. Soc.* 1997, *119*, 8383.

[12] D.E. Discher, A. Eisenberg, Science, 2002, 297, 973.

[13] L. Yang, P. Alexandridis, Curr.Opin. Colloid In., 2000, 5, 132.

[14] C. Allen, D. Maysinger, A. Eisenberg, Colloids Surfaces B, 1999, 16, 3.

[15] Yu Y, Zhang L, Eisenberg A (1998) Macromolecules 31:1144.

[16] Tuzar, Z. and P. Kratochvil, Surface and Colloid Science, 1993, 15, 1.

[17] Price, C., Developments in Block Copolymers, 1982, 1, 80.

[18] De Gennes, P.G., Solid State Physics, Supplement, 1978, 14, 18.

[19] Gao, Z., et al., Macromolecules, 1994, 27(26), 7923.

[20] Rapoport N. *Int. J. Pharm.* 2004, 277, 155.

[21] Shuai X., Merdan T., Schaper A. K., Xi F., Kissel T. *Bioconjug. Chem.* 2004, 15, 441.

[22] Nishiyama N., Okazaki S., Cabral H., Miyamoto M., Kato Y., Sugiyama Y., Nishio K., Matsumara Y., Kataoka K. *Cancer. Res.* 2003, *63*, 8977.

[23] Djordjevic J., Barch M., Uhrich K. E. *Pharm. Res.* 2005, *22*, 24.

[24] M.C. Jones, J.C. Leroux, Eur. J Pharm. Biopharm., 1999, 48, 101.

[25] M. Antonietti and S. Forster, Adv. Mater., 2003, 15, 1323.

[26] L.Chen,H. Shen, A.Eisenberg, J. Phys. Chem., B 1999, 103, 9488.

[27] X. He, F. Schmid, Macromolecules, 2006, 39, 2654.

[28] D. J. Adams, S. Adams, D. Atkins, M. F. Butler, S. Furzeland, J. Cont. Release, 2008, 128, 165.

[29] O. Onaca, D. W. Hughes, V. Balasubramanian, M. Grzelakowski, W. Meier, C. Palivan, *Macromol. Biosci.,* 2010, 10, 531.

[30] P. L. Soo and A. Eisenberg, J. Polym. Sci: Polym. Phys., 2004, 42, 923.

[31] L. Ma and A. Eisenberg, Langmuir, 2009, 25, DOI: 10.1021/la9012729.

[32] J. Du, R. K. O'Reilly, Soft Matter, 2009, 5, 3544.

[33] F. Meng, Z. Zhong and J. Feijen, Biomacromolecules, 2009, 10, 197.

[34] S. Litvinchuk, Z. Lu, P. Rigler, T. D. Hirt and W. Meier, Pharmaceutical Research, 2009, 26, 1711.

[35] O. Onaca, R. Enea, D. W. Hughes and W. Meier, Macromol. Biosci., 2009, 9,129.

[36] S. Egli, M. Nussbaumer, V. Balasubramanian, M. Chami, N. Bruns, C. Palivan, W. Meier, J Am. Chem. Soc., 2011, 133 (12), 4476.

[37] M. Grzelakowski, O. Onaca, P. Rigler, M. Kumar, W. Meier, *small*, 2009, 5 (22), 2545.

[38] Chen, Q., Schoenherr, H. & Vancso, G. J., *Small.*2009, 5, 1436.

[39] P.Tanner, S. Egli, V. Balasubramanian, O. Onaca, C. Palivan, W. Meier, FEBS letters, 2011, DOI: 10.1016/j.febslet.2011.05.003.

[40] C. Nardin, D. Bolikal, J. Kohn, Langmuir, 2004, 20, 11721.

[41] R. Stoenescu, A. Graff, W. Meier, Macromol Biosci, 2004, 4, 930.

[42] C. Nardin, Hirt, T., Leukel, J., Meier, W., Langmuir, 2000, 16, 1035.

[43] Nallani M, Benito S, Onaca O, et al. J Biotechnol 2006;123:50-9

[44] Ranquin A, Versees W, Meier W, et al. Nano Lett., 2005, 5, 2220.

[45] Vocht, C. D; Ranquin, A.; Willaert, R.; Ginderachter, J. V. A.; Vanhaecke, T.; Rogiers, V.; Versees, W.; Gelder, P. V.; Steyaert, J. *J. Control. Release,* 2009, 137, 254.

[46] V. Dongen, S. F. M., Nallani, M., Cornelissen, J. J. L. M., Nolte, R. J. M.,Van Hest, J. C. M., *Chemistry – A European Journal*, 2009, 15, 1107.

[47] C. Nardin, S. Thoeni, J. Widmer, M. Winterhalter, W. Meier,Chemcomm., 2000, 1433.

[48] Kumar M, Grzelakowski M, Zilles J, et al. Proc Nat Acad Sci USA, 2007, 104, 20719.

[49] Graff A, Sauer M, Gelder PV, Meier W. Proc Nat Acad Sci USA, 2002, 99, 5064.

[50] Kohen R, Gati I, *Toxicology* , 2000, 148, 149.

[51] Comporti M, Three models of free radical-induced cell injury. *Chem Biol Interact,* 1989, 72, 1.

[52] Halliwell B, Gutteridge. J. M, *Free Radicals in Biology and Medicine*, third edition. 1999, Oxford University Press,Midsomer Norton, Avon, England.

[53] R. Kohen, A. Nyska, Toxicologic pathology, 2002, 30, 620.

[54] W. Droege, Oxidative Stress, Disease and Cancer, ed. K. K. Singh, Imperial College Press, London, 2006, 885.

[55] J. E. Slemmer, I. J. Shacka, M. I. Sweeney and J. T. Weber, Curr. Med. Chem., 2008, 15, 404.

[56] Davies, K.J.A., *Oxidative stress: the paradox of aerobic life.* Biochemical Society Symposia, 1995. 61, 1.

[57] Stohs, S.J., Oxidative Stress and Antioxidant Defenses in Biology, 1995, 117.

[58] McCord JM, Fridovich I, *J Biol Chem.,* 1969, 244, 6049.

[59] Lardinois O. M, *Free Radic Res,* 1995*,* 22, 251.

[60] Chance B, Sies H, Boveris A (1979). *Physiol Rev* 59: 527–605.

[61] Dore, S. and S.H. Snyder, Annals of the New York Academy of Sciences, 1999, 890, 167.

[62] Maharaj, D.S., B.D. Glass, S. Daya, Bioscience Reports, 2007, 27(6), 299.

[63] Rodriguez, M.C., et al., Muscle & Nerve, 2007, 35(2), 235.

[64] Strazzullo, P. and J.G. Puig, Nutrition, Metabolism & Cardiovascular Diseases, 2007, 17(6), 409.

[65] Yang G, Chan P H, Chen J, Carlson E, Chen S F, Weinstein P, et al. Stroke, 1994, 25, 165.

[66] Oyanagui Y. Biochem Pharmacol., 1976, 25, 1465.

[67] Andreassen O A, Ferrante R J, Dedeoglu A, Albers D W, Klivenyi P, Carlson E J, Epstein C J, Beal M F. Exp Neurol., 2001, 167(1), 189.

[68] Salminen U, Harjula A L, Maasilta P K, Romanska H M, Bishop A E, Polak J M. Transplant Proc 2001, 33, 2477.

[69] Barnes J P. Chronic obstructive pulmonary disease. N Engl J Med., 2000, 343, 269.

[70] Klivenyi P, St Clair D, Wermer H, Yen H C, Oberly T, Yang L, Beal MF. Neurobiol Dis., 1998, 5, 253.

[71] Jiang ZY, Woollard AC, Wolff SP. FEBS Lett., 1990, 268(1), 69.

[72] Guo Dong Mao, anakkezhum. Thomas, Gary. Lopaschuk, and Mark. Poznansky, J. Biol. Chem.,1993, 268(1), 416.

[73] G. Luo, W. Liu, Q. Sun, L. Ding, Z. Zhu, G. Yan, T. Yang, Bifunctional enzymes, Annals New York Academy of Sciences,1996, 799, 50.

[74] Kawada, T., et al., Journal of Applied Physiology, 1992, 73(4), 1326.

[75] Breuer, R., et al., Lung, 1992, 170(1), 19.

[76] Wright, S.E., D.A. Baron, and J.E. Heffner, Journal ofLaboratory and Clinical Medicine, 1995, 125(2), 257.

[77] Jadot, G., et al., Clinical pharmacokinetics, 1995, 28(1), 17.

[78] D. Salvemini, C. Muscoli, D. P. Riley, S. Cuzzocrea, Pulmonary Pharmacology & Therapeutics 2002, 15, 439.

[79] O. Vajragupta, P. Boonchoong, Y. Sumanont, H.Watanabe, Y. Wongkrajang, N. Kammasuda, Bioorganic & Medicinal Chemistry, 2003, 11, 2329.

[80] R. N. Patel, N. Singh, K. K. Shukla, V. L. N. Gundla Spectrochim. Acta Part A, 2005, 61, 1893.

[81] Tamura M, Urano Y, Kikuchi K, Higuchi T, Hirobe M, Nagano T., Chem Pharm Bull, 2000, 48(10), 1514.

[82] Li-Hu, Chen, Liu-Zhan Liu, Han-Xi Shen, Analytica Chimica Acta, 2003, 480, 143.

[83] U. Borgmann, In: Nriagu, J.O. (Ed.), Aquatic Toxicology. Wiley, New York, 1983, 47.

[84] Hidalgo I, Models for Assessing Drug Absorption and Metabolism, Editors: Borchardt RT, Smith PL, Wilson G), Plenum Press, New York, 1996, 35. 1996.

[85] G. Jadot, A. Vaille, J. Maldonado, P. Vanelle, Clin. Pharmacokinet. 1995, 28, 17.

[86] C. Regnault, M. Soursac, M. Roch-Arveiller, E. Postaire,G. Hazebroucq, Biopharm. Drug Dispos. 1996, 17, 165.

[87] J. H. Kang, K. S. Kim, S. Y. Choi, H. Y. Kwon, M. H. Won, T. C. Kang, BBA Gen Subjects 2002, 89, 1570.

[88] A. V. Maksimenko, Curr. Pharm. Des. 2005, 11, 2007.

[89] M. M. Gaspar, O. C. Boerman, P. Laverman, M. L. Corvo, G.Storm, M. E. Cruz, J. Controlled Release 2007, 117, 186.

[90] T. T. Jubeh, S. Antler, S. Haupt, Y. Barenholz, A. Rubinstein,Mol. Pharm. 2005, 2, 2.

[91] M. G. Saifer, R. Somack, L. D. Williams, Adv. Exp. Med. Biol.1994, 366, 377.

[92] Y. Barenholz, Curr. Opin. Colloids Interfaces 2001, 6, 66.

[93] K. Hirakaa, M. Kanehisaa, M. Tamaia, S. Asayamaa, S. Nagaokaa, K. Oyaizuc, M. Yuasa, K. H. Kawakamia, *Colloids and Surf. B: Biointerfaces,* 2008, 67, 54.

[94] H. Nagami, H. Umakoshi, T. Shimanouchi, R. Kuboi, *J. Biochem. Eng.,* 2004, 21, 221.

[95] H. Umakoshi, K. Morimoto, Y.Ohama, H. Nagami, T. Shimanouchi, R. Kuboi, *Langmuir* 2008, 24, 4451.

[96] H. Umakoshi, K. Morimoto, N. Yasuda, T. Shimanouchi, R. Kuboi, Journal of Biotechnology 147, 2010, 59.

[97] Charles Y. Cheung, Suzanne J. McCartney, and Kristi S. Anseth, Adv. Funct. Mater. 2008, 18, 3119.

[98] T. Piacham, C. I. Ayudhya, V. Prachayasittikul, L. Bulowa, L.Ye, *Chem. Commun.* , 2003, 1254.

[99] F. Axthelm, O. Casse, W. H. Koppenol, T. Nauser, W. Meier, C. G. Palivan, J. Phys. Chem. B 2008, 112, 8211.

[100] P. Broz, S. M. Benito, C. L. Saw, P. Burger, H. Heider, M. Pfisterer, S. Marsch, W. Meier, H. Hunziker, J. Control. Rel., 102, 475, 2005.

[101] a) J. Casanova, G. Alzuet, S. Ferrer, J. Latorre, J. A. Ramirez,J. Barras, Inorg. Chim. Acta 2000, 304, 170; b) H. Ohtsu,Y. Shimazaki, A. Odani, O. Yamauchi, W. Mori, S. Itoh, S.Fukuzumi, J. Am. Chem. Soc. 2000, 122, 5733; c) M. L. P.Santos, I. A. Bagatin, E. M. Pereira, A. M. D. C. Ferreira, J.Chem. Soc., Dalton Trans. 2001, 838; d) Q. X. Li, Q. H. Luo, Y. Z. Li, M. C. Shen, Dalton Trans. 2004, 2329; e) U. Weser, L. M. Schubotz, J. Mol. Catal. 1981, 13, 249; f) R. N. Patel, V. L. N. Gundla, D. K. Patel, Polyhedron 2008, 27, 1054; g) R. N. Patel, N. Singh, K. K. Shukla, U. K. Chauhan, J. N. Gutierrez, A. Castineiras, Inorg. Chim. Acta 2004, 357, 2469; h) R. N. Patel, N. Singh, K. K. Shukla, U. K. Chauhan, Spectrochim. Acta, Part A 2005, 61, 287; i) R. N. Patel, N. Singh, K. K. Shukla, V. L. N. Gundla, Spectrochim. Acta, Part A 2005, 61, 1893; j) A. L. Abuhijleh, C. Woods, Inorg. Chem. Commun. 2002, 5, 269; k) F. Afreen, P. Mathur, A. Rheingold, Inorg. Chim. Acta 2005, 358, 1125; l) R. P. Bonomo, F. D. Alessandro, G. Grasso, G. 4638, Eur. J. Inorg. Chem. 2009, 4634; m) M. Devereux, D. O'Shea, M. O'Connor, H. Grehan, G. Connor, M. McCann, G. Rosair, F. Lyng, A. Kellett, M. Walsh, D. Egan, B. Thati, Polyhedron 2007, 26, 4073; n) H. Fu, Y. H. Zhou, W. L. Chen, Z. G. Deqing, M. L. Tong, L. N. Ji, Z. W. Mao, J. Am. Chem. Soc. 2006, 128, 4924; o) D. Li, S. Li, D. Yang, J. Yu, J. Huang, Y. Li, W. Tang, Inorg. Chem. 2003, 42, 6071; p) R. N. Patel, N. Singh, K. K. Shukla, V. L. N. Gundla, U. K. Chauhan, J. Inorg. Biochem. 2005, 99, 651; q) G. Qin, L. X. Yi, L. Q. Bin, L. S. Rong, M. X. Dan, F. X. Long, Chin. J. Chem. 2007, 25, 791; r) A. G. Raso, J. J. Fiol, B. Adrover, P. Tauler, A. Pons, I. Mata, E. Espinosa, E. Molins, Polyhedron 2003, 22, 3255; s) F. Saczewski, E. D. Borys, P. J. Bednarski, M. Gdaniec, Arch. Pharm. Chem. Life Sci. 2007, 340, 333; t) F. Saczewski, E. D. Borys, P. J. Bednarski, R. Grunert, M. Gdaniec, P. Tabin, J. Inorg. Biochem. 2006, 100, 1389; u) M. Tofazzal, H. Tarafder, N. Saravanan, K. A. Crouse, Transition Met. Chem. 2001, 26, 613; v) B. Verdejo, S. Blasco, E. G. Espana, F. Lloret, P. Gavina, C. Soriano, S. Tatay, H. R. Jimenez, A. Domenech, J. Latorre, Dalton Trans. 2007, 41, 4726; w) J. Patole, S. Dutta, S. Padhye, E. Sinn, Inorg. Chim. Acta 2001, 318, 207.

[102] a) K. Jitsukawa, M. Harata, H. Arii, H. Sakurai, H. Masuda, *Inorg. Chim. Acta* 2001, *324*, 108; b) J. Muller, K. Felix, C. Maichle, E. Lengfelder, J. Strahle, U. Weser, *Inorg. Chim. Acta* 1995, *233*, 11; c) J. Muller, D. Schubl, C. M. Mossmer, J. Strahle, U. Weser, *J. Inorg. Biochem.* 1999, *75*, 63; d) R. N. Patel, N. Singh, V. L. N. Gundla, U. K. Chauhan, *Spectrochim. Acta, Part A* 2007, *66*, 726; e) A. S. Fernandes, J. Gaspar, M. F. Cabral, C. Caneiras, R. Guedes, J. Rueff, M. Castro, J. Costa, N. G. Oliveira, *J. Inorg. Biochem.* 2007, *101*, 849; f) E. T. Nomkoko, G. E. Jackson, B. S. Nakani, *Dalton Trans.* 2004, 1432; g) R. N. Patel, N. Singh, K. K. Shukla, J. N. Gutierrez, A. Castineiras, V. G. Vaidyanathan, B. U. Nair, *Spectrochim. Acta, Part A* 2005, *62*,

261; h) C. Urquiola, D. Gambino, M. Cabrera, M. L. Lavaggi, H. Cerecetto, M. Gonzalez, A. L. D. Cerain, A. Monge, A. J. C. Filho, M. H. Torre, *J. Inorg. Biochem.* 2008, *102*, 119; i) Y. H. Zhou, H. Fu, W. X. Zhao, W. L. Chen, C. Y. Su, H. Sun, L. N. Ji, Z. W. Mao, *Inorg. Chem.* 2007, *46*, 734.

[103] a) S. Dutta, S. Padhye, F. Ahmed, F. Sarkar, *Inorg. Chim. Acta* 2005, *358*, 3617; b) I. Schepetkin, A. Potapov, A. Khlebnikov, E. Korotkova, A. Lukina, G. Malovichko, L. Kirpotina, M. T. Quinn, *J. Biol. Inorg. Chem.* 2006, *11*, 499; c) A. L.Abuhijleh, *J. Inorg. Biochem.* 1997, 167; d) M. Devereux, M. McCann, D. O'Shea, M. O'Connor, E. Kiely, V. McKee, D. Naughton, A. Fisher, A. Kellett, M. Walsh, D. Egan, C. Deegan, *Bioinorg. Chem. Appl.* 2006, 1; e) T. Fukuuchi, K. D. Ura, S. Yoshihara, S. Ohta, *Bioorg. Med. Chem. Lett.* 2006, *16*, 5982; f) C. M. Liu, R. G. Xiong, X. Z. You, *Polyhedron* 1997, *16*, 119; g) R. N. Patel, N. Singh, K. K. Shukla, V. L. N. Gundla, U. K. Chauhan, *Spectrochim. Acta, Part A* 2006, *63*, 21; h) R. G. Bhirud, T. S. Srivastava, *Inorg. Chim. Acta* 1991, *179*, 125.

[104] a) M. G. Alvarez, G. Alzuet, J. Borras, L. C. Agudo, J. M. M. Bernardo, S. G. Granda, *J. Biol. Inorg. Chem.* 2003, *8*, 112; b) M. G. Alvarez, G. Alzuet, J. Borras, L. C. D. Agudo, S. G. Granda, J. M. M. Bernardo, *J. Inorg. Biochem.* 2004, *98*, 189; c) M. G. Alvarez, G. Alzue, J. Borras, L. C. Agudo, S. G. Granda, J. M. M. Bernardo, *Inorg. Chem.* 2005, *44*, 9424; d) R. C. Marin, G. Alzuet, S. Ferrer, J. Borras, *Inorg. Chem.* 2004, *43*, 6805; e) M. G. Alvarez, G. Alzuet, J. Borras, B. Macias, J. M. M. Bernardo, S. G. Granda, *Z. Anorg. Allg. Chem.* 2003, *629*, 239; f) E. Kremer, G. Facchin, E. Estevez, P. Albores, E. J. Baran, J. Ellenad, M. H. Torre, *J. Inorg. Biochem.* 2006, *100*, 1167.

[105] a) B. Boka, A. Myari, I. Sovago, N. Hadjiliadis, *J. Inorg. Biochem.* 2004, *98*, 113; b) M. Casolaro, M. Chelli, M. Ginanneschi, F. Laschi, L. Messori, M. M. Miranda, A. M. ini, T. K. Jankowska, H. Kozlowski, *J. Inorg. Biochem.* 2002, *89*, 181; c) Z. Arkosi, Z. Paksi, L. Korecz, T. Gajda, B. Henry, A. Rockenbauer, *J. Inorg. Biochem.* 2004, *98*, 199; d) G.Facchin, M. H. Torre, E. Kremer, O. E. Piro, E. E. Castellano, E. J. Baran, *J. Inorg. Biochem.* 2002, *89*, 174; e) E. G. Ferrer, L. L. L. Tevez, N. Baeza, M. J. Correa, N. Okulik, L. Lezama, T. Rojo, E. E. Castellano, O. E. Piro, P. A. M. Williams, *J. Inorg. Biochem.* 2007, *101*, 741; f) A. Jancso, Z. Paksi, N. Jakab, B. Gyurcsik, A. Rockenbauer, T. Gajda, *Dalton Trans.* 2005, 3187; g) R. Pogni, M. C. Baratto, E.Busi, R. Basosi, *J. Inorg. Biochem.* 1999, *73*, 157.

[106] a) A. M. C. Ferreira, M. L. P. Santos, E. M. Pereira, M. O. Damasceno, W. A. Alvesa, Acad. Bras. Ci. 2000, 72, 51; b) M. L. P. Santos, A. F. Alario, A. S. Mangrich, A. M. C. Ferreira, J. Inorg. Biochem. 1998, 71, 71; c) K. Serbest, A. Colak, S. Guner, S. Karabocek, Transition Met. Chem. 2001, 26, 625.

[107] a) T. Fujimori, S. Yamada, H. Yasui, H. Sakurai, *J. Biol. Inorg. Chem.* 2005, *10*, 831; b) A. Diaz, R. Cao, A. Fragoso, I. Sanchez, *Inorg. Chem. Commun.* 1999, *2*, 358.

[108] a) R. P. Bonomo, V. Bruno, E. Conte, G. D. Guidi, D. L. Mendola, G. Maccarrone, F. Nicoletti, E. Rizzarelli, S. Sortino, G. Vecchio, *Dalton Trans.* 2003, 4406; b) F. Bellia, D. L. Mendola, G. Maccarrone, P. Mineo, D. Vitalini, E. Scamporrino, S. Sortino, G. Vecchio, E. Rizzarelli, *Inorg. Chim. Acta* 2007, *360*, 945.

[109] a) A. Barik, B. Mishra, L. Shen, H. Mohan, R. M. Kadam, S. Dutta, H. Y. Zhang, K. I. Priyadarsini, Free Radical Biol. Med. 2005, 39, 811; b) A. Barik, B. Mishra, A. Kunwar, R. M.

Eur. J. Inorg. Chem. 2009, 4634; L. Shen, S. Dutta, S. Padhye, A. K. Satpati, H. Y. Zhang, K. I. Priyadarsini, Eur. J. Med. Chem. 2007, 42, 431.

[110] a) C. G. Palivan, B. A. Goodman, *Recent Research Developments in Inorganic and Organometallic Chemistry*, Pandalai, India, 2001, 141; b) B. A. Goodman, C. G. Palivan, H. Palivan, S. Tomas, *Appl. Magn. Resn.* 2003, *25*, 13; c) C. G. Palivan, H. Palivan, B. A. Goodman, C. Cristescu, *Appl. Magn. Reson.* 1998, *15*, 477; d) C. G. Palivan, C. Darmon, S. Thomas, *Bull. Magn. Reson.* 1999, *19*, 29.

[111] A. M. Ramandan, *J. Inorg. Chem.* 1997, 183.

[112] a) A. E. O. Fisher, G. Lau, D. P. Naughton, *Biochem. Biophys. Res. Commun.* 2005, *329*, 930; b) Z. Durackova, M. A. Mendiola, M. T. Sevilla, A. Valent, *Bioelectrochem. Bioenerg.* 1999, *48*, 109; c) S. Autzen, H. G. Korth, R. Boese, H. Groot, R. Sustmann, *Eur. J. Inorg. Chem.* 2003, 1401; d) D. K. Demertzi, A. Galani, M. A. Demertzis, S. Skoulika, C. Kotoglou, *J. Inorg. Biochem.* 2004, *98*, 358; e) R. G. Bhirud, T. S. Srivastava, *Inorg. Chim. Acta* 1990, *173*, 121; f) C. A. Boswell, X. Sun, W. Niu, G. R. Weisman, E. H. Wong, A. L. Rheingold, C. J. Anderson, *J. Med. Chem.* 2004, *47*, 1465.

[113] a) I. H. Batinic, I. Spasojevic, R. D. Stevens, P. Hambright, P. Neta, A. M. Okado, I. Fridovich, *J. Chem. Soc. Dalton Trans*. 2004, *11*, 1696; b) R. J. F. Branco, P. A. Fernandes, M. J. Ramos, *J. Mol. Struct. Theochem.* 2005, *729*, 141.

[114] B. J. Hathaway, *Comprehensive Coordination Chemistry,* Pergamon Press, Oxford, 1987, 5, 634.

[115] a) D. Riley, O. F. Schall, *Adv. Inorg. Chem.* 2007, 59, 233.

[116] J. M. McCord, I. Fridovich, *J. Biol. Chem*. 1969, *244 (22)*, 6049.

[117] a) E. Michel, T. Nauser, B. Sutter, P. L. Bounds, W. H. Koppenol, *Arch. Biochem. Biophys.* 2005, *439*, 234-240. b) D.P. Riley, *Chem. Rev*. 1999, *99*, 2573.

[118] J. P. Hart, M. M. Balbirnie, N. L. Ogihara, A. M. Nersissian, M. S. Weiss, J. S. Valentile, D. Eisenberg, *Biochemistry*, 1999, *38*, 2167.

[119] B. A. Goodman, C. G. Palivan, C. Cristescu, *Polyhedron*, 1995, 14, 2523.

[120] Z. H. Chohan, H. Pervez, A. Rauf, K. M. Khan, G. M. Maharvi, C. T. Supuran, J. Enzyme Inhib. Med. Chem., 2004, 19, 161.

[121] 56 Y. Li, Z. Yang and B. Wang, Transition Met. Chem., 2006, 31, 598.

[122] R. P. Bonomo, F. D'Alessandro, G. Grasso, G. Impellizzeri, G. Pappalardo, E. Rizzarelli and G. Tabi, Inorg. Chim. Acta, 2008, 361, 1705.

[123] J. Peisach and W. E. Blumberg, Arch. Biochem. Biophys., 1974,165, 691.

[124] F. Sackzewski, E. Dziemidowicz Borys, P. J. Bednarski, R. Grunert, M. Gdaniec and P. Tabin, J. Inorg. Biochem., 2006, 100, 1389.

[125] K. G. Strothkamp and S. J. Lippard, J. Am. Chem. Soc., 1982, 104,852.

[126] A. Schweiger and G. Jeschke, Principles of Pulse Electron Paramagnetic Resonance, University Press Oxford, Oxford, 2001.

[127] A. Schweiger and Hs. H. Gü̈nthard, Chem. Phys., 1978, 32, 35.

[128] S. Kita, M. Hashimoto and M. Iwaizumi, Inorg. Chem., 1979, 18, 3432.

[129] H. Ukeda, D. Kawana, S. Maeda and M. Sawamura, Biosci., Biotechnol., Biochem., 1999, 63, 485.

[130] J. Serrano, M. Jove, J. Boada, M. J. Bellmunt, R. Pamplona, M. Portero-Otín, *Biochem. Biophys. Res. Commun.*, 2009, 388, 443.

[131] Jensen, D. K.; Kopeckova, P.; Bridge, J. H. B.; Kopecek, J. *Pharm. Sci.* 2001, 3(4), 1.

[132] R. M. Zucker, E. J. Massaro, K. M. Sanders, L. L. Degn, W. K. Boyes, Cytometry Part A, 2010, 77A, 677.

[133] **N. S. Claxton, T. J. Fellers, M. W. Davidson, confocal laser scanning microscopy.**

[134] Musyanovych, A.; Wienke, J. S.; Mailander, V.; Walther, P.; Landfester, K. *Macromol. Biosci.* 2008, 8, 127.

[135] Win K. Y.; Feng, S. S. *Biomaterials.* 2005, 26(15), 2713.

[136] Malich, G.; Markovic, B.; Winder. C. *Toxicology.* 1997, 124, 179.

[137] Tan, A. S.; Berridge, M. V. *J. Immunol. Methods.* 2000, 238, 59.

[138] Granfeldt, D.; Dahlgren, C. *Inflammation,* 2001, 25(3), 165.

[139] Allen, J. M.; Rushton, N. *Promega Notes Magazine.* 45: 7-11; 1994.

[140] Pauser, S.; Keller, K.; Zschunke, A.; Mugge, C. *Mag. Reson. Imaging.* 1993, 11, 419.

[141] Black, A. T.; Gray, J. P.; Shakarjian, M. P.; Laskin, D. L.; Heck, D. E.; Laskin, J. D. *Toxicol. Appl. Pharmacol.,* 2008, 231, 384.

[142] Drechsel, D. A.; Patel, M.; *Free Radic. Biol. Med.,* 2008, 44, 1873.

[143] Chen,   Y.; Ward, E. M.; Kong, S.; Israels, S. J.; Gibson, S. B. *Cell Death and Differ.,* 2008, 15, 171.

[144] J.S. Valentine, P.A. Doucette, S.Z. Potter, *Annu. Rev. Biochem.*, 2005, *74*, 563-593.

[145] S. Stoll, A. Schweiger, *J. Magn. Reson.*, 2006, 178, 42.

[146] Z. L. Madi, S. Van Doorslaer and A. Schweiger, *J. Magn. Reson.*, 2002, 154, 181.

[147] G. Williams, D. C. Watts, S. B. Dev, A. M. North, *Trans. Faraday Soc.,* 1971, 67, 1323.

10. Acknowledgements

It is very difficult to express the great feelings in words, as the gratitude a feel with people who helped me to make this thesis possible. To begin with, I am especially grateful to **PD. Dr. Cornelia. G. Palivan**, without her, this thesis would not have been possible. I sincerely thank her for giving me her valuable time, stimulating suggestions, encouragement and friendship. I would like to express my gratitude to, **Prof. Wolfgang Meier**, University of Basel, Switzerland, who gave the possibility to work on this project in his group.

I am indebted to Prof. Sabine Van Doorslaer and Dr. Maria Ezhevskaya for successful collaboration on detailed EPR experiments. I would like to thank Dr. Ozana Onaca and Pascal Tanner for collaboration and suggestions in all the time of my research in University of Basel. I extend my thanks to other collaborators: Dr. C. Cristescu from CPRI, Bucharest, for providing the ligand for $Cu^{II}ENZm$, S. Dockheer in the group of Prof. W. Koppenol, ETHZ for help with the pulse radiolysis measurements, Vesna Olivieri, Ursula Sauder from ZMB and Gaby for TEM measurements, Verena Jaeggin, Dr. Balasubramanian Sivasankaran from University Hospital, Basel for flow cytometry experiments, Hans Moons for DFT calculations and Markus Neuburger for X-ray crystallographic experiments, Dr. Mariusz Grzelakowski for providing polymers, Dr. Julia Razumovitch for training in cell culture handling, David Hughes for helping me with synthesis of ligand and Dr. Ramona Enea for useful discussions.

I would like to thank all my former and current group colleagues for their friendship and help whenever I needed it, their useful comments, and because of them, I can say that I have a magnificent and friendly work environment. Special thanks go to Dr. Fabian Axthelm for helping me in introducing lab techniques and also comfortable settling down in Lab as well as in Basel. I also thank Mark Inglin for reading and correcting the manuscripts.

I express my heartiest thanks to Anna Vehkaperä for support and care during the hard and stressful times of Ph.D studies.

Many thanks also to my friends in general, and all people who have helped and encouraged me to finish this thesis. Last, but not least, I also want to gratefully acknowledge financial support from SNSF for providing financial support and COST P15 Action for providing financial support a Short Term Scientific Mission at the University of Antwerp.

11. Curriculum Vitae

Vimalkumar BALASUBRAMANIAN, Ph.D

Date of Birth   09.05.1982

Nationality   Indian

Resident permit   B-Permit

Address   Kannenfeldstrasse 59

4056 Basel

Switzerland

Telephone   +41 788809347

Email   v.balasubramanian@unibas.ch

Languages   English (fluent), Tamil (native), Hindi (average), German (beginner)

Short Profile

- Doctoral researcher in Chemistry, Nanoscience

- Experience in small molecule drug discovery and development, polymeric formulations for development of drug carrier/delivery systems

- Expertise in studying the cellular interactions of drugs / nanomaterials

- Seeking to develop my career in a challenging research position

Education

2007- Present   **PhD** in Chemistry (expected submission: May 2011), University of Basel, Switzerland.

2005–2007   **Master of Technology** in Nanotechnology (equivalent to masters in engineering), with excellence (CGPA: 9.1/10.0), Amity University, India

2002-2004   **Master of Science** in Microbiology, first class, Periyar University, India

1999-2002   **Bachelor of Science** in **Microbiology** with first class, Periyar University, India

Research Experience

2007 - Present   PhD research in the Department of Chemistry, University of Basel, Switzerland.

- Synthesis and characterization of small molecules as functional enzyme mimics
- Designing and investigation of polymeric formulations based on encapsulation of proteins, enzymes and enzyme mimics in polymeric vesicles that act as nanoreactors to develop antioxidant therapy
- Detailed study of nanomaterials - cellular interactions in different mammalian cell cultures, toxicity assessment and in-vitro experiments (cellular uptake, viability, cytotoxicity, oxidative-stress, *in-vitro* antioxidant activity and other cell based assays).
- Directly responsible for the maintenance of cell cultures of the department. Supervised Bachelors' students.

2007 M.Tech, master thesis in Laboratoire de Chimie des Polymères Organiques, LCPO) (CNRS), France.

- Synthesis and characterization of hybrid polypeptide block co-polymers for biomedical applications

2006 Internship project in Sun Pharma Advanced Research Center, Baroda, India.

- Tailoring the optical properties of the dendrimer (PAMAM) stabilized gold nanoparticles.
- Synthesis and characterization of doxorubicin loaded gold nanoparticles for the anti cancer drug delivery.

2004 M.Sc, master thesis in Sengunthar arts and science college, Periyar University, India.

- Extended spectrum β-lactamase mediated resistance to Cefepime in Gram-negative organisms.

Technical skills

- Handling of various mammalian and bacterial cell cultures and cellular based assays (*in-vitro* evaluation on viability, cytotoxicity, internalization and pharmacokinetics).

- Synthesis and characterization of nanoparticles, metal complexes, organic, inorganic compounds and block copolymers.

- Spectroscopy techniques (UV-VIS, IR, EPR, NMR, fluorescence and luminescence) and Light scattering, X-ray crystallography.

- Isolation and identification of nucleic acids, proteins, PCR, Hybridization techniques, Western Blotting, Flow cytometry (FACS).

- Microscopy (Light, Fluorescence and Confocal laser scanning microscopy, Transmission electron microscopy).

- Purification techniques (size exclusion, thin layer chromatography, FPLC).

List of Publications

1. **Vimalkumar Balasubramanian**, Maria Ezhevskaya, Hans Moons, Markus Neuburger, Carol Cristescu, Sabine Van Doorslaer and Cornelia Palivan, Structural characterization of a highly active superoxide-dismutase mimic, Phys. Chem. Chem. Phys., 2009, 11, 6778 – 6787.

2. **Vimalkumar. Balasubramanian**, O. Onaca, F. Axthelm, D. Hughes, M. Grzelakowski, W. Meier, C. G. Palivan, How to Reduce Superoxide Anion Concentration using Antioxidant Nanoreactors, Journal of Optoelectronics and Advanced Material, 2009, 1(6), 1083 - 1087.

3. **V. Balasubramanian**, O. Onaca, R. Enea, D. Hughes, C.G. Palivan, Proteins delivery: From conventional drug delivery carriers to polymeric nanoreactors, Expert. Opin. Drug Delivery, 2010, 7(1), 63-78.

4. Cornelia G. Palivan, **Vimalkumar Balasubramanian**, Bernard A. Goodman, Global Structure-Activity Analysis in Drug Development Illustrated for Active Cu/Zn Superoxide Dismutase Mimics, Eur. J. Inorg. Chem., 2009, 31, 4634-4639

5. Ozana Onaca, David W. Hughes, **Vimalkumar Balasubramanian**, Mariusz Grzelakowski, Wolfgang Meier, Cornelia Palivan, SOD antioxidant nanoreactors: Influence of block copolymer composition on the nanoreactor efficiency, Macromol. Biosci., 2010, 10, DOI: 10.1002/mabi.200900379.

6. **Vimalkumar Balasubramanian**, Ozana Onaca, Maria Ezhevskaya, Sabine Van Doorslaer, Balasubramanian Sivasankaran, Cornelia G. Palivan, A surprising system: Polymeric nanoreactors containing a mimic with dual-enzyme activity-submitted to Soft Matter / SM-ART-02-2011-005215.

7. Pascal Tanner, Ozana Onaca, **Vimalkumar Balasubramanian**, Wolfgang Meier, Cornelia G. Palivan, Enzymatic Cascade Reactions inside Polymeric Nanocontainers – A Means to Combat Oxidative Stress, Chemistry a European journal, DOI: 10.1002/chem.201002782.

8. Egli, Stefan; Nussbaumer, Martin; **Balasubramanian, Vimalkumar**; Chami, Mohamed; Bruns, Nico; Palivan, Cornelia; Meier, Wolfgang, Biocompatible Functionalization of Polymersome Surfaces: A new Approach to

Surface Immobilization and Cell Targeting using Polymersomes, **in press-accepted**, Journal of American Chemical Society (JACS) / ja-2010-10275f.

9. Pascal Tanner, Stefan Egli, **Vimalkumar Balasubramanian**, Ozana Onaca, Cornelia G. Palivan, and Wolfgang Meier, Can polymeric vesicles that confine enzymatic reactions act as simplified organelles? FEBS letters, 2011, 10.1016/j.febslet.2011.05.003

Fellowships and awards

2007 - 2011   Swiss national foundation fellowship

2010   Swiss travel award from SCNAT/SCS

2009 - 2010   Received STSM grant from COST action P15

References

1. PD. Dr. Cornelia G. Palivan,
Department of Chemistry,
University of Basel
Switzerland
Email: cornelia.palivan@unibas.ch

2. Prof. Wolfgang Meier,
Department of Chemistry,
University of Basel
Switzerland
Email: wolfgang.meier@unibas.ch